
Single-Molecule Force Spectroscopy of Biological Complexes

Kamila Klamecka



München 2016

Single-Molecule Force Spectroscopy of Biological Complexes

Kamila Klamecka

Dissertation
an der Fakultät für Biologie
der Ludwig-Maximilians-University
München

vorgelegt von
Kamila Klamecka
aus Poznań (Posen)

München, den 17.11.2016

Erstgutachter: Prof. Dr. Heinrich Leonhardt

Zweitgutachter: Prof. Dr. Volker Scheuß

Tag der Abgabe: 17.11.2016

Tag der mündlichen Prüfung: 31.07.2017

Contents

Abstract	xiii
1 Introduction	1
1.1 Molecular interactions in living systems	1
1.1.1 Classical approaches to study molecular interactions	1
1.1.2 Computer simulations	2
1.1.3 Single-Molecule Force Spectroscopy	3
1.2 Bell-Evans model of bond dissociation	10
1.3 Biopolymers	12
1.3.1 Polymer elasticity models	12
1.3.2 Stretching the polymer of DNA: B-S transition	13
1.4 Studying biological interactions	14
1.4.1 Green Fluorescent Protein	14
1.4.2 Recombinant binders	15
1.5 Epigenetic DNA modifications	19
1.5.1 Methylcytosine binding proteins	20
1.5.2 Methylated-CpG binding Protein 2	20
1.6 Biotin-streptavidin bond	21
1.7 Aims of the work	22
2 Materials and Methods	25
2.1 Reagents	25
2.2 DNA, oligonucleotides and primers	26
2.3 Molecular biological methods	27
2.3.1 PCR	27
2.3.2 Cloning	27
2.3.3 Preparation of DNA for AFM measurements	29
2.3.4 DNA methylation	30

2.4	Biochemical methods	30
2.4.1	Protein expression and purification	30
2.4.2	Electrophoretic Mobility Shift Assay	32
2.5	Surface and cantilever chemistry	32
2.6	Biophysical methods	35
3	Results	39
3.1	Single-molecule force measurements of streptavidin-biotin complex	39
3.1.1	DNA construct preparation	40
3.1.2	Streptavidin-biotin force spectroscopy using AFM	40
3.2	Analysis of DNA cross-linking by MeCP2	42
3.2.1	AFM measurements	42
3.2.2	Magnetic Tweezers experiments	47
3.2.3	Loop detection using type II restriction endonuclease - assay test.	48
3.2.4	DNA looping upon MeCP2 binding	52
3.3	GFP-Nanobody binding strength determination	67
3.3.1	Strength of Nb-GFP complex as compared to other biomolec- ular interactions	67
3.3.2	Molecular Force Balance measurements	73
3.3.3	Binding strength of GFP-Enhancer vs. GFP-Modified Enhancer	74
3.3.4	Energy landscape of Nb-GFP complex	78
3.3.5	Specificity control in Nb-GFP force spectroscopy	87
4	Discussion	89
4.1	Streptavidin-biotin bond strength	89
4.2	MeCP2-DNA interaction	90
4.3	GFP-Nb	96
4.3.1	Nb-GFP interface	97
4.3.2	MFB results	97
4.3.3	AFM results	100
4.3.4	Specificity of interactions in AFM	103
4.4	Importance of single-molecule studies of protein complexes	103
4.5	Summary	104
4.6	Outlook	104
A	List of abbreviations	105

Table of Contents	vii
B Declaration	109
Acknowledgements	124

List of Figures

1.1	Schematic of AFM Force Spectroscopy	4
1.2	Schematic of MFA Force Spectroscopy	6
1.3	Schematic of magnetic tweezers	7
1.4	Energy landscape under external force	11
1.5	Force-extension curve of stretched DNA	14
1.6	Schematic depiction of conventional antibody, heavy-chain-only anti-body and Nanobody	18
1.7	Central dogma of molecular biology	19
2.1	Schematic of a flowcell	34
2.2	Typical force-distance curve	35
3.1	Streptavidin-biotin rupture force determination - experimental design.	40
3.2	Determination of rupture force of the streptavidin-biotin complex . .	41
3.3	EMSA of MeCP2	43
3.4	Exemplary B-S transition curve in absence of MeCP2	45
3.5	"Step" pattern of MeCP2-cross-linked DNA.	45
3.6	Intra- vs. intermolecular cross-linking of DNA by MeCP2	46
3.7	DNA constructs	50
3.8	Field of view of magnetic tweezers	51
3.9	Loop detection protocol	53
3.10	300 bp loop DNA; tether length analysis	54
3.11	300 bp loop DNA; long range drift analysis	55
3.12	300 bp loop DNA; short range drift analysis	56
3.13	600 bp loop DNA; tether length analysis	58
3.14	600 bp loop DNA in high salt; tether length analysis	60
3.15	600 bp loop DNA in high salt; long range drift analysis	61
3.16	600 bp loop DNA in high salt; short range drift analysis	62

3.17	1 kb methylated DNA; tether length analysis	64
3.18	1 kb methylated DNA; long range drift analysis	65
3.19	1 kb methylated DNA; short range drift analysis	66
3.20	Nb purified over HisTrap; SDS-PAGE	67
3.21	Nb purified over Superdex 75; SDS-PAGE	68
3.22	Covalent DNA-GFP complexes separated by native PAGE.	71
3.23	Covalent DNA-GFP complexes separated by non-reducing SDS-PAGE.	72
3.24	Protein MFB schematics.	75
3.25	Adjustment of MFA sensitivity	76
3.26	Analysis of different GFP variants for Enhancer interaction strength in a Multiplexed Protein-MFA	77
3.27	Force spectroscopy results; eGFP C anchor	80
3.28	Force spectroscopy results; eGFP N anchor	81
3.29	Force spectroscopy results; eGFP N+C anchor	81
3.30	Force spectroscopy results; wtGFP C anchor	82
3.31	Force spectroscopy results; wtGFP N anchor, cantilever a	82
3.32	Force spectroscopy results; wtGFP N anchor, cantilever b	83
3.33	Force spectroscopy results; wtGFP N+C anchor	84
3.34	Dynamic force spectrum of Nb-GFP complex	85
3.35	Energy landscape of Nb-GFP complex	86
4.1	Schematic explanation of the "step"-pattern in force curves	94
4.2	Alignment of GFP constructs used in MFB	99
4.3	Alignment of GFP constructs used in AFM	102

List of Tables

2.1	Consumables	25
2.2	Cloning oligonucleotides	26
2.3	Sequencing primers	27
3.1	Nb-GFP negative control summary	87
4.1	CpG nucleotide context	92

Abstract

Biomolecular interactions form the basis of all living organisms and their detailed investigation on the molecular level is crucial to the understanding of complex biological systems. With the advent of single-molecule (SM) techniques in response to the growing interest in the molecular nature of interactions, a whole new layer of knowledge has emerged. Hence, bulk-derived characteristics of molecular complexes need to be complemented by more detailed information addressing individual molecules and not only their statistical representatives. This way also interactions that are transient, weak or less abundant in the population are considered. This work focuses on the single-molecule elucidation of different types of biomolecular interactions - from protein-ligand to protein-DNA, to protein-protein ones.

The focus of the presented research is on force measurements, considered both in an absolute manner as well as in comparison to other reference interactions. Comparative analysis is more informative in many cases in which a ranking of interactions against each other is of interest rather than their absolute strengths. Several SM techniques are explored and their complementarity in targeting specific aspects of single-molecule accessibility is discussed.

I present a way to eliminate multiple events' bias in AFM measurements of biotin-streptavidin bond rupture. Despite numerous studies, available data regarding the binding force of the complex are not fully consistent and contain a lot of open questions. Here, the introduced DNA tether provided an intrinsic fingerprint, thus ensuring SM-accessibility. The same assay allowed to address the MeCP2-DNA binding, thought to lead to DNA cross-linking and looping. We observed DNA clustering upon addition of the protein and turned to magnetic tweezers to further analyse the mechanism of MeCP2 action. This instance demonstrates the challenges in proper experimental design in both techniques when it is desired to achieve a truly SM resolution not only in sensing but also in the behavior of the investigated system.

Finally, I characterized the GFP-Nanobody binding as an exemplary protein-antibody interaction. The energy landscape of the complex was explored by the AFM. Interestingly, the force measurements revealed several regimes related to various pulling geometries, as well as force dependence on the type of GFP despite identical epitopes. Then, multiplexed single-molecule measurements by means of Molecular Force Assay demonstrated the usefulness of this pair as a reference in comparative studies.

In this thesis I show that even with dedicated techniques achieving SM resolution may not be a straightforward task. Studying molecular systems often requires a very individualized approach so that native-like conditions can be mimicked while the focus is strictly confined to one molecule only. To sum up, we have designed assays to analyze biomolecular interactions on the SM level and demonstrate how to ensure SM resolution by making use of intrinsic features of biomolecules. The presented work contributes to the expansion of the existing SM techniques in the field of protein research and provides binding force data for the GFP-Nanobody complex - a promising molecular reference.

Chapter 1

Introduction

1.1 Molecular interactions in living systems

Force underlies motion and thus drives biological processes. As living systems are defined by biological pathways involving interacting molecules, understanding cellular dynamics and structure is only feasible through detailed elucidation of the molecular mechanisms. Interactions in living systems occur in a spatially and temporally regulated manner, therefore they should be studied in a physiological context. This explains the need for meticulous identification and characterization of the relations between their components. Numerous methods have been developed that provide various parameters of interest when describing interactions on the molecular level. These can be divided into three groups: classical (indirect) approaches, computer modeling and Single-Molecule Force Spectroscopy.

1.1.1 Classical approaches to study molecular interactions

Biochemical methods aimed at detection and identification of interaction partners include co-immunoprecipitation (Co-IP), Western blot analysis and affinity purification. They all rely on the principle of ‘fishing’ the specific interaction partner out of a solution (e.g. cellular lysate). A genetic yeast two-hybrid (Y2H) system is based on co-expression of putative interaction partners as fusion proteins and reconstruction of the transcription activator upon their binding. Due to its simplicity, low cost and rapidness, Y2H is particularly popular for high throughput screening. Phage display

is another example of an assay suitable for large library analysis, allowing for the identification of high-affinity binders.

In addition, also biophysical techniques have been developed: Dynamic and Static Light Scattering determine the size distribution of molecules in solution, Circular Dichroism exploits the chiral nature of biomolecules, Isothermal Titration Calorimetry provides binding affinity as well as thermodynamic parameters (enthalpy ΔH , Gibbs energy change ΔE and entropy change ΔS). Microscale Thermophoresis provides binding affinities and kinetics derived from the observation of particle movement in a temperature gradient. Surface Plasmon Resonance detects mass changes upon analyte build-up on a biosensor with an immobilized ligand. Fluorescence-based approaches depend on the labeling of molecules or their intrinsic fluorophores. Fluorescence Resonance Energy Transfer (FRET) - a non-radiant, distance-dependent energy transfer is applicable particularly for smaller molecules. This length (size) constraint does not apply to Fluorescence Correlation Spectroscopy or its two-channel version - Fluorescence Cross-Correlation Spectroscopy. Both these techniques are capable of measurements inside living cells and determine binding stoichiometry and binding constants. Fluorescence Polarization provides quantitative information on molecular interactions as well as enzymatic activity. This method is based on reduced mobility caused by molecules binding to form complexes.

Yet another possibility to map interaction networks is chemical cross-linking resulting in covalently linked binding partners, which can then be subjected to further analysis by Mass Spectroscopy.

Using a combination of the abovementioned techniques allows for - besides recreating interaction networks - the determination of parameters describing the affinity, stoichiometry, energetics and kinetics of the interaction. A common weakness of all these assays is that the conclusion is drawn based on averaging over a large number of molecules. This indirect character results in transient or weak interactions being lost or masked due to washing or simply scarcity. Yet even the statistically insignificant events do play an important role in nature and so need to be considered.

1.1.2 Computer simulations

Theoretical approaches by means of computer modeling are of immense help in gaining thorough understanding of the interactions. Detailed simulations remain, however, laborious, time-consuming and computationally expensive. Computer simulations rely on structural data (X-ray or NMR) and utilize equations of motion

to predict mechanical details of the particles' dynamics. Due to limits in computational capacity, it is not possible to model laboratory or physiologically meaningful timescales. Therefore, computer simulations are best exploited as complementary to experimental studies.

1.1.3 Single-Molecule Force Spectroscopy

Studying forces on the single-molecule level is crucial for an in-depth understanding of the mechanisms steering the living systems. A range of techniques has been developed to perform single-molecule force spectroscopy, most widespread ones being: Atomic Force Microscopy, Magnetic Tweezers, Optical Tweezers and Biomembrane Force Probe. The single-molecule approach reveals features otherwise out of reach for ensemble-averaged bulk measurements, such as the mechanical stability of proteins or receptor-ligand complexes, as well as rare events. Currently, sensitivities down to single angstrom (\AA) in length and a femtonewton (fN) in force can be achieved.

Single-molecule techniques exploited in this work are described below.

Atomic Force Microscopy

Invented in 1986, Atomic Force Microscope (AFM) [Binnig et al., 1986] is one of the tools of the Scanning Probe Microscopy family. The instrument utilizes a microstructured probe - a cantilever with a sharp tip at its end - controlled with a piezoelement to scan the surface under investigation, as schematically depicted in Fig. 1.

Considering the movement of the tip over the sample, AFM can operate in contact, non-contact or tapping (intermittent contact) mode. Initially conceived as a conductivity-independent imaging technique, soon after its introduction the AFM became a basic tool in single-molecule biophysics, proving successful in both unfolding as well as unbinding studies of biomolecules. The following description of the technique focuses on the use of the AFM for force spectroscopy. The central part of the instrument is a cantilever oscillating vertically over the sample surface. The movement of the cantilever is optically monitored and a force-distance curve is generated after each approach-retract cycle. The cantilever acts as a soft spring and exerted forces cause it to bend. In a typical single-molecule rupture experiment interacting molecules of interest are attached to the cantilever and substrate surface respectively. As the cantilever is brought in contact with the surface, the complex forms and upon cantilever retraction it is stretched until rupture, represented as a

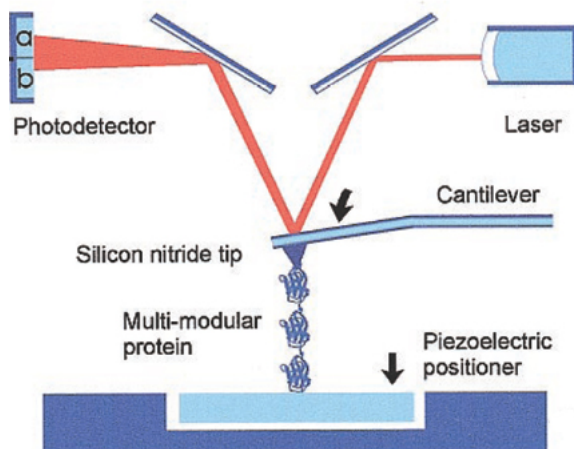


Figure 1.1: Schematic of the principle of AFM Force Spectroscopy. The biomolecule is tethered between the cantilever tip and the surface resting on a piezo-stage. A laser beam is projected onto the top of the cantilever and reflected off it to reach the photodetector. Upon piezostage movement in the z-direction, the molecule is stretched and exerts force on the cantilever, which bends. Deflection of the cantilever changes the position of the laser spot on the detector. (Fig. source: [Oberhauser et al., 2001] copyright 2001 National Academy of Sciences.)

sharp peak in the force-distance graph. Repeating the cycle for a couple of hundred times yields a Gaussian distribution of measured forces centered around the most probable rupture force.

In unfolding studies, molecules are probed in a similar manner, the difference being that a series of peaks representing domains or fragments unfolding precedes the final rupture peak. Transforming the recorded force-distance trace into the force-contour length one allows for mapping the unfolding pattern to the investigated structure.

Molecular Force Assay

Molecular Force Assay (MFA) is a multiplexed differential single-molecule technique developed to test binding strength of a complex relative to that of a known reference. In other words, a previously characterized molecular bond is employed as a force transducer. MFA does not determine the absolute rupture force value, rather the mutual relation of the two interactions, which is often more meaningful when

explaining the mechanistic aspects of a system. In MFA, a single measurement cycle provides statistics for the evaluation of the investigated interactions in the order of 10^9 as this many force balances are screened [Albrecht et al., 2003].

The experiment is conducted using a custom-built instrument based on an inverted epifluorescence microscope and a piezo-controlled head above it. The force balances are built by stepwise deposition of the molecules on a glass slide. Covalent immobilization of the balance to the slide and specific pairing within the balance results in two breakable bonds in series. The actual principle of the balance is exercised by bringing the top surface in contact with the functionalized glass slide and then retracting it. The top surface constitutes an elastomer stamp with 16 pads (1 mm^2 each) corresponding to the 16 spots on the sample slide. Streptavidin is covalently bound to the pads and upon contacting the lower surface, binds the biotinylated ends of the force balances. Retraction of the stamp exposes all assembled force balances to load and in consequence in each of them either the test bond or the reference bond ruptures. The position of the middle strand after the stamp removal indicates which was the case. In its initial form the technique utilizes oligomeric double-stranded DNA pulled against each other (see Fig. 1.2).

Shorter bottom and top single strands are cross-linked by one longer strand creating two double-stranded fragments. Fluorescent labels attached to the middle (Cy5) and top (Cy3) DNA strands allow for coupling efficiency determination, as correct assembly of a single balance brings the two fluorophores close together, creating a FRET pair.

Fluorescence scans before and after the probing of the force balances allow for ratio calculation of both the *RED* signal (Cy5 channel), giving the proportion of intact bottom bonds:

$$Ratio_{RED} = \frac{RED_{final}}{RED_{initial}} \quad (1.1)$$

and the *FRET* signal, giving the proportion of intact top bonds:

$$Ratio_{FRET} = \frac{FRET_{final}}{FRET_{initial}} \quad (1.2)$$

Now it is crucial to correct for the force balances that failed to couple to streptavidin on the stamp and thus were not probed. Therefore, the coupling efficiency (*CE*) is determined as:

$$CE = 1 - Ratio_{FRET} \quad (1.3)$$

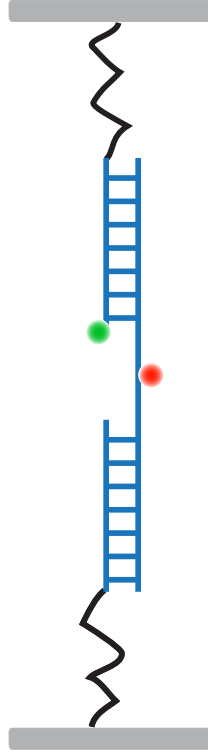


Figure 1.2: Schematic visualization of Molecular Force Balance. Upper DNA strand is labeled with Cy3 (green) and middle one with Cy5 (red).

Based on that, the ratio of broken test bonds as compared to reference bonds is expressed as the normalized fluorescence (NF):

$$NF = \frac{(Ratio_{RED} - Ratio_{FRET})}{CE} \quad (1.4)$$

NF equals 0.5 for test and reference bonds of the same strength, since then any of them ruptures with a 50 % chance. Difference in bond strength skews the NF accordingly, while it always takes values from 0 to 1.

Magnetic tweezers

The idea of magnetic tweezers (MT) was first demonstrated by Crick and Hughes in 1950 [Crick and Hughes, 1950]. Here, a biological polymer of interest (DNA, RNA,

structures thereof or a nucleosome fiber) is tethered between the flowcell bottom and a micron-sized superparamagnetic bead as depicted in Fig. 1.3. In the most common experimental design, the flowcell is placed between an inverted microscope and a pair of magnets, the height of which can be regulated. The magnetic field induces a magnetic moment in the bead and the bead experiences a force proportional to the gradient of the field, thus stretching the tether. The acting force can be inferred from vibrations in the x-y plane, while the z-position of the bead (relative to a surface-bound reference bead) gives the so called tether contour length. Since the characteristic length scale over which the field gradient varies is large (typically of the order of 1 mm), the exerted force can be considered constant over the distance penetrated by the bead. Force range from a few pN to about 100 pN can be covered by Magnetic Tweezers, tunable by varying bead size, gap between the magnets and their distance from the flowcell.

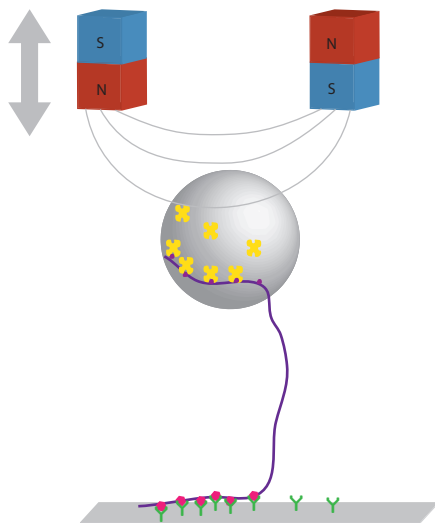


Figure 1.3: Schematic of magnetic tweezers. The biopolymer is spread between sample surface and a superparamagnetic bead, which can be manipulated in the field gradient.

Interestingly, magnetic tweezers offer parallel single molecule tracking, unachievable by other SM techniques. The throughput of multiplex measurements (involving many tethers manipulated at the same time) depends on the number of trackable beads in the field of view of the camera. With optimized surface chemistry, to date

double-digit numbers of tethers have been successfully scanned in parallel. For larger numbers of tracked beads online calculation of bead positions becomes cumbersome and can be replaced by post-measurement data analysis to make the measurement feasible.

Theoretical background of magnetic tweezers

Force exerted on a bead can be determined based on its lateral fluctuations and extensions of the tether:

$$F = \frac{1}{2} \nabla (\vec{m} \cdot \vec{B}) \quad (1.5)$$

where m is the induced magnetic moment of the bead in the external magnetic field \vec{B} .

The total potential energy of the tether is composed of mechanical energy stored in the nucleic acid (dependent on its end-to-end extension l) and a magnetic component:

$$E_p = E_{NA} + E_m = A(l) - Fz \quad (1.6)$$

where F denotes magnetic force acting on the bead and z - tether extension.

Due to Brownian motion, the bead constantly fluctuates. Therefore its potential energy can be expressed by:

$$\langle E_p \rangle = \frac{1}{2} \frac{F}{l} \langle \delta x^2 \rangle \quad (1.7)$$

where $\frac{F}{l}$ is the effective trap stiffness in the x direction (i.e. direction of the field) and

$$var\langle \delta x \rangle \equiv \langle \delta x^2 \rangle - \langle \delta x \rangle^2 = \langle \delta x^2 \rangle \quad (1.8)$$

(x - bead position in the direction of the field).

Since, by the equipartition theorem, the energy of one degree of freedom equals $\frac{1}{2}k_B T$,

$$F = \frac{k_B T l}{\langle \delta x^2 \rangle} \quad (1.9)$$

At forces higher than ~ 1 pN the above formula results in a systematic error [Vilfan et al., 2009], that can be corrected for by Allan variance (AV), which is half of the ensemble-averaged variance of the difference between two consecutive samples of position, where each sample is itself a local average of the probe position [Lansdorp and Saleh, 2012]:

$$\sigma(t) = \frac{1}{2} \langle (\bar{x}_{\tau,j+1} - \bar{x}_{\tau,j})^2 \rangle \quad (1.10)$$

Allan variance is a time-domain analysis, hence it does not entail any aliasing or spectral leakage [Lansdorp and Saleh, 2012]. It assumes a finite averaging time, which matches the video tracking instrument function, so no additional corrections of instrumental response are necessary.

Other single-molecule techniques

Biomembrane Force Probe

Introduced in 1995, Biomembrane Force Probe [Evans et al., 1995], comprises a microbead attached to a cell membrane (or synthetic lipid bilayer) spread over the aperture of a glass micropipette. The bead serves to probe the investigated surface. Here, the stiffness of the force transducer can be regulated by changing the suction pressure of the membrane and force sensitivity below 0.1 pN can be achieved.

Laser Optical Tweezers

In Optical Tweezers, also referred to as optical trap, a tightly focused laser beam is used to spatially confine a dielectric particle. The particle is polarized by the optical field and interacts with the steep gradient near the focus. The steepness of the gradient, the power of the laser and the polarisability of the particle all determine the stiffness of the trap, referred to as spring constant. The broad size range of trappable molecules (from ~ 20 nm up to several μm) makes it possible to trap single cellular organelles as well as whole cells or microstructured beads.

1.2 Bell-Evans model of bond dissociation

As described above, different measurement methods describe the same interaction with various parameters, which - although not equivalent - are related to each other. Hence, studying the system far from its equilibrium makes it feasible to derive equilibrium constants. A molecular bond is characterized by a dissociation rate k_{off} determining its lifetime $t_{off} = \frac{1}{k_{off}}$, that is the time necessary for it to break spontaneously.

Breaking the bond requires the system to overcome an energy barrier, the height of which describes the bond strength. A molecular complex is confined to an energy well, the depth of which is given by:

$$\frac{\Delta G^0}{k_B T} = \ln K_D - \ln 55 \quad (1.11)$$

where ΔG^0 is the binding free energy, K_D the dissociation constant in mole fraction and $k_B T$ sets the energy scale. The term $-\ln 55$ is a result of converting the dissociation constant into a unitless value by normalizing to molarity of H_2O (55 M) [Paul, 2003].

There may also exist an additional activation barrier separating the bound and unbound states of the system. Bond dissociation is possible owing to the thermal energy of the system, contributing transient impulses of force. Also under external load it is still the thermal energy that is responsible for bond breaking but in this case it is aided by the applied force. The energy landscape describes the complex by a set of energetic minima separated by energy barriers that need to be overcome in order to dissociate the molecules. External force tilts the energy landscape, diminishing the barriers as shown in Fig. 1.4.

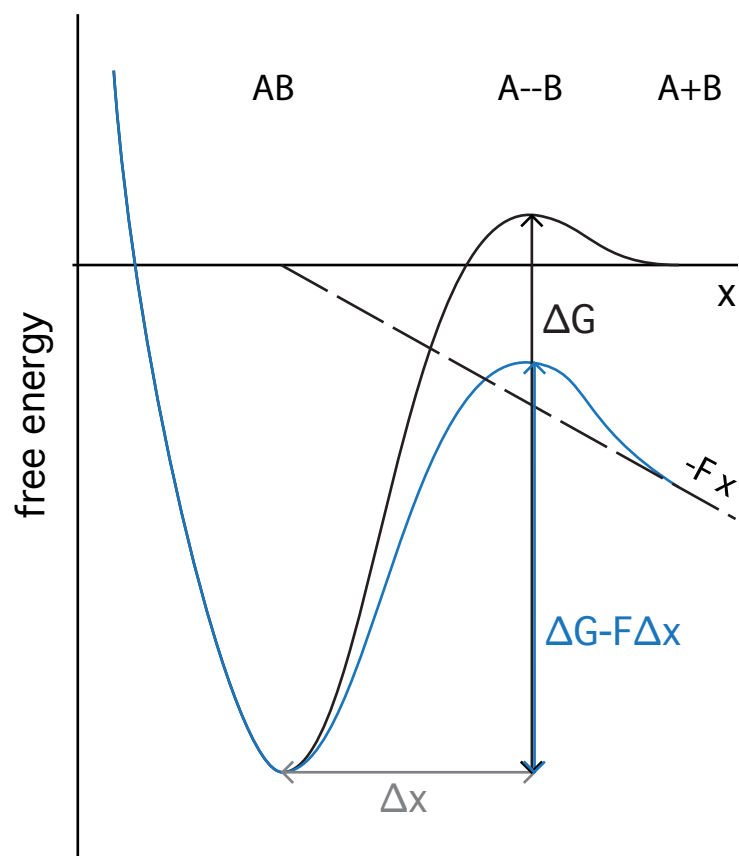


Figure 1.4: External force tilts the energy landscape lowering the energy barriers to dissociation. Black: reaction pathway without force; blue: reaction pathway under force.

Kinetics of a system subjected to external load (external force) is described by dynamic spectrum of rupture forces depending on the loading rate. The longer the force is applied, the more it affects the barrier; hence the observed dependence of rupture force on loading rate (force/time). The Bell-Evans model describes the most probable rupture force F^* as a function of temperature T and loading rate \dot{F} :

$$F^* = \frac{k_B T}{\Delta x} \ln \frac{\dot{F} \Delta x}{k_B T \cdot k_{off}} \quad (1.12)$$

where Δx denotes the position of the energy barrier and $k_B T$ thermal energy of the complex.

1.3 Biopolymers

On the molecular level, living systems are assemblies of molecules organized into complexes and organelles. A great deal of biomolecules falls into the category of polymers, prominent examples being nucleic acids and proteins. Thus, studying their mechanics requires appropriate physical models describing molecules' behavior.

1.3.1 Polymer elasticity models

Polymers are long, linear chains of repeated subunits. Proteins are folded polypeptides composed of amino acids, while building blocks of DNA or RNA are nucleotides. Despite the vast diversity of the biopolymer world, these macromolecules share common mechanical properties stemming from their similar overall architectural concept. Semi-flexible polymers are, to a good approximation, described by the Freely Jointed Chain (FJC) and Wormlike Chain (WLC) models.

Freely Jointed Chain

In the FJC model, the polymer is perceived as a chain of N stiff segments of define length l known as Kuhn length (double the persistence length), characteristic for the polymer. Thus the total length L of the polymer chain is:

$$L = Nl \quad (1.13)$$

The rotational freedom of the chain is restricted only to the joints. The theoretical Kuhn length not necessarily resembles the size of molecular segments of the polymer, for instance the best fit of FJC for a typical dsDNA molecule gives l of about 100 nm compared to the 0.34 nm contour length per basepair.

Wormlike Chain

More complex is the Wormlike Chain (WLC) model [Marko and Siggia, 1995], which assumes a polymer to behave like a fluctuating, isotropic and linearly elastic rod. It can be viewed as the limiting case of FJC, with Kuhn length approaching zero.

$$\frac{FA}{k_B T} = \frac{z}{L} + \frac{1}{4(1 - z/L)^2} - \frac{1}{4} \quad (1.14)$$

where F is the applied external force, A the bending stiffness of the molecule, k_B the Boltzmann's constant, T the absolute temperature, z the extension of the molecule and L the total molecular contour length. The WLC model provides a good fit for force-extension traces of many biopolymers, like double-stranded DNA or RNA, and polypeptides.

1.3.2 Stretching the polymer of DNA: B-S transition

For a long time the mechanics of DNA under load remained vaguely understood with several competing models trying to elucidate the nature of this biopolymer's overstretching. Relaxed double-stranded DNA (dsDNA) molecule has a form of β -helix described in the seminal work by Watson and Crick [Watson and Crick, 1953]. Under external load, B-DNA first reaches its contour length of 3.4 nm/bp. Upon further stretching, the molecule elongates by 70 % assuming an S-form, with maintained - at least partially - double-stranded structure. This constitutes a transient form on the way to full mechanical denaturation (melting), observed at several hundred pN resulting in two separate strands. Depending on the attachment geometry, the B-S transition occurs at 65 pN (for dsDNA anchored at opposite ends) or 110 pN (when both ends of the same strand are probed) and in both cases manifests itself with a plateau in a force-distance trace (Fig. 1.5).

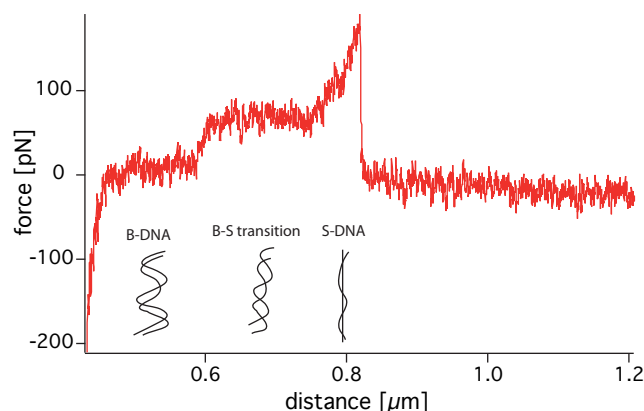


Figure 1.5: Force-extension curve of double-stranded λ -DNA. While retracting the cantilever from the surface with a velocity of $16 \mu\text{m/s}$ the double-stranded λ -DNA is stretched. At a force between 65 and 70 pN the well-known highly cooperative B-S transition is observed. During this transition the DNA duplex lengthens by a factor of 1.7. After this transition the force increases to a value of ~ 170 pN, at which the DNA finally ruptures. Adapted from [Morfill et al., 2007]

1.4 Studying biological interactions

1.4.1 Green Fluorescent Protein

Green Fluorescent Protein (GFP) was first mentioned by [Shimomura et al., 1962] but it was not until three decades later when it was cloned by Prasher [Prasher et al., 1992], which resulted in an explosion of its popularity due to the unusual ability of this protein to generate visible light. Understanding the mechanisms driving GFP fluorescence led to an immediate breakthrough in biological sciences, honored with the Nobel Prize in 1998. Employed as a molecular tag, GFP revolutionized cell biology, facilitating *in vivo* imaging without any disturbance to the visualized cells.

The bimodal excitation (absorbance) spectrum of the wtGFP displays the main peak at 395 nm and a less pronounced one at 475 nm [Chalfie, 1995]. The major peak corresponds to the chromophore in the anionic (deprotonated) state whereas the minor one - to the neutral state. In its natural environment, wtGFP converts the energy transferred from calcium-dependent aequorin into green fluorescence [Prasher et al.,

1992]. In laboratory conditions, GFP excitation is achieved by direct illumination with UV or blue light. Rather poor folding efficiency of the wtGFP variant prompted the development of a humanized, enhanced form of GFP (eGFP) [Zhang et al., 1996]. The introduced mutations in the chromophore (F64L, S65T) made the protein 35 times brighter than its wild-type predecessor. EGFP features the two mentioned absorbance peaks but the one for higher wavelength becomes predominant (and also slightly red-shifted to 488 nm). Besides these two most common representatives of the GFP family, a vast number of other color variants exists, spanning most of the visible light spectrum. This opens up extensive multiple-color imaging possibilities as well as applications exploiting FRET. Yet another interesting example of engineered GFP is a variant characterized by improved folding kinetics useful in expression when fused to poorly folding proteins - called superfolder GFP (sfGFP) [Pédelacq et al., 2006].

Green fluorescent proteins can also be isolated from species other than *Aequorea*, like e.g. a hydroid *Obelia* or a sea pansy *Renilla* [Morin and Hastings, 1971]. Other than *Aequorea* GFP, only the one produced by *Renilla* has been biochemically well characterized and despite the apparently identical chromophore, it differs from the former in amino-acid sequence, physical parameters like extinction coefficient, pH-tolerance and tendency to dimerize [Ward et al., 1980]. This explains the unquestionable domination of the *Aequorea*-derived GFP and variants thereof in research use.

Full length wtGFP comprises 238 amino acids, which fold into an eleven-stranded β -barrel closed on one end by a short α -helix. The molecule is about 2.4 nm in diameter and 4.2 nm long. Both N- and C-termini protrude from the same side of the barrel and another α -helix runs axially through it. The chromophore is formed by three adjacent amino acids (residues 65-67) within this helix, through a cyclization process involving molecular oxygen.

The mechanical stability of GFP has been investigated by Dietz and Rief [Dietz and Rief, 2004]. They observed the β -barrel unfolding through two intermediate states: by first losing the N-terminal seven-residue-long α -helix at about 35 pN, followed by removal of one of the terminal β -strands at higher forces, before the whole structural integrity is lost at over 100 pN.

1.4.2 Recombinant binders

Studying biological interactions requires specific probes for identification, visualization and purification, both inside the living cells as well as *in vitro*. Thus, versatile

binders are needed, which are not only easy to produce but also tailored to specific needs of a particular approach. Revolutionary hybridoma technology introduced by Kohler and Milstein [Kohler and Milstein, 1975] brought research in the field of antibodies to a thrive. These are, however, clearly of limited use due to expensive production, low tissue penetration, complex architecture and bivalent or multivalent mode of action as well as in many cases - patent issues. Several alternative strategies are the subject of ongoing efforts, aimed at overcoming the obstacles beyond reach for the traditional antibody-based approaches. These can be classified into two groups: antibody-derivatives and non-antibody binders. Small binders share a number of advantages over traditional antibodies, such as ease and reduced cost of production, more efficient tissue penetration and fast renal clearance. Possible therapeutic use of any type of small protein binders relies either on the unmodified versions or on their conjugates (or fusion proteins).

Antibody mimetics

The class of non-antibody binders, also referred to as antibody mimetics, features a number of scaffolds. One example is a 10 kDa fibronectin protein fold based on human fibronectin type III domain (FN3). The FN3 forms a β -sandwich structure similar to that of immunoglobulin domains. This inspired its use as a scaffold for engineering novel binding proteins referred to as monobodies or Adnectins [Koide et al., 1998]. Twice as large - yet still in the range of small binders - are 20 kDa anticalins derived from the family of extracellular proteins, lipocalins, responsible mainly for transport and storage of physiologically significant molecules [Flower, 1996]. Lipocalins share a structural motif of an eight-stranded β -barrel enclosing an internal ligand-binding site, particularly suited for small, hydrophobic molecules (but types of ligands vary throughout the family). Domain of protein A of *Staphylococcus aureus* has in turn become a template for affibodies, with α -helical structure and molecular weight of only 6.5 kDa [Nord et al., 1996].

Designed ankyrin repeat proteins (DARPin) [Amstutz et al., 2006; Binz et al., 2003] constitute another novel class of binders which may outperform monoclonal antibodies. These small - typically 14-21 kDa - single domain proteins, characterized by high temperature stability (midpoint denaturation at 65-95 °C) and no aggregation tendency are modular molecules usually composed of 4-6 segments: amino- and carboxy-terminal cap and 2-4 inner segments. A single segment is made of 33 amino-acids (3.5 kDa), 7 of which are variable. Libraries based on just two variable segments reach diversities over 10^{14} [Stumpp et al., 2008]. Ankyrin proteins natu-

rally occur in erythrocytes and belong to the most abundant proteins encoded in the human genome. Therefore, DARPin drugs are expected to be well tolerated by the immune system [Vogel et al., 2007; Stumpp et al., 2008]. Their natural function is recognition and binding of large epitopes. In many organisms the immune system relies on repeat proteins. Free of intrinsic cysteines, DARPins can be easily modified by introduction of a thiol group for convenient site-specific chemical coupling.

Antibody-derived binders

Antibodies (also referred to as immunoglobulins) are the active agents of the vertebrate immune system responsible for recognition, binding and inactivating foreign agents in the organism. Among the five classes of antibodies (IgG, IgM, IgA, IgD and IgE), IgG are the most abundant and play the key role both in their natural habitat as well as in biotechnological applications. An IgG molecule is a large, 150 kDa, glycoprotein formed by two heavy and two light sugar-modified polypeptide chains kept together by disulphide bridges and hydrophobic interactions on their interface. Parts of one heavy and one light chain contribute to the formation of each of the two antibody binding sites on the termini of the Y-shaped monomer. Hence, isolating this domain was the most straightforward approach to create a small binder. The resultant molecule is Fab (Fragment, antigen-binding) with a molecular weight of 50 kDa, composed of one constant and one variable domain of the heavy and light chain of the antibody. Thermal stability of such molecule is weak, since within the antigen-binding site there is no covalent link between the two chains.

Nanobodies

The discovery of heavy-chain-only antibodies (HCAbs) in camelids [Hamers-Casterman et al., 1993] inspired completely new approaches in antibody engineering. Devoid of light chains, HCAbs recognize their antigens using single protein domains; unlike their conventional counterparts, which need parts of both heavy and light chain to bind the epitope. Derived from HCAbs, so-called Nanobodies (Nbs) constitute the smallest functional antigen-binding domain (see Fig. 1.6). Their average molecular mass of about 15 kDa makes them ten times smaller than typical antibodies, yet they remain competitive in their binding affinity and specificity. Nanobodies can be raised against a desired antigen, easily cloned and expressed in heterologous hosts, including bacteria [Arbabi Ghahroudi et al., 1997]. Interestingly, they combine the

advantages of conventional antibodies with greatly improved tissue permeability owing to their reduced size and increased hydrophilicity [Muyldermans et al., 1994]. Nanobodies show a high degree of identity with human type 3 VH domains and humanization strategies have been proposed [Vincke et al., 2009; Vaneycken et al., 2010]. Therefore, it is not surprising that nanobodies were considered potent agents in therapeutics and immunodiagnostic methods early on.

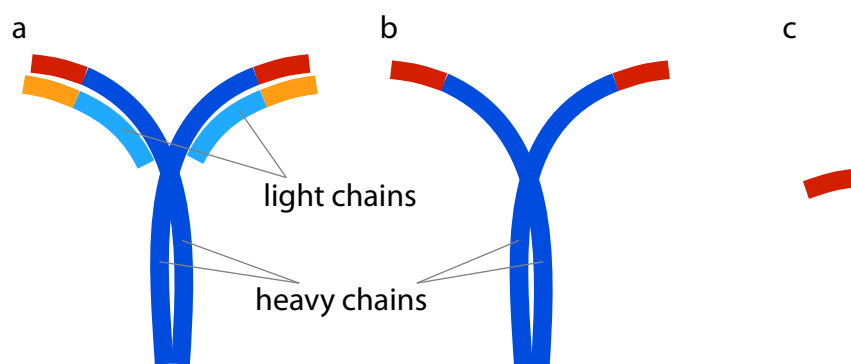


Figure 1.6: Schematic depiction of conventional antibody (a), heavy-chain-only antibody (b) and Nanobody (c). Constant regions depicted in dark and light blue, variable regions in red and orange.

Nanobodies are versatile reagents that are useful in a broad variety of applications. Of particular interest is the use of Nanobodies in *in vivo* imaging techniques [Chakravarty et al., 2014; Herce et al., 2013; Goethals et al., 2014; Gainkam et al., 2008; Vaneycken et al., 2011; De Groeve et al., 2010; Rothbauer et al., 2006]. Noninvasive (and repeatable) visualization is for example important when screening the progress of a disease. Here, the Nanobodies' small size and lack of adverse effects help bypass the limitations typical of conventional antibodies. In recent years, Nanobodies have proven successful in therapy [Vandenbroucke et al., 2009; Overbeke et al., 2014] and their bispecific derivatives are expected to aid in tumor treatment by cross-linking otherwise unrelated antigens [Els Conrath et al., 2001; Hmila et al., 2010]. Medical uses beyond oncology [Cortez-Retamozo et al., 2004; D'Huyvetter et al., 2012; Altintas et al., 2012] include monitoring arthritis [Zheng et al., 2014], atherosclerosis [Broisat et al., 2012] and other inflammatory diseases [Baral et al., 2006; Stijlemans et al., 2011].

1.5 Epigenetic DNA modifications

Life relies on genetic information passed from generation to generation by means of a four-letter genetic code. The central dogma of molecular biology (illustrated in Fig. 1.7) explains how genes, encoding proteins, shape living organisms. But genes constitute only a part of the final picture. In its native form, DNA is rarely a bare string of nucleotides. Rather, it is subject to epigenetic modifications, turning genes on and off and regulating the functioning of the genome in each individual cell.



Figure 1.7: Schematic illustration of the central dogma of molecular biology explaining the directed flow of information leading from DNA to RNA to protein.

The term "epigenetics" refers to genome alterations not involving changes in DNA sequence. These mechanisms are crucial for X chromosome inactivation as well as for the course of cell differentiation [Holliday, 2006]. DNA methylation is the most abundant epigenetic mark in eukaryotes and occurs exclusively at cytosine residues, predominantly at CpG dinucleotides [Bird, 1986]. In mammals 60-90 % of CpGs are methylated with the exception of CpG islands, mostly found in gene promoter regions and generally left unmethylated. Introduction and maintenance of the methyl tags is accomplished by methyltransferases: *de novo* methyltransferases DNMT3a and DNMT3b, modifying previously unmethylated DNA, and maintenance DNMT1 responsible for copying methylation pattern onto the nascent strand during replication [Jeltsch, 2006]. The latter, however, has been shown to also possess *de novo* methylation activity [Fatemi et al., 2002; Pradhan et al., 1999]. On the other hand there are enzymes specialized in reading the epigenetic information: the MBD (Methyl-DNA Binding Domain) family [Hendrich and Bird, 1998], the Kaiso family [Daniel and Reynolds, 1999; Filion et al., 2006] and the Uhrf family [Hopfner et al., 2000; Bronner et al., 2007]. Yet another group of epigenetically-sensitive DNA binders constitute the family of Tet (ten-eleven translocation) proteins responsible for 5-methylcytosine (5mC) conversion to 5-hydroxymethylcytosine (5hmC), 5-formylcytosine (5fC) and 5-carboxycytosine (5caC) [Mohr et al., 2010].

It is epigenetics that makes cells of a single organism, sharing the same genetic material so different as to be parts of completely unrelated tissues and specialize in totally distant functions. Genomes of various organisms display different levels of

dependence on methylation and even within a single organism significant changes in methylation pattern occur throughout its life, in relation to developmental stages and environmental factors [Bogdanović and Veenstra, 2009]. Similar mechanisms underlie slight differences in the phenotypes of monozygous twins, a phenomenon confirmed by extensive research [Fraga et al., 2005; Singh et al., 2002; Petronis, 2006; Bell and Spector, 2011]. Epigenetic discrepancies in otherwise genetically identical twins were found to accumulate with age and reflect factors such as exposure to toxins (e.g. smoking), medical history, diet, stress or physical activity. Changes in the epigenome also affect the CpGs within promoter regions, potentially affecting gene expression. Another interesting example of epigenetic regulation through methylation is the social structure organization in the honeybee, in which queens and worker bees develop sharing the same genetic material and differing only in the type of food received from early on [Barchuk et al., 2007; Colhoun and Smith, 1960].

1.5.1 Methylcytosine binding proteins

Five proteins: MBD1, MBD2, MBD3 and MBD4 as well as MeCP2 form the MBD family [Hendrich and Bird, 1998]. Their common feature is the domain responsible for specific binding of methylated CpG dinucleotide - the MBD domain. Apart from mammalian MBD3 and the long form of amphibian MBD3 (MBD3 LF), all these proteins specifically recognize and preferentially bind methylated over unmethylated DNA. Lack of this specificity in MBD3 is a result of insertion in its MBD region [Wade et al., 1999]. Additionally, MBD1 can also bind DNA via its CxxC3 zinc-finger domain [Jørgensen et al., 2004]. The preference for methylated over unmethylated DNA is three- to tenfold throughout the family and may as well be influenced by the nucleotide context.

1.5.2 Methylated-CpG binding Protein 2

The multifunctional mammalian protein MeCP2 (Methyl-CpG binding Protein 2), first described by [Lewis et al., 1992], is involved in transcription activation and repression, RNA processing and chromatin organization. It is expressed in all tissues and displays extremely high abundance in neuronal chromatin. Mutations in MeCP2 are associated with Rett Syndrome (RTT) and autism spectrum disorders [Amir et al., 1999], as well as certain cancers (reviewed in [Parry and Clarke, 2011]). MeCP2 localizes to both promoter and intergenic regions in the nuclei of neuronal cells [Yasui

et al., 2007]. Deviations from its normal expression level have drastic effects on proper brain function.

Intact MeCP2 has a theoretical molecular weight of 53 kDa but during electrophoretic analysis it co-migrates with markers of 81 kDa [Nan et al., 1993]. Full length protein is composed of 486 amino acids, among which 60 % are unstructured, 35 % folded into β -strand or turn and 5 % α -helix [Adams et al., 2007; Ghosh et al., 2008].

The key domain of MeCP2, responsible for specific binding to methylated CpG sites Methylated-CpG Binding Domain (MBD) spans amino acid positions 78-162 [Nan et al., 1993], accounts for 17 % of its full length and is one of the few regions with organized secondary structure. The MBD core consists of an α/β sandwich and recognizes the hydration pattern of methylated CpG dinucleotide rather than the methyl group per se [Ho et al., 2008].

To date, several other domains have been identified; these include AT-hooks responsible for DNA-methylation-independent chromatin binding [Baker et al., 2013], the DNA-binding domain and binary chromatin-binding sites [Nikitina et al., 2007], protein-protein-interacting regions present within these domains, including a dimerizing domain as well as a WW domain-binding region (WDR) [Buschdorf and Strätling, 2004] also mediating interactions between proteins. Thanks to the wide attention MeCP2 has experienced in the past years its structural composition and biochemistry has been well described, yet the mechanism of its binding to DNA still lacks a detailed understanding.

1.6 Biotin-streptavidin bond

Streptavidin (SA), first described by [Chalet and Wolf, 1964], is a 60 kDa protein composed of four identical subunits. It is isolated from soil bacteria *Streptomyces avidinii*. The tetramer assembles as a dimer of dimers, exposing four β -barrel-shaped binding pockets for its ligand - biotin. Each β -barrel is composed of eight antiparallel β -strands [Kurzban et al., 1990]. A complex of single biotin with streptavidin is stabilized by the residues of the beta-barrel of one subunit and a single tryptophan (Trp120) of a neighboring one, which upon binding moves towards the binding site inducing structural change of the whole protein [Weber et al., 1989]. Rearrangement of one surface-exposed loop of streptavidin (closing the pocket) plays an additional role in the complex formation [Freitag et al., 1997]. The unusual strength with which streptavidin binds its ligand relies mainly on hydrophobic and van der Waals

interactions, aided by seven hydrogen bonds, five of which are buried deep in the pocket and protected from competing solvent molecules.

The unusually low K_d of 10^{-15} M [Chaiet and Wolf, 1964; Green, 1975] places the biotin-streptavidin complex among the strongest non-covalent ones in nature, intensely studied as a model receptor-ligand pair. The fact that streptavidin readily accommodates not only free but also derivatized biotin has led to the common use of this system in protein purification and biomolecules immobilization. Surface-exposed lysine side chains provide primary amines facilitating convenient chemical modifications of the protein. Other members of the biotin-binding protein family include hen egg avidin - a glycoprotein which shares just 38 % of sequence identity with SA (yet displays high structural similarity), and its deglycosylated version - neutravidin (NA) [Marttila et al., 2000]. All these proteins share the high K_d but differ in pI values (10 for avidin, ± 7 for SA, 6.3 for NA), which plays a role in surface interactions with solid support or other molecules. Monovalent streptavidin has also been reported, offering similar affinity to biotin as the wild-type form [Howarth et al., 2006].

Streptavidin-biotin interaction has received a lot of attention over the past years. Available data is, however, not quite consistent. Many attempts to determine binding strength of the complex resulted in force values ranging from 120 pN to even 450 pN [Yuan et al., 2000; Stevens et al., 2002] and not always all the interesting parameters are provided. Although the now growing in prominence cohesin-dockerin system withstands much higher forces - in the order of 700 pN - the biotin-streptavidin pair still remains one of the most popular complexes used for anchoring biomolecules to solid support.

1.7 Aims of the work

Molecular interactions shape the living systems and only through their detailed elucidation are we able to fully understand the mechanisms of life. Currently available single-molecule techniques are designed to ensure enhanced precision and sensitivity. The objective of this work is to provide insight into different types of biomolecular complexes. Using the advantages of diverse single-molecule techniques, examples of protein-ligand, protein-DNA and protein-protein interactions are characterized in a manner unavailable for classical approaches.

First, I aimed at demonstrating the usefulness of AFM-based force spectroscopy

in discriminating specific interactions, in this work between biotin and streptavidin. Despite extensive attention this receptor-ligand pair has attracted over the years, the existent data provide a broad range of forces and are not always complete in terms of presented measurement parameters. Therefore, I incorporated a dsDNA tether providing a clear B-S transition fingerprint to easily select only the single-molecule events.

Next, using a similar experimental design, I tackled the interaction of methyl-DNA-dependent protein MeCP2 with specific and unspecific targets. The protein is believed to loop DNA upon binding to it but little is known about the nature of this phenomenon. Single-molecule assays were meant to address the putative role of MeCP2 in DNA cross-linking. I employed two different single-molecule techniques (AFM and MT) to achieve the required single-molecule resolution and analyze the putative effect of DNA loop formation. I also designed several DNA substrates to provide various sequence contexts optimal for the looping to occur.

Furthermore, inspired by the popularity of the GFP tag in protein research, I focused on the GFP-Nb pair, starting with the complex's rupture force determination. I tackled this aspect both in terms of absolute force values (provided by AFM force spectroscopy) as well as relative ones (using Molecular Force Assay), at which on the one hand the technique was adapted to and tested for screening protein-protein interactions and on the other hand - the GFP-Nb system was considered a potent reference for measuring those.

Chapter 2

Materials and Methods

2.1 Reagents

All common chemicals were purchased from Sigma (Deisenhofen, Germany) or Roth (Karlsruhe, Germany), unless otherwise stated. Restriction endonucleases and methyltransferases, Phusion Polymerase and Phusion High-Fidelity PCR Master Mix were purchased from New England Biolabs (NEB; Ipswich, Massachusetts). Kits for DNA cleanup (gel extraction, PCR product purification, plasmid DNA isolation) were purchased from Qiagen (Qiagen AB, Sollentuna, Sweden). Consumables are listed in Table 2.1.

Consumables	Supplier
glass slide A+ (aminosilane coating)	Nexterion
glass slide E (epoxysilane coating)	Nexterion
cantilevers MLCT	Bruker
cantilevers BioLever mini	Olympus
Malhex-NH-PEG-O-C ₃ H ₆ -CONHS	Rapp Polymere

Table 2.1: Consumables

2.2 DNA, oligonucleotides and primers

Gene/sequence	forward DNA 5'-3'	reverse DNA 5'-3'	elongation time	T _a
Nb C anchor	GTCACCGTCTCC TCACACCACCAT CACCATCACTGC TAATAGTCTAG	AATTCTAGACTA TTAGCAGTGATG GTGATGGTGGTG TGAGGAGACG	-	70 °C
eGFP N anchor	CATGGCATGCAG CAAGGGCGAGGA GCTGTTCAACCG	GTGAACAGCTCC TCGCCCTTGCTG CATGC	-	70 °C
eGFP C anchor	GTCACCACCATC ACCATCACTGCT AGTAAG	AATTCTTACTAG CAGTGATGGTGA TGGTG	-	60 °C
T4 1.1 kb fragment	biotin-TGGAGAAG GAGAATGAAGAA TAATA	HS-CGGTGCTAAA TTTATTATGACT TCA	30 s	58 °C
mtweez loop300	CAGCTAGCTCGA GTGGAGAAGGAG AATGAAGAATAA TA	GTCAGGTACCGT GAAGTAAGTAAT AAATGGATTGA	30 s	61 °C
GA eGFP N+C anchor eGFP	gatcgggccgtgggtATG GTGAGCAAGGGC GA	ttaatttcagtgtgaccA CCCTTGACAGC TCGTC	30 s	61.7 °C
GA eGFP N+C anchor hAGT	GGTCACCATGAA ATTAAACTGGTG	ACCCACGGCCCG ATCCT	3.5 min	67.9 °C
GA loop600_v	TACAGAATCCCT AAACGC	ACCTGTCAAAGC AGGCA	3 min	59.1 °C
GA loop600_i	gcctgcttgacaggtGG GACCTGCGCTCT GTC	cgtttaggattctgtaGT ATGTTTGGCATT AGTTCAATC	30 s	62.1 °C
GA mtweez basic XhoI-CGC	ctcgagAGCTGTTT GTAACTTGC	cgCTTTTAATCTG CTGTTTGCTC	1 min	58.2 °C
GA mtweez basic CG-C	caaacagcagattaaaagc gCTGCAGGAGTC AATGGGA	tggagcgcCAGTACA CCACATCACTTT C	2 min	61.2 °C
GA mtweez basic C-XhoI	gtgtactggcGCTCCA CCTTTTTTCCCCA G	gcaagttaacaaacagctct cgagGACTGAATTTC CATACCACATTT G	30 s	62.4 °C
MT handle EcoRI	ATGAAAATTTGG AGCAAAGAAGAG G	AAAAAAGAATTC ACTTCCGGATTA CGGCTG	15 s	58 °C
MT handle XbaI	AAAAAACTCGAG GATGAAAAA ACTGTTTACCAC CATTAAAGG	CAGCAGGCGTTTC AATATTGCG	15 s	58 °C

Table 2.2: Cloning oligonucleotides

Name	5'-3' sequence
Nb_seq	ATACCTATTGCCTACGG
pBADrev	GTCGACGGCGCTATTCAG
pBADfor	CACTTTGCTATGCCATAGC
eGFPup	GGACACGCTGAACTTGTG
eGFPdown	CCAGTCCGCCCTGAGC
tit_rev_seq	CCATTGAATGCTTAGTGCC

Table 2.3: Non-standard sequencing primers

2.3 Molecular biological methods

Unless otherwise indicated, the oligos were purchased from Eurofins MWG (Ebersberg, Germany).

2.3.1 PCR

A typical 20 μ l PCR reaction mix consisted of 10 μ l HF Phusion Master Mix, 7 μ l H₂O, 1 μ l DNA template (of 200 pg/ μ l to 100 ng/ μ l) and 1 μ l each 10 μ M forward and reverse primer. PCRs using Phusion polymerase (not in a Master Mix) were usually performed in a total volume of 50 μ l. 5 μ l 5x Phusion GC buffer, 1 μ l polymerase, 1 μ l dNTPs (PeqLab, Erlangen, Germany) 10 mM each, 1 μ l DNA template and 0.5 μ l each of forward and reverse primers were added to 36 μ l H₂O.

Cycling conditions were adjusted for each reaction according to the manufacturer's instructions.

2.3.2 Cloning

Cloning of N+C-anchored eGFP, 600-bp-loop and 600-bp-loop-basic constructs was performed using Gibson Assembly (GA) method. The other constructs were obtained through restriction cloning. In both cases chemically competent *E. coli* (DH5 α unless otherwise specified) were used for subsequent transformation. Primer sequences along with annealing temperatures and elongation times are listed in Table 2.2. Positive

clones were confirmed by sequencing. Table 2.3 contains the list of custom-designed sequencing primers.

Gibson Assembly cloning

Gibson Assembly cloning was performed using GA kit (NEB) and NEB online tool for primer design, according to the manufacturer's instructions. Following PCR, each reaction mix was diluted 1:20 with H₂O and added to 10 µl of 2x GA mix in proportions determined based on the fragments' length ratio.

Cloning of N+C-anchored eGFP

The eGFP insert was PCR amplified using pRSET5D_eGHis as a template and pBAD_hAGT-TitGFP-hAGT-Strep was used as a template for backbone PCR. Both fragments were combined using Gibson Assembly assay.

Cloning of single-anchored eGFP

N-terminal cystein was introduced to pRSET5D_eGHis by replacing an NcoI/BseRI cut fragment by a synthetic insert with complementary overhangs. Similarly, the C-terminal modification was achieved and the extra cystein was placed right after the HisTag.

Cloning of Nanobodies

Terminal cystein was introduced by replacing EcoRI/BstEII cut C-terminal fragment of cAbGFP4 in pHen6 by a synthetic insert with complementary overhangs, introducing the cystein right after the HisTag, and an additional XbaI restriction site enabling easy identification of positive clones.

Cloning of DNA constructs for magnetic tweezers

All constructs for the use with magnetic tweezers were based on the pCpGfree-lacZ plasmid (InVivogen, San Diego, California). Chemically competent *E.coli* GT115

(InVivogen) cells allowing for Zeocin (InVivogen) selection were used for transformation.

300-bp-loop construct was obtained by PCR amplifying 1.1-kb fragment with primers introducing NheI and XhoI (forward) and Acc65I (reverse) restriction sites. Both pCpGfree vector and PCR product were digested with NheI and Acc65I and ligated with each other. The resulting construct features two EcoRI and one XhoI sites, and upon linearization with those enzymes, a 5 kb fragment with 300 bp loop was isolated.

600-bp-loop construct was generated through site directed mutagenesis of the 300-bp-loop one (by GA cloning), introducing two M.HhaI sites 624 bp apart.

600-bp-loop-basic was prepared via assembly (GA) of three fragments, all PCR-produced using pCpGfree-lacZ plasmid as a template. The resulting construct contains single EcoRI and XhoI sites in close proximity to each other to simplify tether preparation procedure.

To enable proper attachment of the DNA to the bead and the lower surface of the flowcell, DNA handles were used, carrying several biotin or digoxigenin labels. The labels were incorporated during a PCR reaction as described in [Dekker et al., 2004], in which regular PCR mix was supplemented with biotin- (at a final concentration of 375 μ M) or digoxigenin-labeled dUTP (at a final concentration of 30 μ M) (Jena Bioscience, Jena, Germany). In both reactions, a fragment of BcnI sequence was used as template. The 314 bp-long biotin handle was then digested with EcoRI and the 400 bp-long digoxigenin handle with XhoI.

Actual tethers for the use with magnetic tweezers were prepared by ligating the EcoRI/XhoI-linearised fragments with the two pre-digested handles.

2.3.3 Preparation of DNA for AFM measurements

1.1-kb-long T4 DNA fragment was PCR amplified using primers carrying terminal functional groups: thiol for covalent attachment to gold or maleimide, and biotin for attachment to streptavidin.

2.3.4 DNA methylation

Two-site methylation of DNA with defined loop length was achieved enzymatically using M.HhaI methyltransferase (NEB) according to the manufacturer's instructions. Methylated DNA was then test digested with HhaI restriction endonuclease cutting unmethylated sites, ensuring that only completely methylated DNA was probed in the experiments.

Full methylation of AFM constructs was achieved through PCR substituting dCTP of the dNTPs mix with 5-methyl-dCTP (Jena Bioscience). This way all cytosine residues of the PCR product were methylated.

2.4 Biochemical methods

2.4.1 Protein expression and purification

DNA constructs not mentioned in the Cloning section (2.3.2) were already available in the library of either Gaub lab or Leonhardt lab.

In general, 1-5 l LB medium was inoculated with an overnight culture, grown to OD₆₀₀ in the range of 0.6-0.8, at which point they were induced with 0.25-0.5 mM β -D-1-thiogalactopyranoside (AppliChem, Darmstadt, Germany) and overexpression was carried out overnight at 20 °C (Nb) or 28 °C (GFP). The cultures were then harvested by centrifugation at 5000 g for 10 min. The pellet was frozen at -80 °C for at least 15 min, then thawed and resuspended in 10 ml of binding buffer (1x PBS, pH 8.0, 0.5 M NaCl, 20 mM imidazole, 1 mM PMSF, 10 g/l lysozyme; see below for ybbR-tagged protein). After incubation for 1 h at 4 °C, it was sonicated (6x 10 second pulse) on ice. Following centrifugation at 20000 g for 20 min, soluble fraction was applied to a pre-equilibrated 1 ml HiTrap column (GE Healthcare, Freiburg, Germany) and purified. Bound proteins were eluted by a linear gradient of imidazole (20-500 mM).

Purified protein was dialyzed (overnight at 4 °C) into storage buffer (1x PBS unless otherwise stated) and stored at 4 °C for up to 4 weeks or flash frozen and stored at -80 °C until further use.

Nanobodies

Nanobodies were expressed in *E.coli* JM109 strain suited for periplasmic expression due to internal disulphide. Both Nanobody constructs harbor a pelB leader sequence for periplasmic export and a C-terminal HisTag for purification. Modified Enhancer was expressed from pHEN6-cAbGFP4FTAThis6 vector, encoding GFP-binder preceded by TAT peptide (GRKKRRQRRRPQ).

GFP

His-tagged GFP (both single-anchored eGFPs and ybbR-tagged wtGFP) were expressed in *E.coli* BL21 (DE3).

ybbR-tagged GFP [Pippig et al., 2014] was purified using Tris buffer system (lysis in 50 mM Tris pH 7.5, 100 mM NaCl, 5 % glycerin, 15 mM imidazole and 10 mM β -mercaptoethanol) and dialyzed into storage buffer (30 mM Tris pH 7.5, 100 mM NaCl, 5 % glycerin, 2 mM DTT), then stored at -80 °C.

pGEX-2T-GFP-hAGT vector was used for expression of wtGFP with a C-terminal hAGT anchor. The expressed GFP was fused to a GST tag used for purification. The protein was purified in Tris/NaCl pH 8 using GST affinity column (GE Healthcare, Freiburg, Germany) according to the manufacturer's instructions. The GST tag was cleaved off during purification using thrombin. The protein was stored in 1x PBS at 4 °C.

Both wtGFP and eGFP with N- and C-terminal handles were expressed in *E.coli* BL21 (DE3) from pBAD-hAGT-TitGFP-hAGT-Strep vector, N-anchored wtGFP from pBAD-hAGT-TitGFP-Strep. In each case the resulting GFP was flanked by two stretches of four Ig domains each and featured an hAGT domain on respective termini, as well as a C-terminal StrepTag II. The cultures were induced with arabinose at a final concentration of 0.2 %, the protein was expressed overnight at 30 °C and then purified using StrepTrap HP (GE Healthcare, Freiburg, Germany), eluted in Tris/NaCl pH 8 and stored in 100 mM Tris 150 mM NaCl, 2 mM DTT, 5 % glycerin, 10 μ M ZnCl₂ pH 7.8 at -80 °C.

GFPs for MFB [Aschenbrenner et al., 2014] were expressed from pET28a vectors (EMD Group, Merck KGaA, Darmstadt, Germany) in *E.coli* BL21 DE3 CodonPlus cells (Agilent Technologies, Inc., Santa Clara, CA, USA). All three constructs (wt-GFP, eGFP and sfGFP) feature an N-terminal HisTag for purification followed by

the ybbR-tag (DSLEFIASKLA). After purification with HisTrap HP columns (GE Healthcare, Freiburg, Germany), the protein was stored in 30 mM Tris pH 7.5, 100 mM NaCl, 5 % Glycerin, 2 mM DTT at -80 °C.

MeCP2

GFP-tagged MeCP2 was provided by the Cardoso lab. The protein was expressed in Sf9 cells and purified using the GFP-Trap (Chromotek, Martinsried, Germany). It was eluted from the beads with 4 M MgCl₂. Next, buffer exchange against 1x PBS was performed using a 30 kDa Amicon filter (Merck Chemicals GmbH, Darmstadt, Germany). The protein was then stored in single-use aliquots at -80 °C.

2.4.2 Electrophoretic Mobility Shift Assay

Depending on the size of the analyzed molecules, Electrophoretic Mobility Shift Assay (EMSA) was performed either using polyacrylamide or agarose gels. Non-reducing-PAGE was performed to analyse covalent oligonucleotide-protein complexes and 1 % agarose gel to screen DNA-binding capacity of MeCP2.

2.5 Surface and cantilever chemistry

In house modified surfaces were prepared using 1 mm-thick glass slides. These were first sonicated in 50 % (v/v) 2-propanol in ddH₂O for 15 min and oxidized in a solution of 50 % (v/v) hydrogen peroxide (30 %) and sulfuric acid for 30 min. Following washing in ddH₂O and drying under nitrogen flow, desired modification was performed.

Evaporation of gold surfaces

A 250 Å layer of gold was deposited on clean glass slides precoated with chromium-nickel (25 Å) to promote hydrophobic gold adhesion to otherwise hydrophilic glass surface.

Preparation of amino- and epoxy-functionalized slides

Glass slides were silanized by soaking in a solution of 90 % (v/v) ethanol, 8 % ddH₂O and 2 % epoxysilane or its 3-aminopropyldimethyl derivative (ABCR, Germany) for 1 h. Subsequently they were washed twice in isopropanol and ddH₂O and dried at 80 °C for 40 min. At this stage the glass slides were stored under argon atmosphere for up to two months and further functionalization steps were performed directly before the measurement.

Alternatively, commercial amino- or epoxy-functionalized slides (Nexterion) were used.

Slide and cantilever functionalization for AFM

Maleimide-thiol chemistry: Maleimide-thiol chemistry was performed using amino-slides. The amino groups were deprotonated by incubation in sodium-borate buffer at pH 8.5 for 0.5 h at room temperature. Next, heterobifunctional PEG crosslinker with NHS and maleimide groups (MW 5000 Da, Rapp Polymere, Tübingen, Germany) was applied at 30 mM in sodium borate buffer at pH 8.5 for 1 h at room temperature. After washing in ddH₂O, the slides were dried and protein with a free, reduced thiol group was applied.

ybbR chemistry: anchoring of ybbR-tagged proteins was performed using amino-slides. Following deprotonation and pegylation as described above, the slides were washed with H₂O and incubated with 50 µl. After 1 h, 1 µl TCEP was applied for 5-10 min to destroy unreacted maleimide groups. The slides were then washed with H₂O and protein mix (40 µl of 2.5 µM ybbR-GFP in 1x PBS, 1 µl SFP and 4.6 µl SFP buffer) was applied. After 2 h of incubation at room temperature, the slides were washed in 1x PBS.

hAGT chemistry: hAGT anchoring was performed on epoxy-functionalized slides. Heterobifunctional PEG crosslinker with -NH₂ and -COOH functional groups (MW 5000 Da, Rapp Polymere, Tübingen, Germany) was applied at 50 mM in sodium-borate buffer at pH 8.5 and incubated overnight at room temperature. After rinsing with water, -COOH groups were activated with 100 mM EDC/NHS solution (in H₂O). Following 20 min incubation, the slides were rinsed with ddH₂O and 150 µl of 4 mM NH₂-PEG-BG (stored as 40 mM stock in DMF) in 100 mM EDC/NHS in borate buffer was applied for 3 h at room temperature. After rinsing with water, hAGT-tagged GFP was applied and incubated for 45 min.

Cantilever functionalization: Cantilevers were cleansed (activated) by exposition to UV radiation under ozone atmosphere for 10 min. Then they were silanized by immersing for 1 min in 3-aminopropyldimethylepoxysilane diluted 1:1 in ethanol with addition of 1 μ l of H₂O. Following washing in toluol and water, and drying, they were incubated at 80 °C for 30 min. Subsequently, either 1 mM streptavidin in 1x PBS was applied directly or pegylation followed by Nb application was performed as described for slide functionalization.

Preparation of flow cell for MT

Schematic of a flowcell for magnetic tweezers is presented in Fig. 2.1. Two rectangular coverslips are separated by a thin layer of parafilm, which also keeps them together and seals the edges of the cell. The top coverslip features two apertures - inlet and outlet. Inlet chamber is made of the wide part of pipet tip attached to the inlet and acts as a liquid reservoir. Tubing attached to the outlet is connected to a syringe operated by an automated motor.

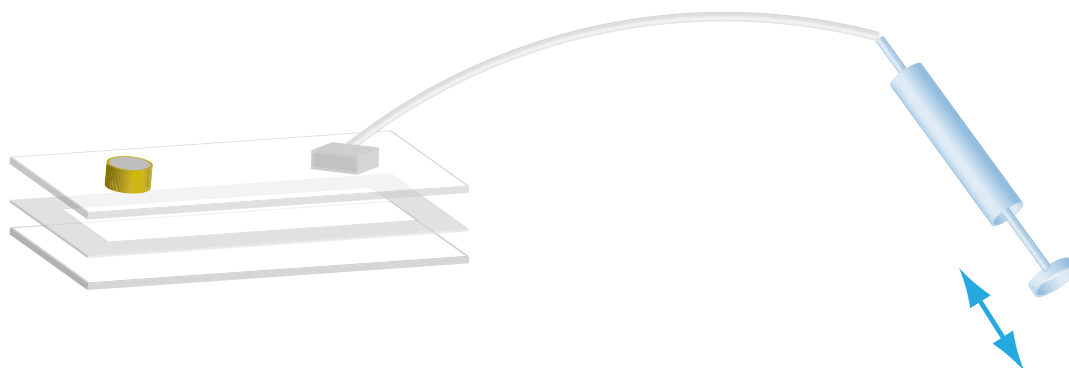


Figure 2.1: Schematic of a flowcell for magnetic tweezers experiment. Parafilm between the upper and the lower surface of the cell (rectangular coverslips) acts both as an adhesive and a spacer. Flow of liquid from the reservoir (yellow) towards the outlet is regulated by an engine-operated syringe.

2.6 Biophysical methods

Atomic Force Microscopy

Single-molecule force spectroscopy experiments were performed using commercial MFP-3D AFM (Asylum Research) and a custom built instrument with an MFP-3D controller. Two types of cantilevers were used: MLCT (cantilever C) by Bruker and Biolever mini (BL-AC40TS-C2) by Olympus. Cantilever and slide were modified each with one of the interaction partners to be investigated. For each measurement cantilever spring constants were calibrated in solution using the equipartition theorem [Butt and Jaschke, 1995]. The bond strengths were tested in series of measurements at various pulling speeds ranging from 300 nm/s to 10000 nm/s. A single measurement cycle consisted of approach, short (< 1 s) dwell at the surface and retraction of the cantilever with constant velocity. An exemplary force-distance curve resulting from a single probing cycle is shown in Fig. 2.2.

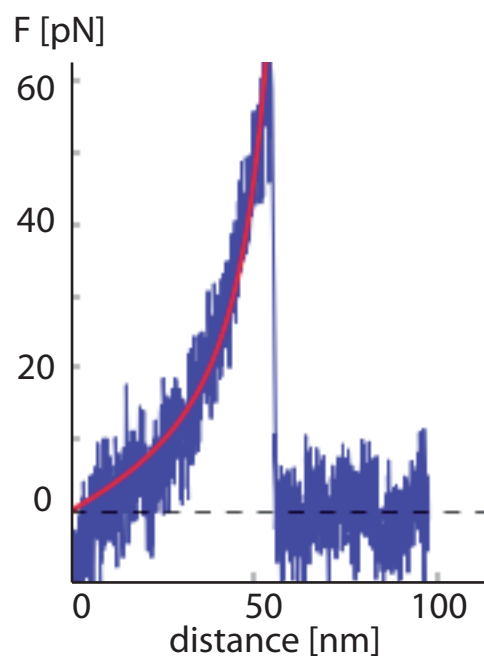


Figure 2.2: A typical force-distance curve resulting from single-molecule probing with AFM. Blue trace - experimental data, red curve - fitted WLC model.

Molecular Force Assay

MFA measurements were performed using a custom-built set-up based on an inverted epifluorescence microscope with piezo-actuated head moving the PDMS stamp against the probed surface. Each Molecular Force Balance (MFB) consisted of a Nb-GFP pair and a DNA oligonucleotide duplex (oligos for MFA were purchased at Biomers.net, Ulm, Germany). To ensure attachment of complete duplexes, CoA-labeled strand was premixed with a 2-fold excess of a biotinylated strand. The Nbs were immobilized on the glass surface via a polymer linker and then GFP-DNA complexes were bound to them. A complementary DNA strand was attached to the PDMS stamp. The stamp format (4x4 patches) allows for analysis of 16 different MFBs in a single experiment. As in the standard MFA, DNA oligonucleotides carried Cy3 and Cy5 labels allowing fluorescence readout. The fluorescence of GFP was not essential for the evaluation of the outcome but provided a convenient online control of sample quality. Indeed, GFP fluorescence signal colocalized with that of Cy3 and Cy5, confirming the specific interaction and correct assembly of protein force balances.

In each experiment fluorescent scans in both red and FRET channel were performed prior to, as well as right after stamping. In between, the stamp was moved towards the surface and kept there for 10 min to allow for correct MFBs assembly by biotin-streptavidin coupling. A piezo actuator controlled stamp retraction at a constant speed of 1 $\mu\text{m/s}$ (corresponding to a loading rate in a range of 10^5 pN/s) resulted in force build-up along each MFB and subsequent failure, statistically of the weaker of the two bonds. The outcome of the experiment was determined based on the ratio of the fluorophores remaining at the surface. The "red" ratio informed of the remaining intact bonds as compared to the initial number of bonds while the FRET ratio referred to the complexes which were not probed and thus allowed the correction for false positive signal. Since all the pictures are affected by the gaussian shape of the illuminating beam, pixel-by-pixel analysis was applied as it has proven to effectively cancel out the resulting inhomogeneities.

Magnetic tweezers

Magnetic tweezers experiments were performed using two different custom-built set-ups, both based on permanent magnets. Single-bead set-up allowed for tracking of one tether molecule along with one reference bead. On the other hand, multiple-bead set-up offered the possibility of subsequent tracking of many beads (both tethered

and reference ones). The actual number of tracked tethers in one experiment was limited by their availability in the field of view. Usually 5 to 9 tethers were analyzed, and only the ones behaving correctly throughout the whole measurement process were included in the final calculations.

The pattern of diffraction rings depends on the distance of the bead to the focal plane. Before the actual measurement, a z-Look-Up-Table was created to enable tether length determination based on the image of the bead. For this purpose, the objective was moved stepwise in the z-direction and a picture was taken at every 100 nm step. By interpolation, the position can be estimated with about 10 nm accuracy using this method [Gosse and Croquette, 2002].

In a typical experiment, streptavidin-coated superparamagnetic Dynabeads M-270 ($\varphi = 2.8 \mu\text{m}$) (Thermo Fischer Scientific, Braunschweig, Germany) were used to create tethers and $1.0 \mu\text{m}$ polystyrene beads (Polysciences Europe GmbH, Eppelheim, Germany) as reference beads, unspecifically stuck to the bottom of the flowcell. The flowcell was mounted on an oil immersion objective and could be manipulated by two motorized stages: a linear one and a rotary one allowed for the automated movement of the magnets resulting in manipulation with the beads. The objective mounted on a piezo stage was moved in the z direction against the flowcell. The beads were introduced to the flowcell once it was mounted on the instrument so that the tethers could be controlled throughout the preparation phase. The measurement consisted of two parts: first bare tethers were scanned at different forces, then protein was added and after a short (a few min) equilibration time, the actual measurement according to the same force pattern was performed.

Chapter 3

Results

This chapter presents the results of single-molecule screening of protein-ligand, protein-DNA and protein-protein interactions. First, force measurements of the streptavidin-biotin complex were performed using AFM to test single-molecule accessibility and at the same time provide quantitative data on the strength of the complex under external load. Next, this and several other techniques were used to tackle the challenge of single-molecule accessibility and to complement each other in explaining biomolecular interactions.

3.1 Single-molecule force measurements of streptavidin-biotin complex

The streptavidin-biotin complex was subjected to single-molecule force measurements using Atomic Force Microscope (AFM). Experimental design assumed incorporation of a 1.1-kilobase-long DNA linker between the gold surface and the biotin molecule, as presented in Fig. 3.1, providing a B-S transition fingerprint upon stretching under load. This way force-extension curves displaying only single interactions could be extracted for further analysis. All measurements were carried out in 1x PBS.

3.1.1 DNA construct preparation

1.1 kb dsDNA fragment was produced by PCR with primers introducing two terminal modifications: a thiol group at one terminus and biotin at the other one. The thiolated end facilitated covalent attachment of the molecule to the gold surface.

3.1.2 Streptavidin-biotin force spectroscopy using AFM

Within a single cycle, the cantilever functionalized with covalently immobilized streptavidin was brought in contact with the surface allowing surface-bound biotinylated DNA to bind to the SA. The cantilever was then retracted causing the DNA tether to overstretch and finally rupture. Biotin-streptavidin bond was considered the weakest link here (apart from the long DNA duplex held together by multiple non-covalent bonds, it was the only non-covalent one) and so statistically should break first.

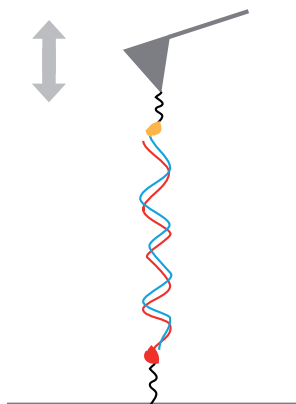


Figure 3.1: Streptavidin-biotin rupture force determination - experimental design. A 1.1-kb-long dsDNA fragment is stretched between an SA-functionalized cantilever and surface. B-S transition of DNA observed upon external load provides a fingerprint thus allowing the selection of single-molecule events.

The analysis comprised 542 curves collected at pulling velocity of 2 $\mu\text{m/s}$, out of which 102 were qualified based on full single B-S transition trace. Force-distance plot representing the selected events is shown in Fig. 3.2 along with a histogram of measured rupture forces. Fitting a Gaussian to the force distribution resulted in

the most probable rupture force of 165.6 ± 3.1 pN. The force distribution also shows a shoulder at larger values.

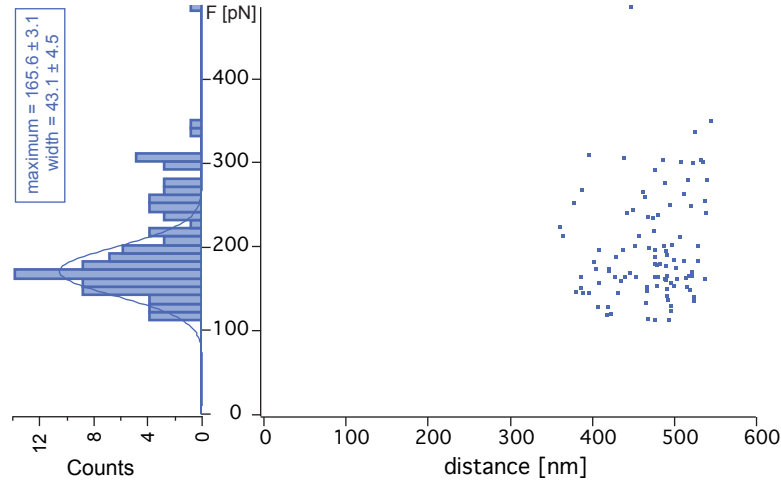


Figure 3.2: Determination of rupture force of the streptavidin-biotin complex: force-distance plot for the selected curves. Gaussian fit to the histogram of measured forces provides the most probable rupture force.

3.2 Analysis of DNA cross-linking by MeCP2

Owing to the wide attention MeCP2 has experienced in the past years, its structural composition and biochemistry have been well described, yet the mechanism of its binding to DNA still lacks a detailed understanding. Here, the MeCP2-DNA complex was investigated using single-molecule techniques: Atomic Force Microscopy and Magnetic Tweezers. In both cases the behavior of a specifically designed single DNA molecule during stretching in absence or presence of MeCP2 is analyzed, focusing on intramolecular versus intermolecular DNA cross-linking upon protein binding.

Loops created upon MeCP2 cross-linking of DNA have been observed by AFM imaging [Ghosh et al., 2010a]. There, nodes harboring both single as well as multiple protein moieties were identified.

3.2.1 AFM measurements

The following section describes experiments performed in part together with another PhD student, Philip Severin.

We performed AFM measurements using a similar setup as described in section 3.1. Initially, two types of DNA constructs were investigated: a non-methylated one - described above - and a fully methylated one.

Preparation of fully methylated DNA

Fully methylated DNA was prepared by PCR using 5mC instead of standard cytosine in the nucleotide mix. This way all 35 CpGs of the 1.1-kb-long fragment were methylated. The same primers with terminal modifications were used as for the non-methylated product.

MeCP2 binding to DNA - EMSA test

The ability of MeCP2 to recognise its DNA target was checked by an EMSA test. A 2-fold dilution series of the stock protein (stock concentration 2.3 μ M) was mixed with fully methylated DNA and after 5-10 minutes of incubation subjected to electrophoresis using a 1 % agarose gel, presented in Fig. 3.3. Band shifts can be

observed for the first two dilutions of MeCP2. In all lanes a secondary band can be seen, representing DNA dimers due to terminal thiols forming disulphide bonds.

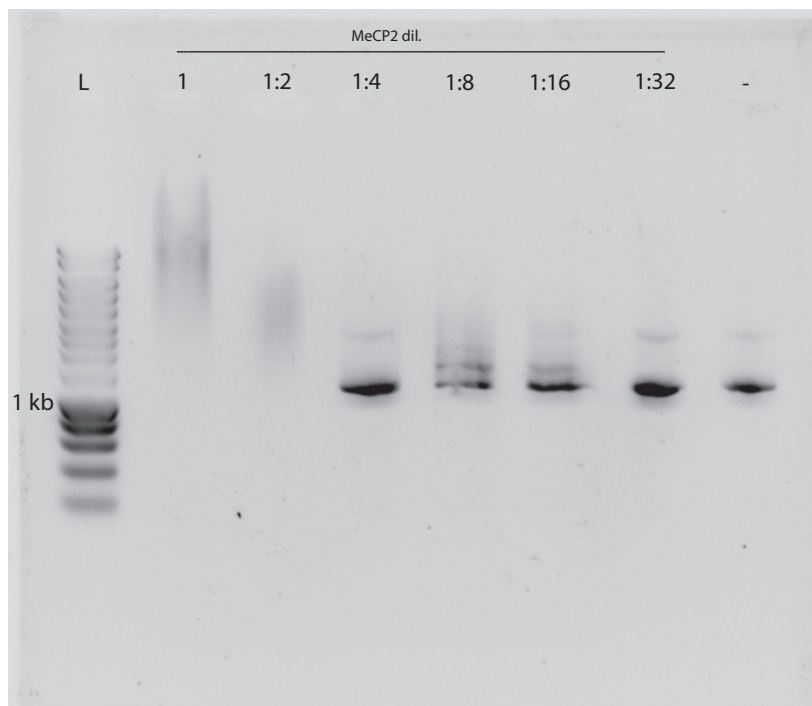


Figure 3.3: Electromobility Shift Assay of MeCP2-bound DNA. MeCP2 bands appear upshifted in the second and third lane. Secondary band at around 2.2 kb can be observed in the other lanes due to DNA dimerising via thiolated ends.

Overstretching non-methylated and fully methylated DNA

First, the surface was probed with a cantilever functionalized with covalently immobilized SA to ensure decent picking efficiency, that is around 10 % of curves representing a single DNA tether. It is important to mention that a full B-S transition curve can only be recorded for a nick-free dsDNA, i.e. one featuring a continuous sugar-phosphate backbone. As nicks occur spontaneously due to mechanical shearing during preparation and handling of the DNA as well as when it is dried on the surface, some curves display only part of the expected pattern, with the rupture happening already in the plateau region. Yet the proportion of full B-S curves was a deciding factor in determining whether to proceed further with the sample. Apart

from providing sample quality information, the measurement prior to addition of the protein constituted also a control for comparison with the effects caused by its presence.

Effect of MeCP2 and MBD on the behavior of probed DNA

For sample quality determination, the surface was first probed a few dozen times prior to addition of the protein and if a sufficient frequency of B-S transition fingerprint (see Fig. 3.4) in the recorded curves was observed, the experiment proceeded to the next step - involving protein. Typically 40 μ l of freshly thawed MeCP2 was added to the approximate volume of 1 ml buffer on the surface and mixed by gently pipetting. Due to evaporation issues, during longer measurements supplementation of buffer was necessary. The sample was left to equilibrate for 20 minutes before force spectroscopy was performed. In all experiments with fully methylated DNA, after addition of MeCP2 no more B-S transition curves were observed. Instead, a hump-shaped peak of up to a few hundred pN appeared right at the beginning of the force-distance curve when retracting the cantilever from the surface. To get a deeper insight into the origin of the "hump", the automated cycling of the cantilever was replaced by a hand-controlled procedure using the "Hamster" knob of the MFP-3D controller. This allowed for a more gentle probing as the cantilever was retracted once it touched the surface, without indenting it further. The resulting force-distance profiles display a behavior not observed previously: the force first built up to over 100 pN to then drop stepwise as the cantilever was retracted further away. The pattern of regular steps of about 28 pN each is presented in Fig. 3.5. This phenomenon occurred a few times more in the analyzed set of a few hundred curves.

Interestingly, addition of MBD (in case of either DNA type) instead of MeCP2 did not affect the shape of the force curves and full B-S transition patterns were recorded also in its presence. Neither did non-methylated DNA show any change in behavior upon addition of the full-length MeCP2.

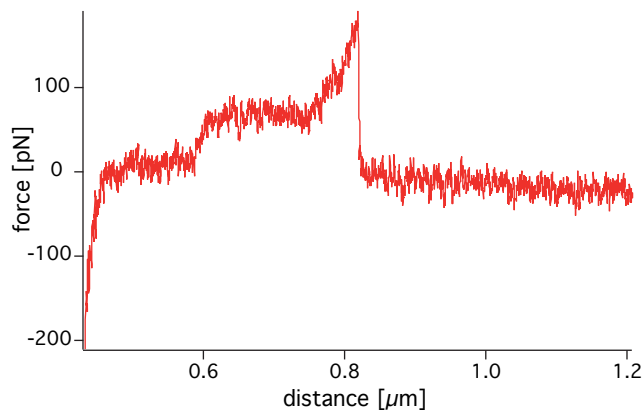


Figure 3.4: An exemplary force-distance curve obtained during overstretching the DNA in absence of MeCP2 displays the well-known B-S transition pattern.

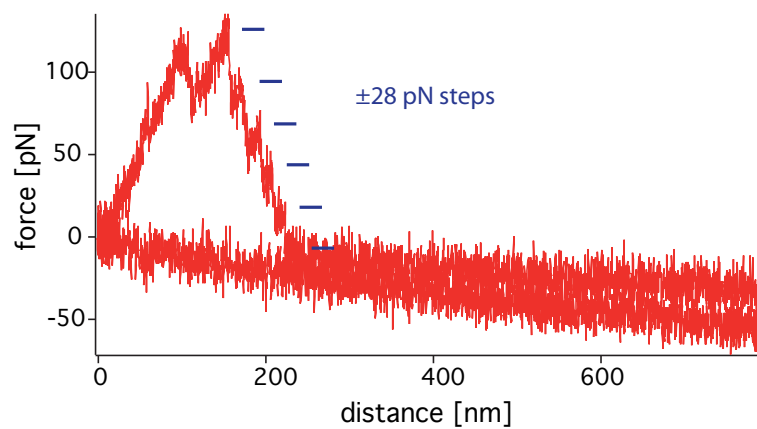


Figure 3.5: Force-distance curve obtained for stretching DNA in presence of MeCP2 shows a pattern of regular steps of about 28 pN each.

2-site methylated DNA

The intriguing pattern of steps inspired further AFM experiments with DNA constructs designed so as to facilitate formation of a loop of a strictly defined size. To realize this, the 1.1 kb DNA fragment was *in vitro* methylated using M.HhaI methyltransferase, recognizing 5'-GCGC-3' palindromic sequence and adding a methyl group to the internal cytosine. The DNA fragment used harbors two recognition sites for this enzyme, separated by 309 bp which corresponds to double the persistence length of dsDNA and, hence, was considered optimal for efficient MeCP2-stabilized loop formation. Stretching such dsDNA was expected to yield a B-S transition trace of a molecule with contour length shorter by the loop size - up to the force high enough to open up the loop, at which the tether should regain its initial contour length.

However, also for 2-site methylated DNA only the hump pattern was observed in presence of the protein. Despite numerous attempts, it was not possible to achieve single-molecule resolution with AFM. Apparently, surface density of DNA required to ensure sufficient picking efficiency disturbed single-molecule events by causing intermolecular cross-links (see Fig. 3.6). Therefore we decided to proceed with an alternative single-molecule technique, offering better possibilities in this respect.

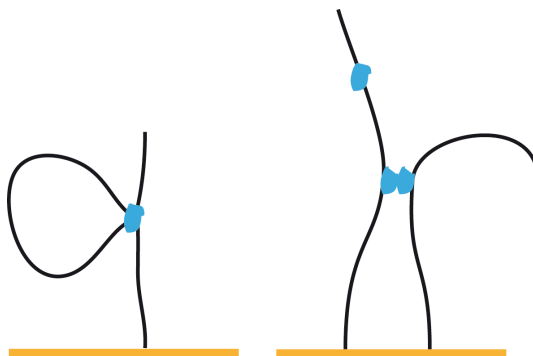


Figure 3.6: Intra- vs. intermolecular cross-linking of DNA by MeCP2 cannot be resolved using AFM due to too high surface density of molecules.

3.2.2 Magnetic Tweezers experiments

The following section presents experiments performed together with a master student, Philipp Walker.

After the promising initial results, we looked for complementary techniques which could help overcome the limitations intrinsic to the AFM. Magnetic tweezers (MT) seemed to be a perfect approach, offering control over single DNA tethers.

MT DNA constructs preparation

Several custom-designed DNA constructs were prepared, all utilizing the same principle of ligating three fragments: an insert and two "handles" responsible for anchoring the molecule to the bead and the surface. The handles were universal for all constructs. Both were produced by PCR: the biotin-labeled one was 314 bp long and the digoxigenin-labeled one 400 bp. Modified dUTP was added to the PCR mixture to compete with standard thymidine during strand elongation, resulting in the handles containing on average about 20 labels each. Prior to ligation, each handle was digested with the respective restriction endonuclease creating single-stranded overhangs complementary to those of the digested insert DNA. Figure 3.7 presents a schematic sketch of produced DNA constructs.

Design of MT DNA inserts

The purpose of using magnetic tweezers was to complement the AFM findings regarding MeCP2-DNA binding mechanisms. Therefore, the previously used T4-1.1 kb-fragment DNA construct was adjusted to match the MT requirements. As such, the molecule would be too short to be well resolved with the MT. Therefore, it had to be incorporated in a longer DNA. Commercially available pCpGfree-LacZ plasmid, carrying the CpG allele of the lacZ gene, was chosen as the framework DNA as this way no further CpG sites were introduced, which could interfere with the expected pattern of specific MeCP2 binding. The newly cloned plasmid contained XhoI and two EcoRI restriction sites and linearization with these endonucleases resulted in a 5 kb fragment. All pCpGfree-lacZ constructs were transformed into *E.coli* GT115 cells.

Two constructs suited for MT measurements were obtained. The initial cloning of the 1.1 kb fragment into CpG free plasmid yielded a 5 kb DNA tether with 300 bp

loop. The loop was then extended to 600 bp in the second construct by introducing two point mutations - one removing one of the methylation sites and the other creating it 300 bp upstream. Doubling the distance between the methylated sites was supposed to provide more flexibility in the loop formation and thus loosen it. The second construct was also optimized for the process of MT DNA preparation - the additional EcoRI restriction site was removed, which saved up an additional gel purification step. In this case the resulting tether was 6 kb long.

***In vitro* DNA Methylation**

Methylation of DNA designed to form a loop was achieved enzymatically. M.HhaI methyltransferase recognizing the 5'-GCGC-3' was used to prepare the 2-site methylated DNA. For a single-molecule experiment, during which only a few molecules are screened, highest efficiency of the reaction is crucial. The extent of *in vitro* methylation was therefore verified by subsequent digestion with HhaI restriction endonuclease discriminating between methylated and thus protected GCGC sequences and unmethylated ones, which were cut. Only fully methylated constructs remained full-length and formed complete tethers in the flowcell.

The construct with fully methylated T4 1.1 kb insert for assay test was obtained by methylating the DNA with M.SssI methyltransferase, recognising the 5'-CG-3' dinucleotide. Here the objective was to get a few sites within a DNA molecule methylated among the 35 available CpGs and the efficiency of the reaction was not tested.

3.2.3 Loop detection using type II restriction endonuclease - assay test.

In order to test the feasibility of loop detection by the assay, we employed a type II restriction endonuclease EcoRII (Thermo Fischer Scientific, Braunschweig, Germany), which binds a dsDNA molecule interacting with two or three recognition sites. Under optimal conditions, one of the sites is cut, while the others act as allosteric activators. Since the objective here was to observe the shortening of DNA tether upon multiple sites binding by one enzyme moiety, the endonuclease activity was blocked by not providing essential magnesium ions and addition of EDTA. This way, upon binding, the enzyme should remain fixed to the DNA. All measurements were

performed using standard reaction buffer recommended by the manufacturer but devoid of Mg^{2+} and supplemented by EDTA. The measurements were conducted at room temperature.

The procedure was similar as in the case of MeCP2 experiments. M270 beads were used and four DNA tethers were analyzed, as shown in Fig. 3.8 a). First the tethers were stretched in absence of EcoRII to make sure no shortening occurs. Following addition of the enzyme, the system was screened at four different force values (2 pN, 4 pN, 10 pN and 16 pN) applied in separate force cycles. A single cycle consisted of eight repetitions of the following protocol: equilibration at low force (0.16 pN) for 90 seconds followed by stretching the tethers at a given force for 300 seconds and then rupturing all the remaining loops at high force (25 pN) for 15 seconds. The force of 25 pN proved to be high enough to restore the initial contour length of the tethers. Eight cycles of blank measurement yielded a single tether length change, whereas for measurements involving the enzyme 63 length changes were recorded for the 2 pN force trace and 30 for the 4 pN one. At 10 pN only one length change was observed and no changes occurred at 16 pN.

Finally, after buffer exchange against EcoRII-optimal one, all tethers were lost during a 300 s incubation at 0.16 pN, indicating successful cleavage of the DNA (Fig. 3.8 b) - before and c) - after cleavage).

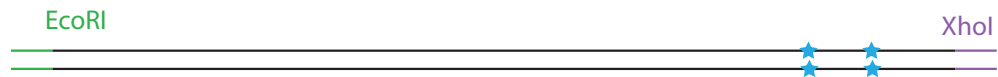
1136 bp T4 DNA fragment for AFM
C* (GCGC): 797 & 1106; (CCGG): 564, 818 & 1077



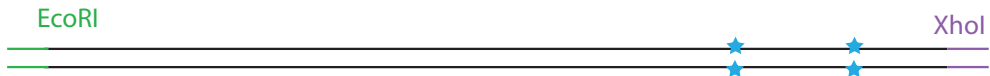
1136 bp T4 DNA fragment for AFM
fully methylated



300 bp loop DNA for magnetic tweezers
5 kb long, C* (GCGC): 3902 & 4211



600 bp loop DNA for magnetic tweezers
5 kb long, C* (GCGC): 3587 & 4211



600 bp loop DNA for magnetic tweezers
6 kb long, C* (GCGC): 3554 & 4145



1 kb insert DNA for magnetic tweezers
5 kb long, incl. 1 kb methylated fragment



Figure 3.7: DNA constructs used to investigate MeCP2-induced DNA cross-linking. Stars indicate methylated CpG sites recognized by MeCP2.

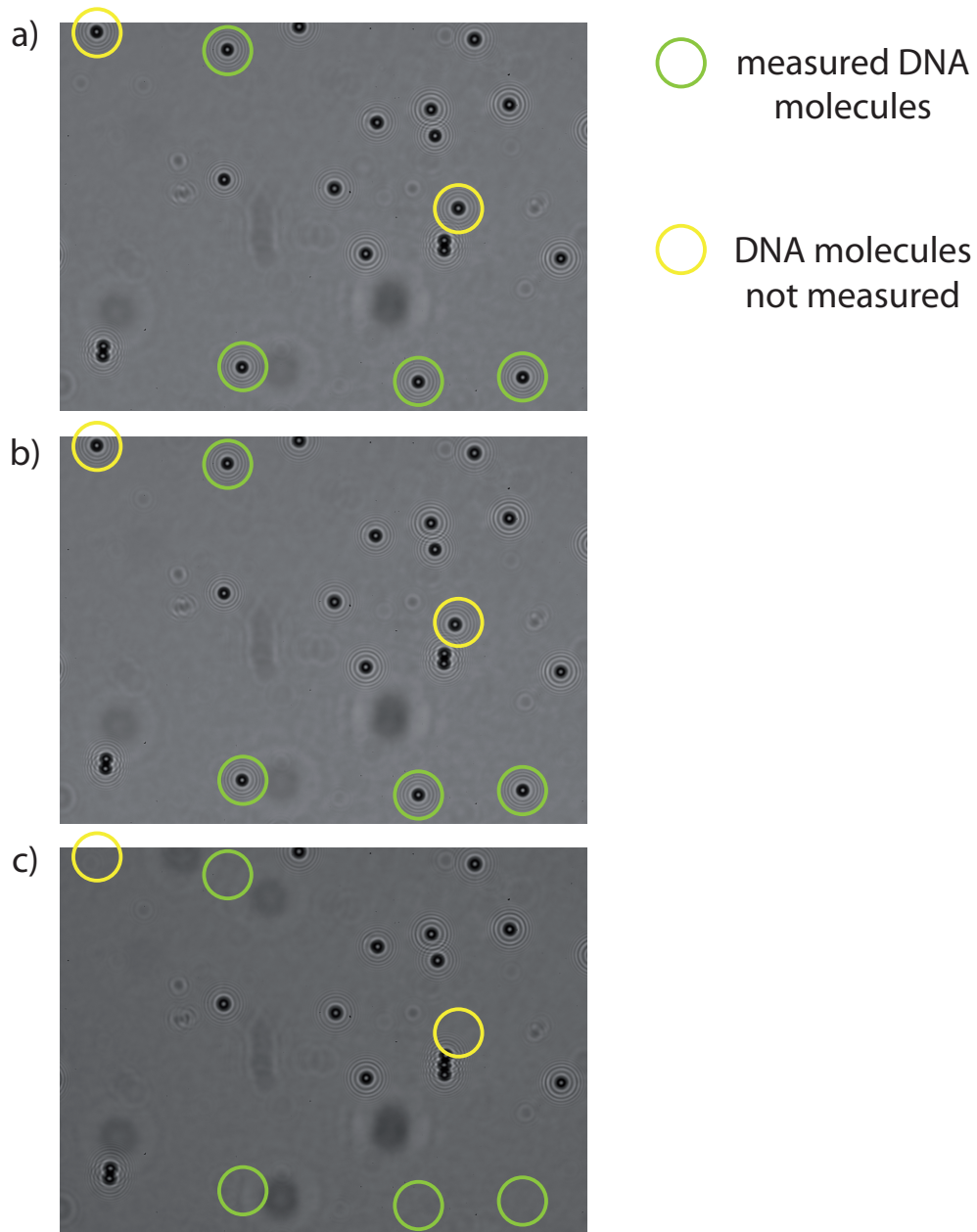


Figure 3.8: Loop detection assay test - field of view of the magnetic tweezers. Circular markers show locations of beads representing single, measurable tethers (in green) as well as a double tether and a tether appearing too close to the edge of the field of view, both of which could not be measured (yellow). The same field of view is pictured at 10 pN stretching force without Mg^{2+} (a), with Mg^{2+} - right after buffer exchange (b), and after 300 seconds incubation (c) - when all tracked beads are gone. (Fig.: P. Walker)

3.2.4 DNA looping upon MeCP2 binding

300 bp loop

The ability of MeCP2 to stabilize DNA loops was first investigated using the 300 bp loop DNA construct. The defined positions of methylated sites recognized by the protein determined the predicted size of the loop. We expected to observe MeCP2-stabilized loop formation manifested by the shortening of the tether contour length by the length of the loop. Conversely, opening up an existing loop would result in tether elongation. The change of contour length is force-dependent and for the 300 bp loop size, based on the WLC model equals respectively 89 nm for 1 pN, 94 nm for 2 pN, 98 nm for 5 pN and 101 nm for 9 pN.

Nine tethers from nine independent experiments using the single-bead setup were measured, first without and then with MeCP2. Blank measurements (in absence of the protein) constituted a reference and were performed according to the same protocol as the ones with MeCP2. All these experiments were performed in 1x PBS buffer to provide comparable conditions to those from the AFM measurements. The force was applied in several series, starting at 0.1 pN, to 1 pN, to 2 pN, to 5 pN and finally 9 pN, after which the cycle was repeated. Fig. 3.9 presents an exemplary fraction of the force protocol applied for loop detection. A total of several hundred cycles were applied in each experiment. During the low force step (0.1 pN) the DNA was rather relaxed, yet the tethered bead was prevented from getting irreversibly stuck to the surface. For the same reason, during the addition of MeCP2 the tethers were stretched at 10 pN to compensate for the shear flow of the liquid inside the flow cell. The algorithm of loop searching assumed comparison of the z positions of a given bead at a given force in two consecutive force cycles. This way the influence of long term drift was minimized. Negative values represent tether shortening and positive ones - elongation. Fig. 3.10 illustrates tether length changes between each two consecutive force plateaus. For the evaluation, for each force value, data from all nine experiments were pooled together and plotted as a histogram of z position changes. Ideally, there should be almost no changes for the blank measurements and in the presence of MeCP2 (loop forming) two peaks: one at the negative and one at the positive value of the expected contour length change were expected.

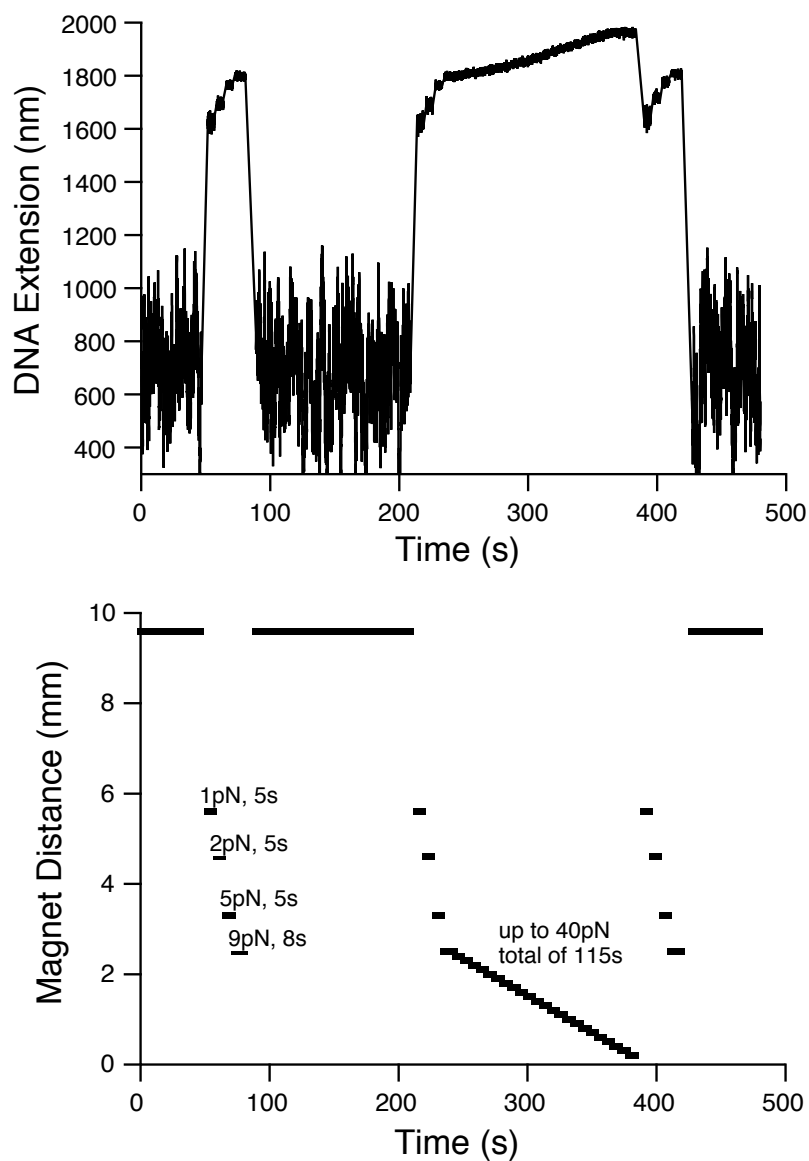


Figure 3.9: Loop detection. Top: tether length changes during force protocol application. Stretching the tether results in a remarkable decrease of the noise. Bottom: force protocol resulting in the force trace presented above. Force values are determined by the distance between the flow cell and the magnets. (Fig.: P. Walker)

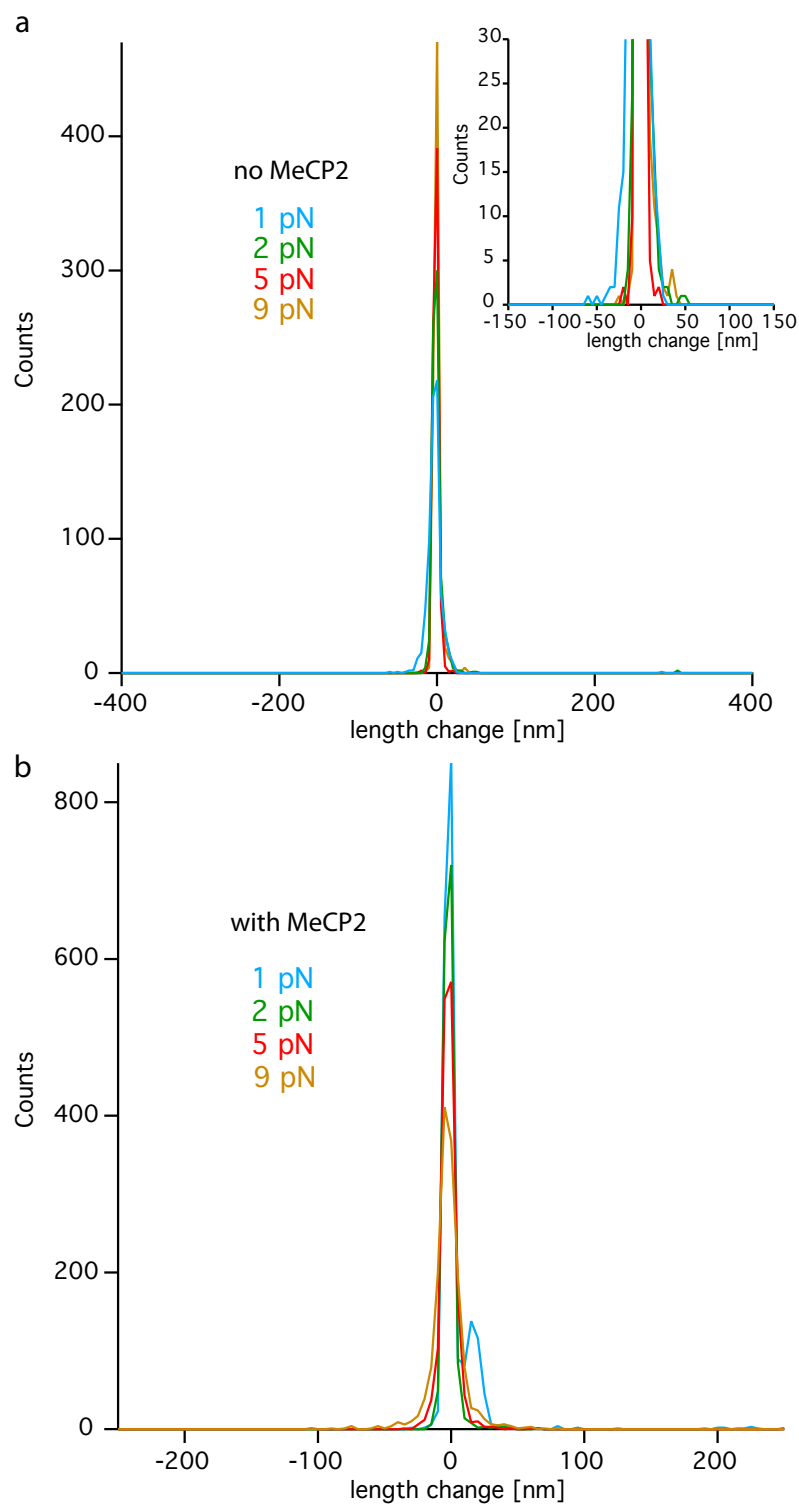


Figure 3.10: 300 bp loop DNA: contour length analysis of 9 tethers at various pulling forces, over all force cycles; top: no MeCP2, inset shows zoomed-in peak, bottom: with MeCP2. Histograms show tether length changes between two consecutive force plateaus. Top: blank measurement, bottom: measurement with MeCP2.

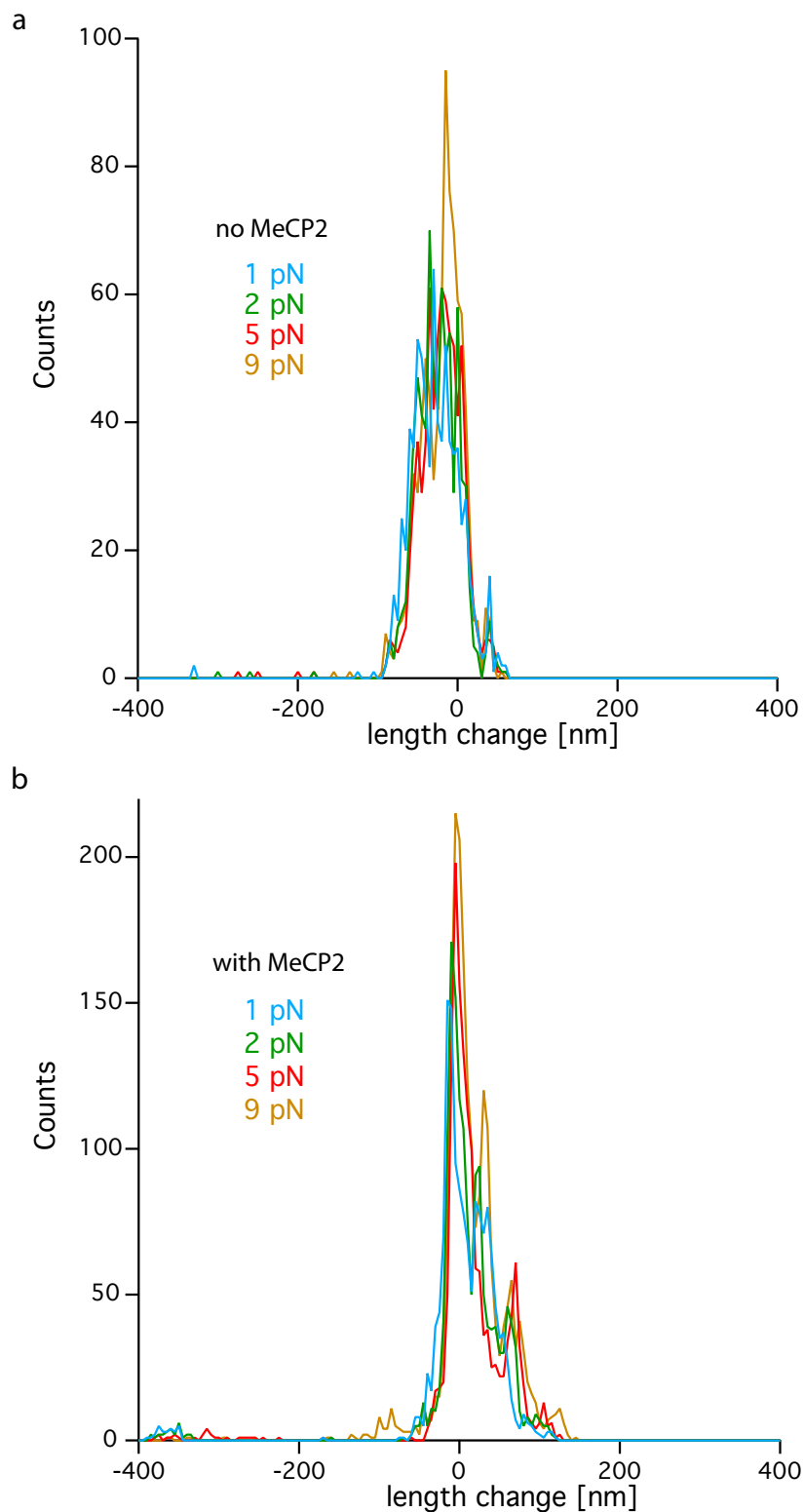


Figure 3.11: 300 bp loop DNA: contour length analysis of 9 tethers at various pulling forces, over all force cycles. Histograms of tether length changes for each plateau as compared to the first plateau at a given force regime. Top: blank measurement, bottom: measurement with MeCP2.

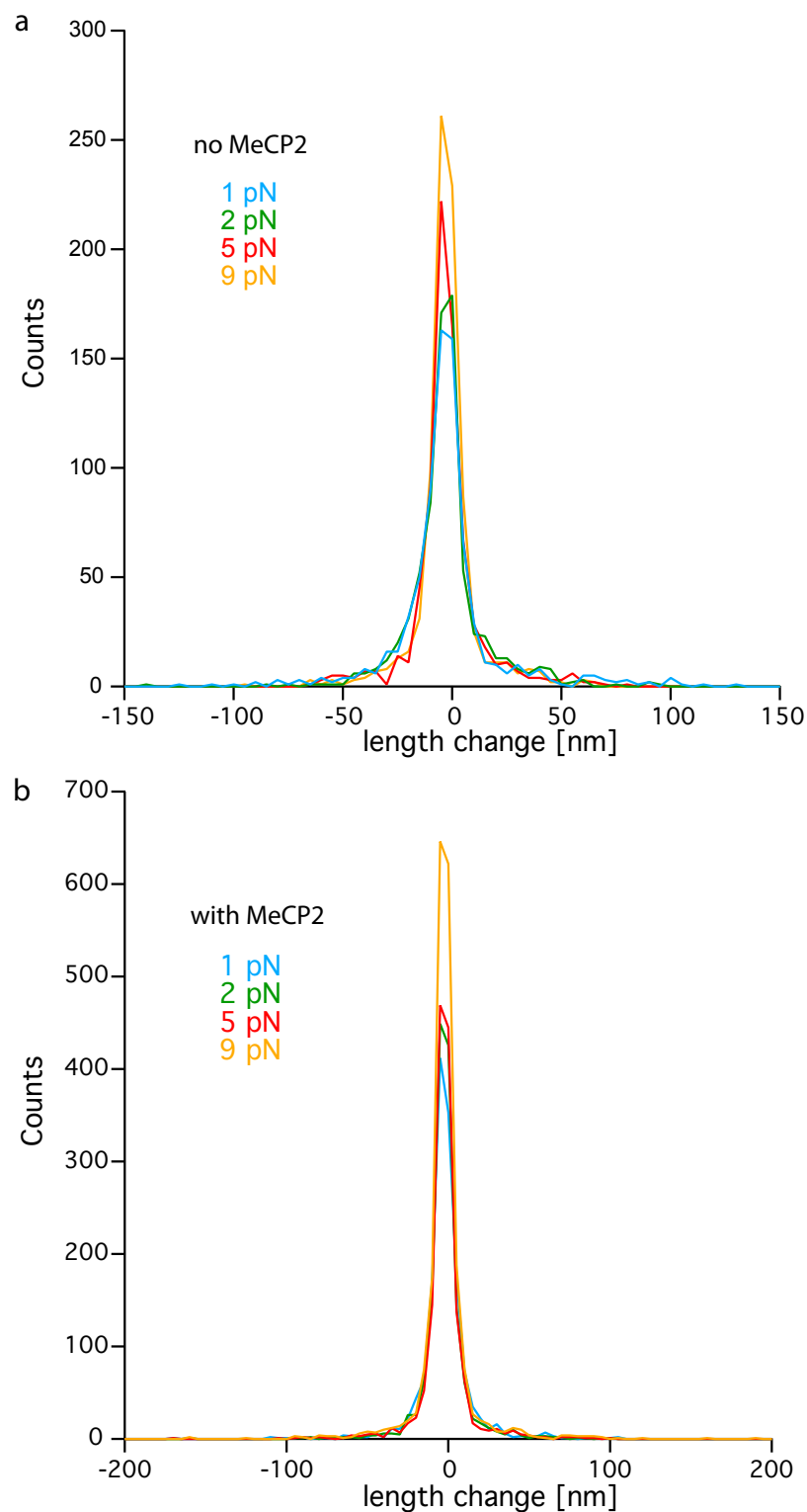


Figure 3.12: 300 bp loop DNA: contour length analysis of 9 tethers at various pulling forces, over all force cycles; top: blank measurement, bottom: with MeCP2. Tether length stability within each plateau for each force regime. Histograms show differences between the mean of the first 60 points and the mean of the last 60 points within each plateau.

For all blank measurements, the great majority of contour length changes fell into the ± 20 nm regime. There was a negligible number of changes recorded around the values expected for the specific loop. Fig. 3.11 presents the relation of each plateau at a given force to the first plateau at that force in the measurement. The shift of the centre of the distribution reflects the observed longterm drift of the setup. On the other hand, stability of the measurements within a single plateau is confirmed by the last histogram in the series (Fig. 3.12), in which the difference between the mean of the last and the first 60 points of each plateau is plotted.

Measurements in presence of MeCP2 did not show the expected pattern of the histograms. Sparse events at the expected distance from zero did not constitute evidence for loop detection in either of the applied force regimes. The same holds true for the comparison of the z position of all plateaus to the first plateau in the measurement. Similarly as in blank measurements, due to the system drift the centre of the contour length change distribution was shifted in all histograms (Fig. 3.11), while within plateaus no significant change could be observed (Fig. 3.12).

600 bp loop

To check if a more flexible loop would be more likely to form or more easily resolved by the assay, measurements with DNA carrying two methylated sites separated by 600 bp were performed at two different force steps. Here buffer conditions described in [Ghosh et al., 2010a] were used, i.e. Tris at pH 7.5, 200 mM NaCl, 0.5 mM EDTA. The expected contour length changes upon loop formation were again calculated based on the WLC model and yielded: 180 nm for 2 pN and 193 nm for 9 pN.

The experiment was performed using the Multibead setup with M270 beads and three tethers from a single measurement qualified for the analysis. For the contour length changes a similar protocol as above was applied, only two force steps (2 pN and 9 pN) were implemented. The resulting histograms of observed contour length changes are presented in Fig. 3.13. In both cases almost no events could be found in the range of interest. The histograms for measurements at 9 pN look a lot "cleaner" than those for 2 pN, in which a lot of drift could be observed resulting in a shoulder of the central peak towards positive values (reaching almost 200 pN). Interestingly, that shoulder is more pronounced in the blank measurement than in any of the measurements with MeCP2 present. In either case it is not accompanied by a peak on the negative half-axis. All histograms for the 9 pN step are centered close to zero and events of lengthening or shortening are sparse, if any.

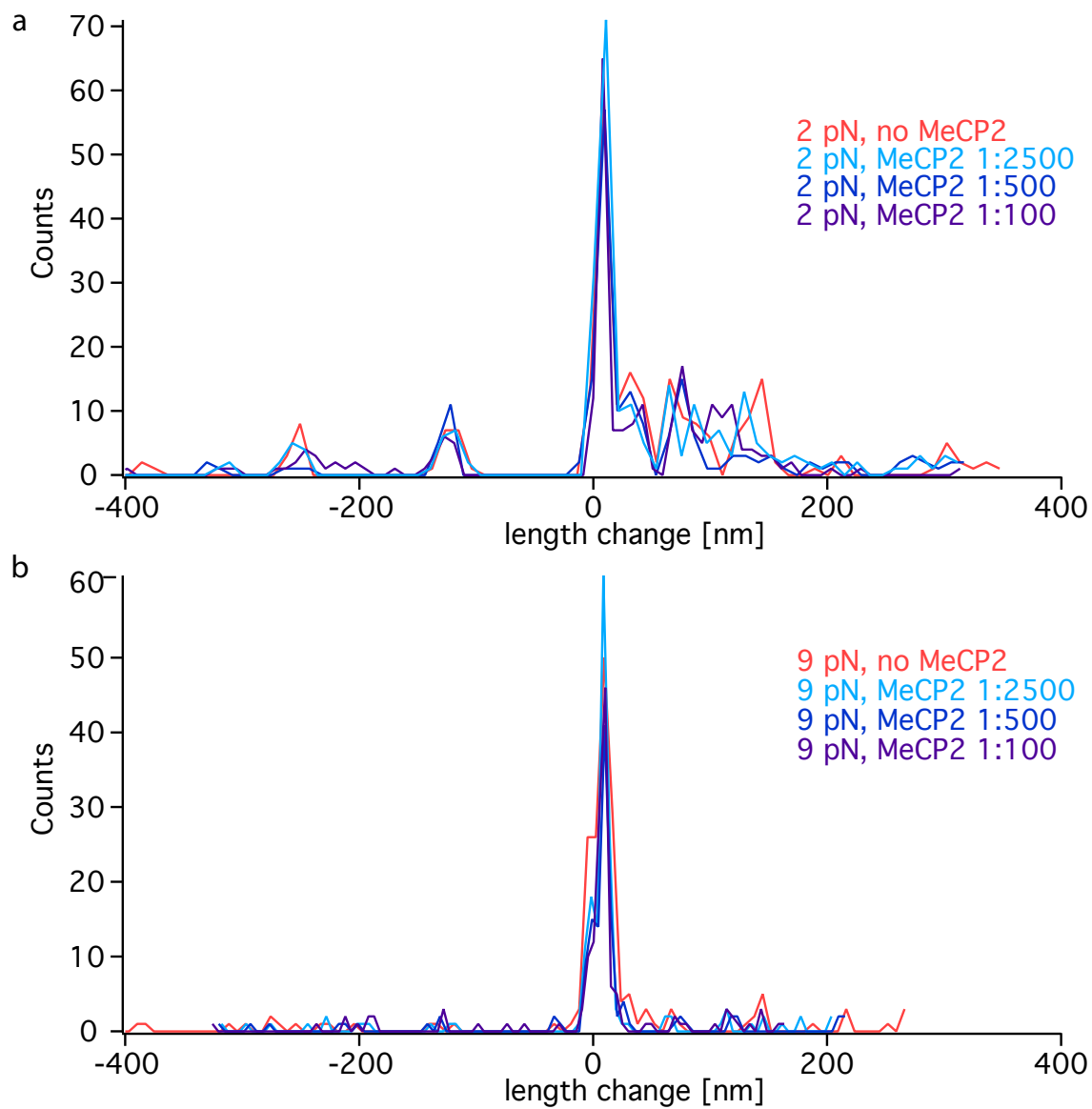


Figure 3.13: 600 bp loop DNA contour length analysis at 2 pN (a) and 9 pN (b) with MeCP2 at various stock dilutions.

600 bp loop DNA in high salt buffer

Next, to increase the specificity of MeCP2 recognition of its target sequence, NaCl concentration in the assay buffer (1x PBS) was increased to 300 mM. The persistence length of dsDNA remains comparable to that in pure 1x PBS so expected values of tether shortening did not change.

This time the blank measurement comprised 3 tethers from three separate flow cells and three additional tethers were analyzed in presence of MeCP2 resulting in six tethers contributing to the histograms of MeCP2 measurements. Fig. 3.14 presents tether length changes between two consecutive force plateaus, Fig. 3.15 - tether length stability over the whole duration of the measurement and Fig. 3.16 shows tether length stability within plateau. No contour length changes in the expected range can be found either in the blank measurements or in the measurements in presence of the protein indicating that no MeCP2-stabilized loops could be observed. Unexpected peaks appear in blank measurement histograms of long range drift: at around 100 nm in the 1 pN trace and around 80 nm in the 2 pN trace, while the other two traces look normal (Fig. 3.15 (a)). The satellite peaks result most probably from a dust particle disturbing part of the readouts.

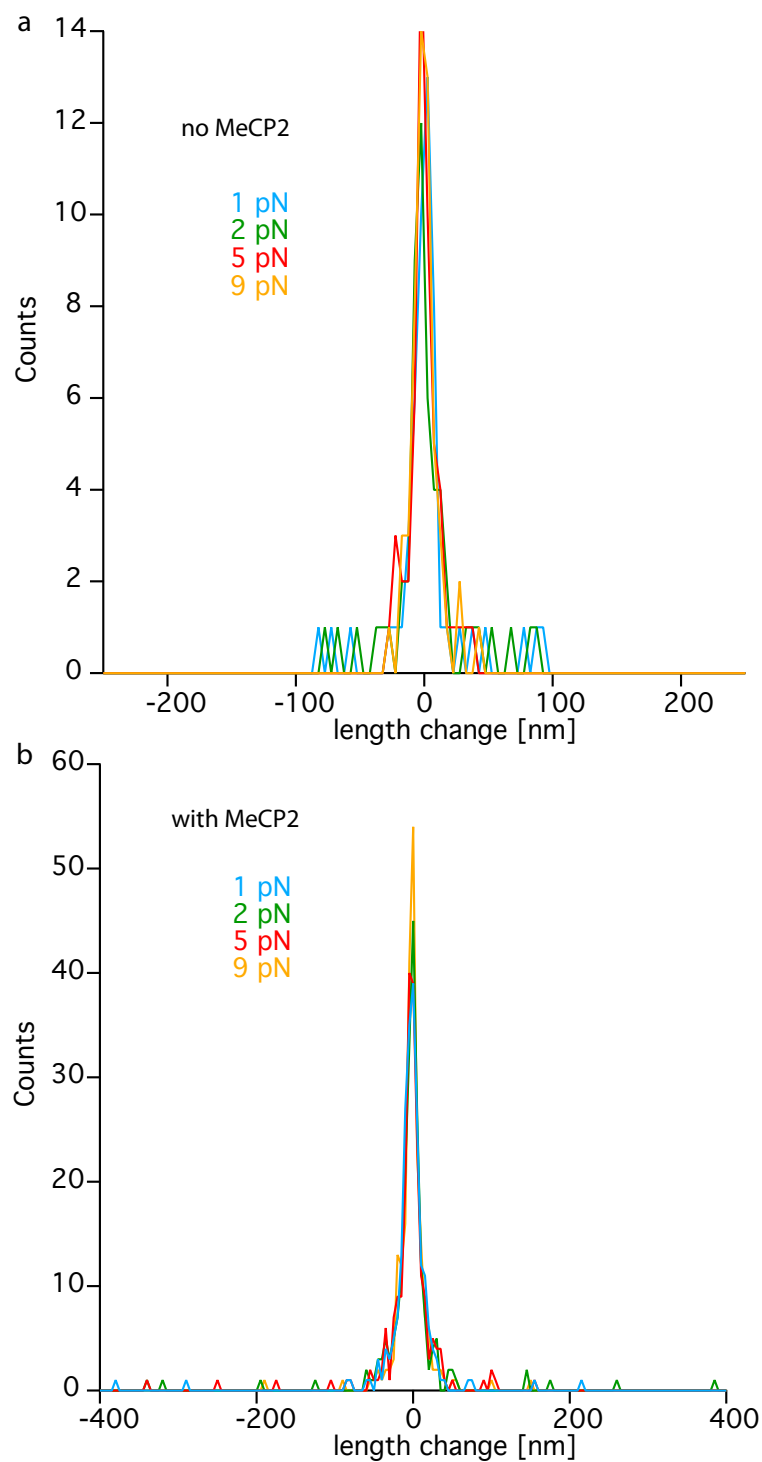


Figure 3.14: 600 bp loop DNA contour length analysis of 6 tethers in high salt buffer at various pulling forces, over all force cycles. Histograms of the tether length changes between two consecutive force plateaus. Top: blank measurement, bottom: with MeCP2.

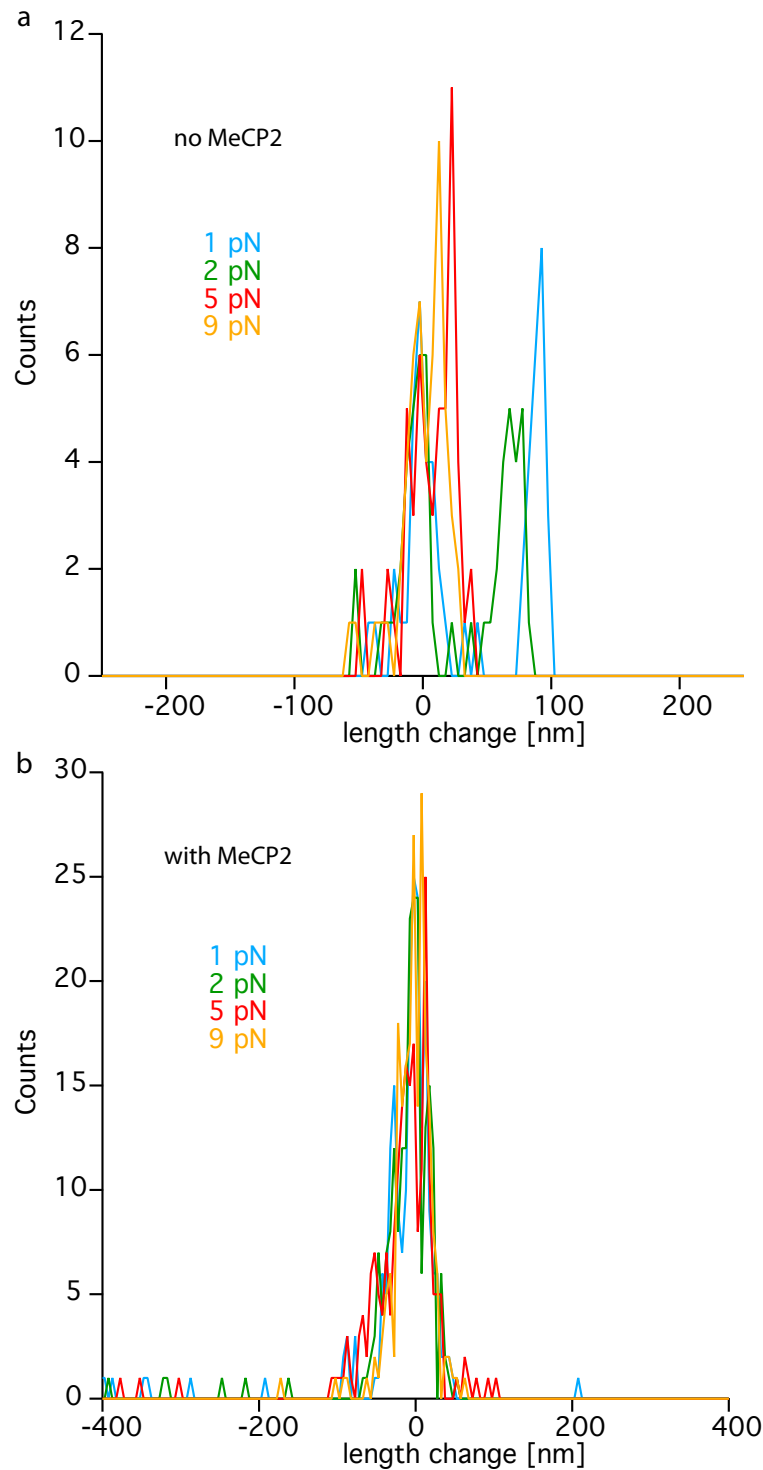


Figure 3.15: 600 bp loop DNA contour length analysis of 6 tethers in high salt buffer, at various pulling forces, over all force cycles. Histograms of tether length changes for each plateau as compared to the first plateau at a given force regime. Top: blank measurement, bottom: with MeCP2.

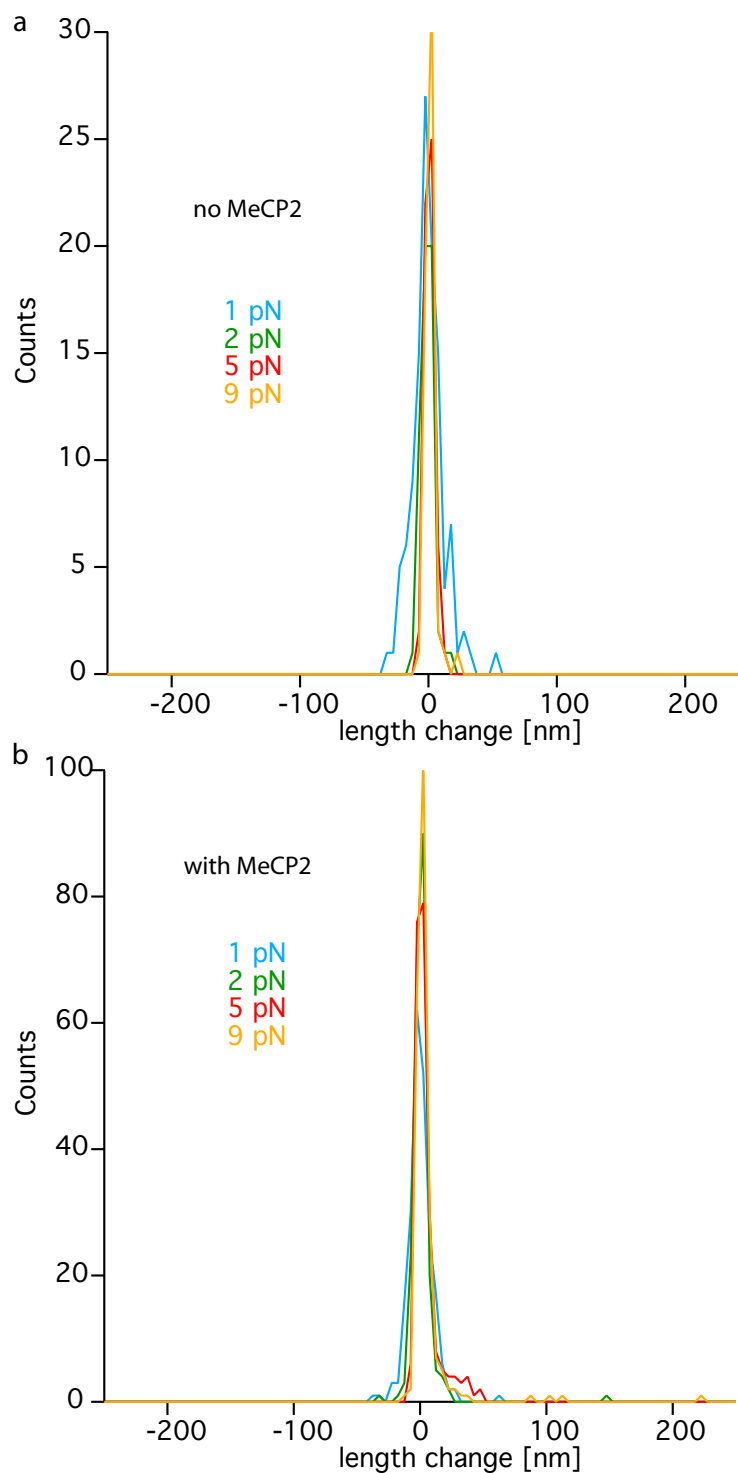


Figure 3.16: 600 bp loop DNA contour length analysis of 6 tethers in high salt buffer at various pulling forces, over all force cycles; top: blank measurement, bottom: with MeCP2. Graph illustrates tether length stability within each plateau for each force regime. Histograms show differences between the mean of the first 60 points and the mean of the last 60 points within each plateau..

Fully methylated 1.1 kb fragment

Here the DNA construct with 35 methylated MeCP2 recognition sites spread across a 1.1 kb stretch was used, providing methylated CpG sites in diverse nucleotide contexts. The resultant protein-stabilized loops of various size were expected and a shortening corresponding to up to around 1 kb loop should be observed. The exact size of the formed loop (or loops) was not the central point in this test, rather the sole possibility to observe shortened DNA tether upon MeCP2 interaction with it. Again, the blank measurements were followed by ones in the presence of MeCP2. In either case, almost no events could be observed. Loop search by comparing two consecutive plateaus resulted in a single sharp peak at 0 nm (3.17). Few deviations from 0 can be observed in the histogram of tether length changes between two consecutive plateaus (3.18) or in the histogram of tether length changes within a one plateau (3.19). The single examples of tether shortening recorded in the ± 200 nm range did not provide enough basis for reasonable statistics.

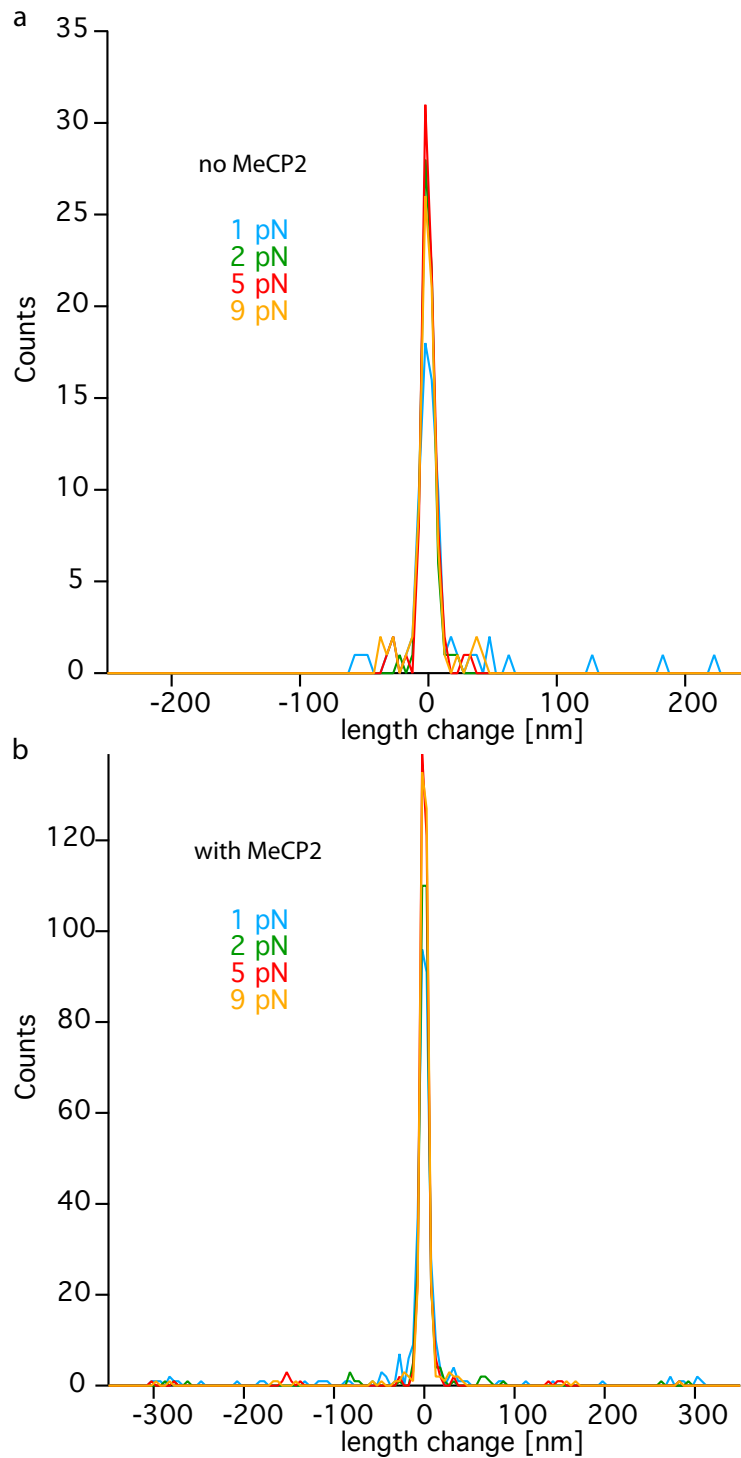


Figure 3.17: 1 kb methylated DNA contour length analysis of 6 tethers at various pulling forces, over all force cycles. Histograms of the tether length changes between two consecutive force plateaus. Top: blank measurement, bottom: with MeCP2.

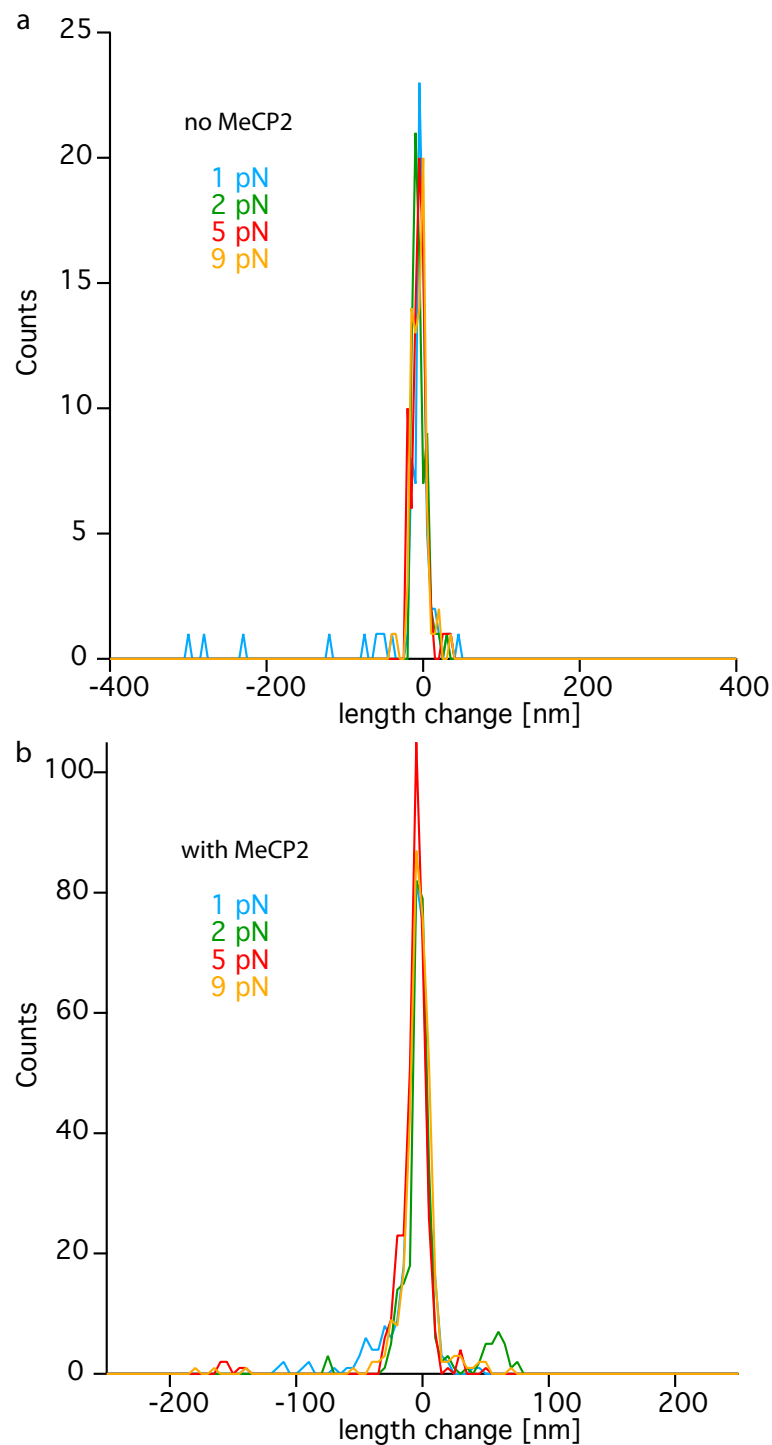


Figure 3.18: 1 kb methylated DNA contour length analysis of 6 tethers at various pulling forces, over all force cycles. Histograms of tether length changes for each plateau as compared to the first plateau at a given force regime. Top: blank measurement, bottom: measurement with MeCP2.

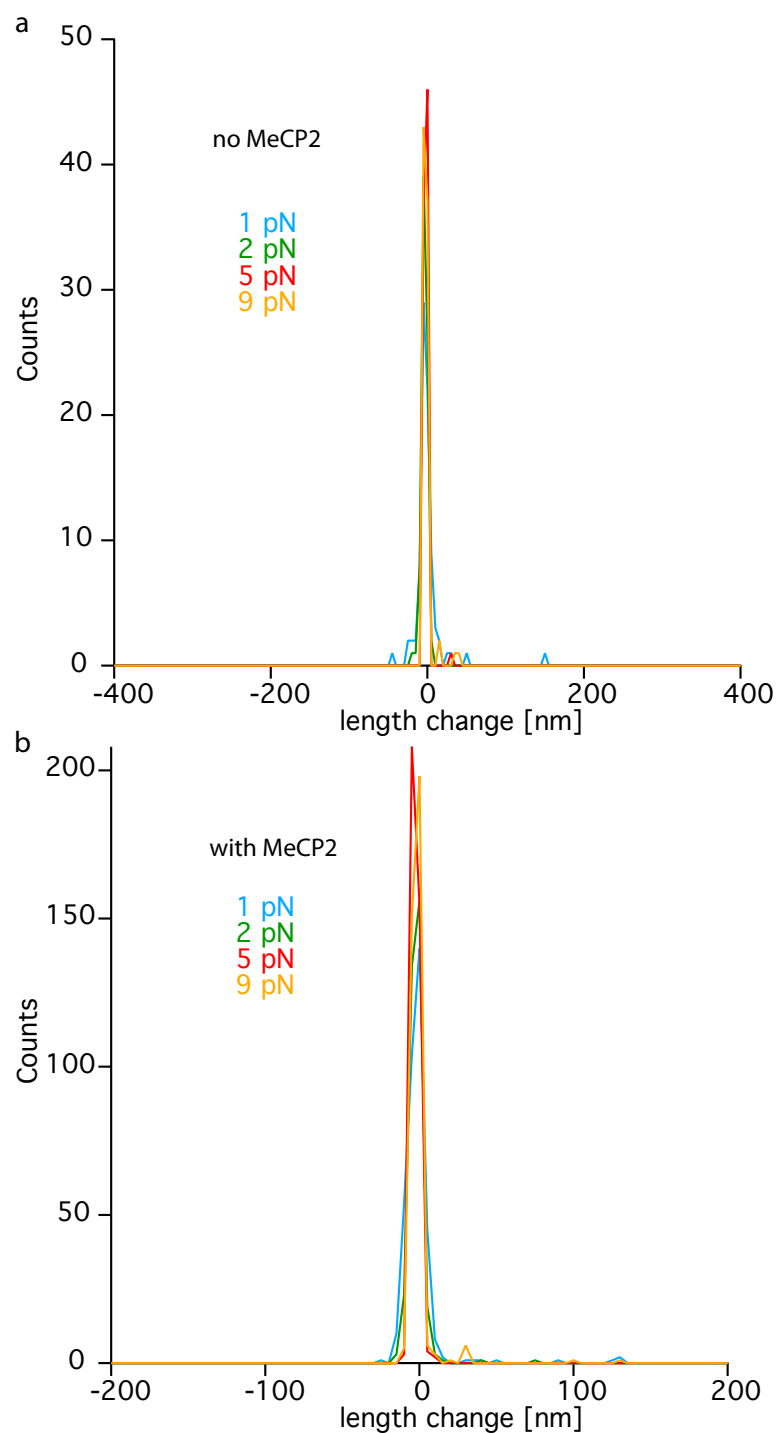


Figure 3.19: 1 kb methylated DNA contour length analysis of 6 tethers at various pulling forces, over all force cycles; top: blank measurement, bottom: with MeCP2. Graph illustrates tether length stability within each plateau for each force regime. Histograms show differences between the mean of the first 60 points and the mean of the last 60 points within each plateau.

3.3 GFP-Nanobody binding strength determination

Given the versatility of the Nb-GFP complex and the multitude of its practical applications, it is interesting to describe these binding partners both in the absolute values as well as in relation to other known biomolecular complexes. The former point was accomplished by incorporating the protein pair in the Molecular Force Balance. The latter - by performing Single-Molecule Force Spectroscopy using AFM. Next, the complex was tested towards its usefulness in Single-Molecule Cut&Paste.

3.3.1 Strength of Nb-GFP complex as compared to other biomolecular interactions

Cloning, expression and purification of Nanobody for subsequent covalent immobilization

For the purpose of this work, the Nanobody with a C-terminal cystein for covalent immobilization was cloned and expressed as described in chapter 2, section 2.3.2. Expression in a 10 l culture yielded about 6 mg pure protein. Stepwise results of a two-step purification procedure are presented in figures 3.20 and 3.21.

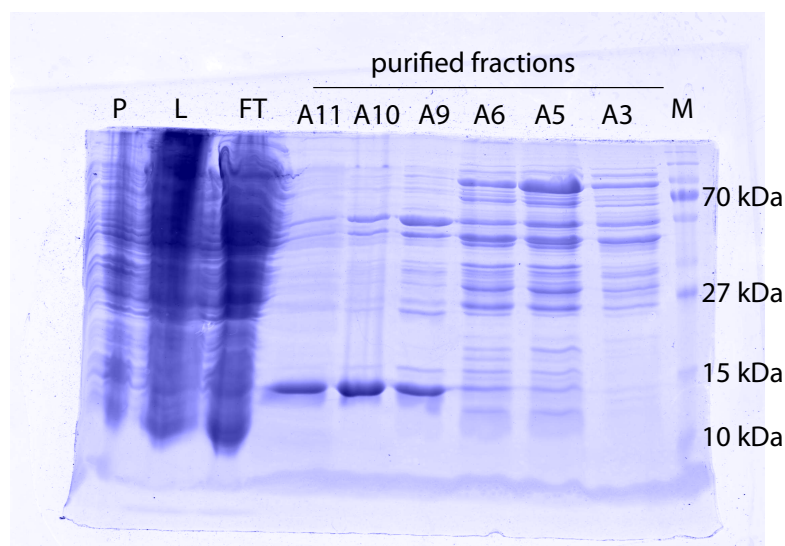


Figure 3.20: Nb-Cys sample purified over HisTrap column analyzed on 15 % SDS PAGE. P - pellet, L - lysate, FT - flow through, M - protein molecular weight marker.

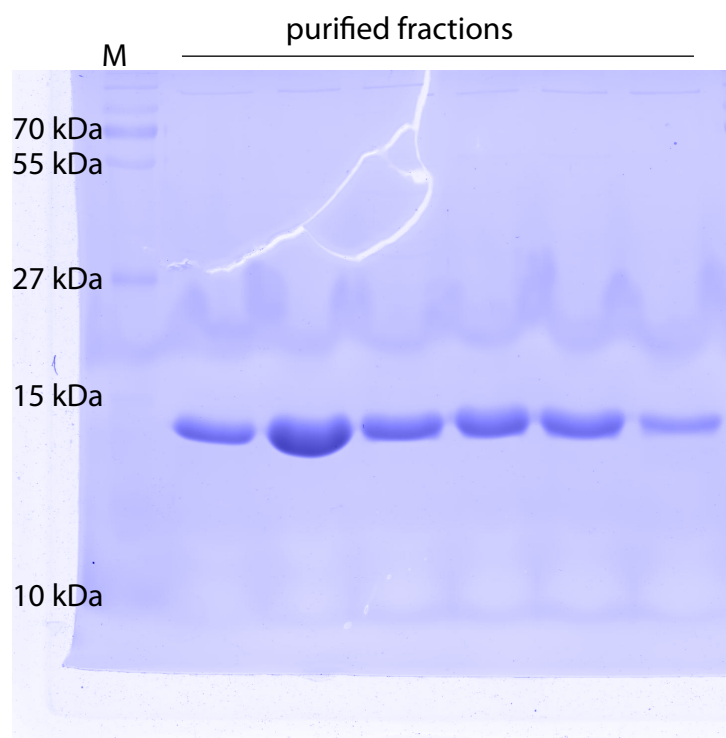


Figure 3.21: Nb-Cys sample after the second step of purification - over Superdex 75 column analyzed on 15 % SDS PAGE. M - protein molecular weight marker.

Preparation of covalent protein-DNA complex

To correctly place the Nb-GFP interaction in a wider context of biomolecular interactions, Molecular Force Balance - so far limited to DNA samples - was adapted to the use of proteins. The first challenge was to efficiently attach the DNA oligonucleotide to the protein of interest. Several strategies were tested, some leading to a fraction of reagents correctly coupled, yet leaving the majority of both DNA and protein unreacted. Exemplary results of an attempt to covalently couple maleimide-modified DNA strand to GFP exposing reduced cysteine are shown in Fig. 3.22. Two reducing agents TCEP (at a final concentration of about 50 mM) and DTT (at a final concentration of 10 mM) were used to maintain thiols on the GFP in a reduced state. After incubation, samples were separated by non-reducing electrophoresis and then scanned against GFP and Cy3 attached to the DNA. The picture presents an overlay of both channels. The fact that GFP fluorescence depends on intact tertiary structure of the protein indicates that the use of reducing agents at the applied concentrations is not harmful to its integrity. Overlapping bands (outlined in pink) represent protein-DNA complexes. However, they constitute only a minor fraction of the total amount of material loaded. The DNA control lane displays also a band near the level of the band representing the complex. A respective band can also be seen in the third lane (GFP-DNA-TCEP), clearly distinctive from the one representing the complex.

In another approach, maleimide-functionalized streptavidin was reacted to eGFP carrying a terminal thiol group and hybrids formed in this way were mixed with biotinylated ssDNA. Streptavidin was used in a 10-fold dilution series in 1x PBS, starting at a concentration of 1 mg/ml. In this assay 10 μ l of SA solution was mixed with 3 μ l of TCEP-reduced eGFP-SH and following one-hour incubation, biotinylated DNA was added (1 μ l of 0.033 μ M DNA in 1x PBS per sample). Cy3 labels on the DNA allowed for direct visualization of the complexes, which were analyzed with an EMSA using non-reducing SDS-PAGE. Figure 3.23 presents the scan of the gel as an overlay of blue (GFP) and green (Cy3) channels. Strong bands can be seen in the upper part of the gel in the lanes 2-5. The position of the band in lane 5 in the scan deviates from the other ones only due to gel wrapping on the edges during the scan as these bands appear very close to the edge due to the large size of the complexes and, hence, their very limited mobility. The first four lanes display also smeared Cy3 signal in the middle range, strongest for the highest SA concentration and no free DNA can be observed there. The reference lanes of GFP and DNA are free of any signal in the upper part of the gel.

Optimization of the abovementioned approaches - although possible - was considered too laborious and failure-prone, especially that an alternative solution has proven successful. GFP carrying a short N-terminal ybbR tag for site-specific surface attachment was employed instead [Yin et al., 2006].

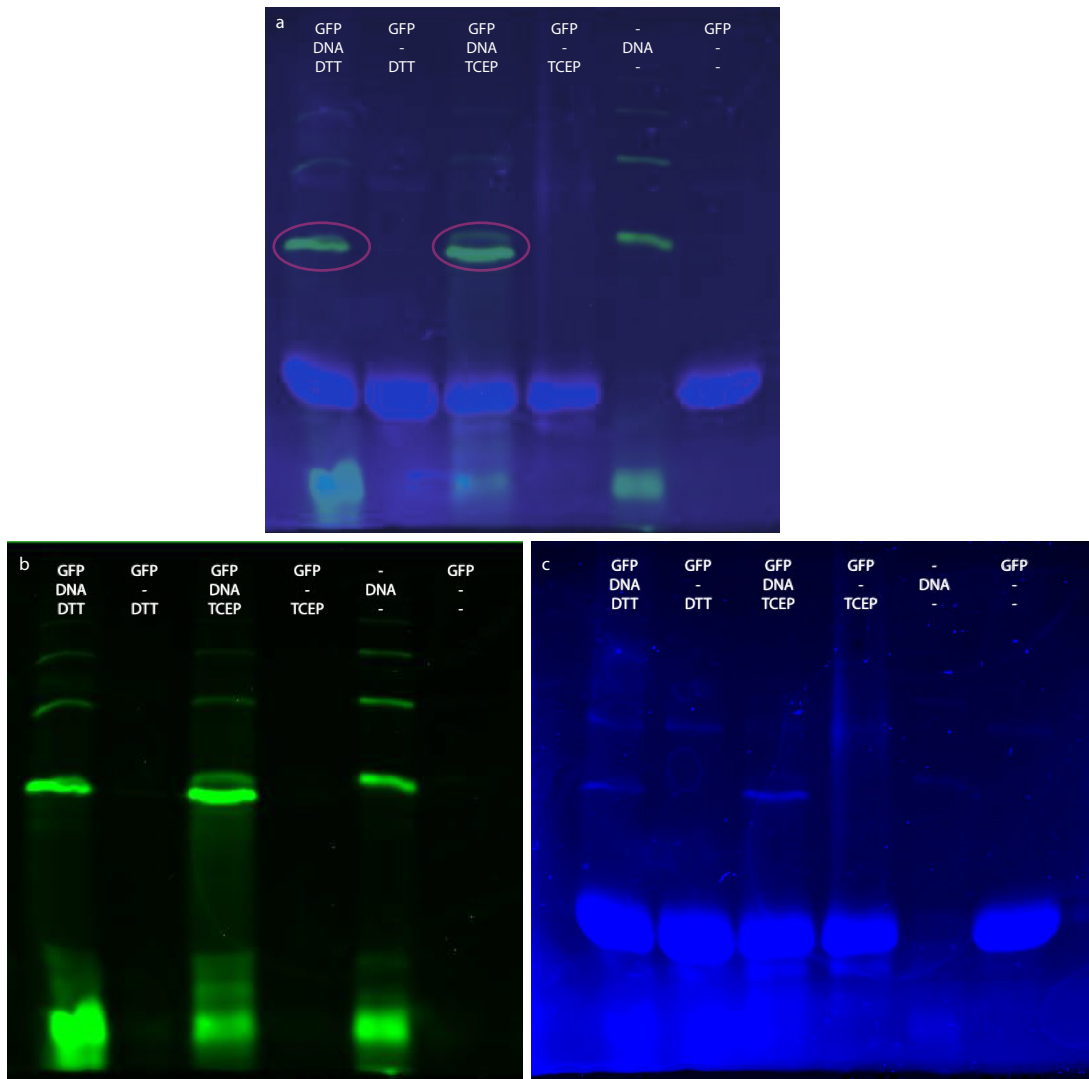


Figure 3.22: Covalent DNA-GFP complexes separated by native PAGE. a: Overlay of blue (GFP) and green (DNA) channels displays a band representing successfully formed complex (outlined in pink), b: green channel, c: blue channel; lane 1: GFP + DNA + DTT; lane 2: GFP + DTT control; lane 3: GFP + DNA + TCEP, lane 4: GFP + TCEP control; lane 5: DNA reference; lane 6: GFP reference.

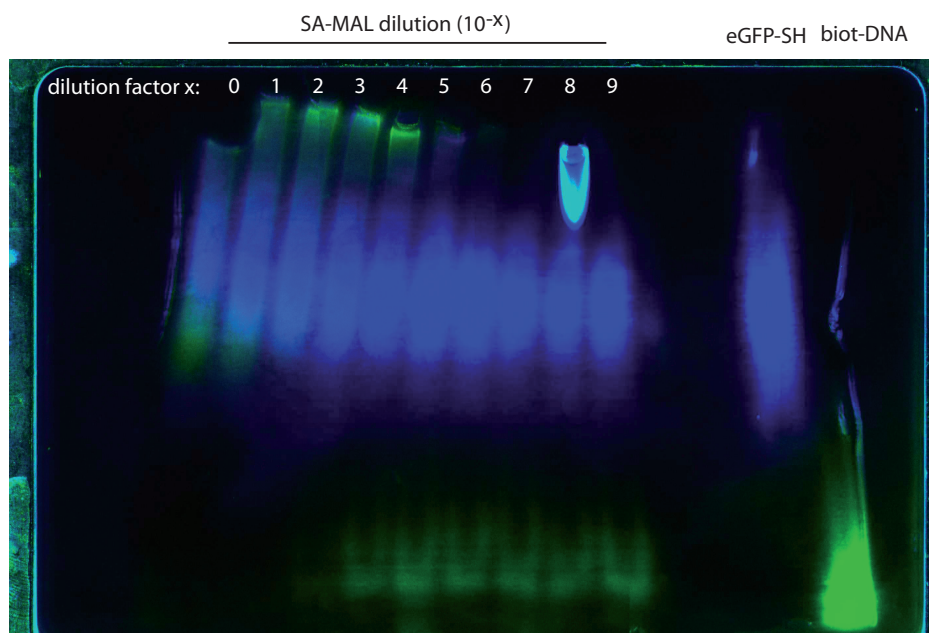


Figure 3.23: Covalent DNA-GFP complexes separated by non-reducing SDS-PAGE. Overlay of blue (GFP) and green (Cy3-DNA) channels (each at 50 % transparency). 10-fold dilution series of maleimide-functionalized SA incubated with eGFP carrying a terminal thiol group and with biotinylated, Cy3-labeled DNA, loaded along with GFP and DNA references. A readout artifact appears in lane 8, however it does not interfere with the bands. Complexes containing both GFP and DNA can be seen in the lanes 2-5 (dilution factor 1-4) in the upper part of the gel. The apparent shifts in bands' positions are due to gel wrapping as the complexes barely enter the gel and are not able to penetrate it further.

3.3.2 Molecular Force Balance measurements

The following section describes experiments performed together with another PhD student, Daniela Aschenbrenner.

Here for the first time the Molecular Force Balance (described in section 1.1.3) was adapted to probe protein-protein pairs. A single force balance consisted of the Nb-GFP pair and an oligonucleotide duplex, as presented in Fig. 3.24. Two types of GFP-binding Nanobodies were tested (for convenience later in this section referred to as Enhancer and Modified Enhancer) against three GFP constructs: wild-type, enhanced and superfolder GFP (sfGFP). The Nbs were immobilized on the glass surface via a polymer linker and then GFP-DNA complexes were bound to them. A complementary DNA strand was attached to the PDMS stamp. The stamp format (4x4 patches) allows for analysis of 16 different MFBs in a single experiment. As in the standard MFA, DNA oligonucleotides carried Cy3 and Cy5 labels allowing fluorescence readout. The fluorescence of GFP was not essential for the evaluation of the outcome but provided a convenient online control of sample quality. Indeed, GFP fluorescence signal colocalized with that of Cy3 and Cy5, confirming the specific interaction and correct assembly of protein force balances.

The surface density of the Protein MFBs estimated from the Cy5 signal was comparable to previous MFA experiments [Ho et al., 2009; Severin and Gaub, 2012], about 10^4 MFBs per μm^2 . Since the relevance of the conclusions drawn from comparative measurements largely depends on maintaining all the measurement conditions (including stamp pressure and loading rate), different constructs were analyzed against each other only within a single stamping experiment.

Unlike for the model DNA-based MFA, adjusting the strength of the reference bonds in case of protein-protein interactions was not that straightforward, as binding force cannot be inferred simply from the structural data. For the sake of measurement accuracy, however, it was crucial to keep the NF values as close as possible to 0.5, which provides the best resolution. Therefore, reference DNA stability was tuned using two approaches: intrinsic modification and by employing DNA-binding ligands. DNA duplex integrity is largely affected by its base composition and relies mostly on base stacking interactions aided by hydrogen bonds between complementary nucleotides. The modified pyrimidines exploited here carried a 5'-propynyl group, extending into the major groove and enhancing base stacking. Altogether 13 cytidines and 7 thymines of the biotinylated reference strand were modified. On the other hand, three different sequence-specific polyamides were used to stabilize DNA in a ligand-induced manner. Their binding to the minor groove of DNA was mediated

by a pyrrole-imidazole hairpin. To ensure saturation of the DNA with polyamides, they were used in 1 μ M concentration, that is in about 1000-fold excess. The three polyamides (denoted P1, P2 and P3) used here offered a range of affinities, with K_D values of 105 pM for P1, 44 pM for P2 and 1442 pM for P3 [Ho et al., 2009].

3.3.3 Binding strength of GFP-Enhancer vs. GFP-Modified Enhancer

Binding strength was estimated based on the NF value. For all three references (unmodified, propynyl-modified and with polyamide ligand) Modified Enhancer was found to bind GFP stronger than Enhancer. The calculated NF values ranged from 0.2 to almost 1, depending on the type of GFP and reference (see Fig. 3.25). In case of sfGFP, polyamide P1-bound 20 bp reference oligonucleotide provided the best resolution with NF values for both Nanobodies falling in the optimal range (around 0.5). Indeed, this example showed the largest spread between the two NF values, while in other cases that difference was also observed, however not that prominent.

All of the used DNA modifications resulted in duplex stabilization. The NF was visibly reduced for 40 bp reference with propynyl bases and an even stronger effect was observed for polyamides, which were therefore applied in combination with short, 20 bp, duplexes. Moreover, the stability enhancement by polyamides reflected their affinity - P2 with lowest K_D showed the strongest effect. P1 turned out to be the perfect stabilizer for the Nb-GFP pair, shifting the NF values close to 0.5. As expected, here also the largest spread between the two compared values could be observed.

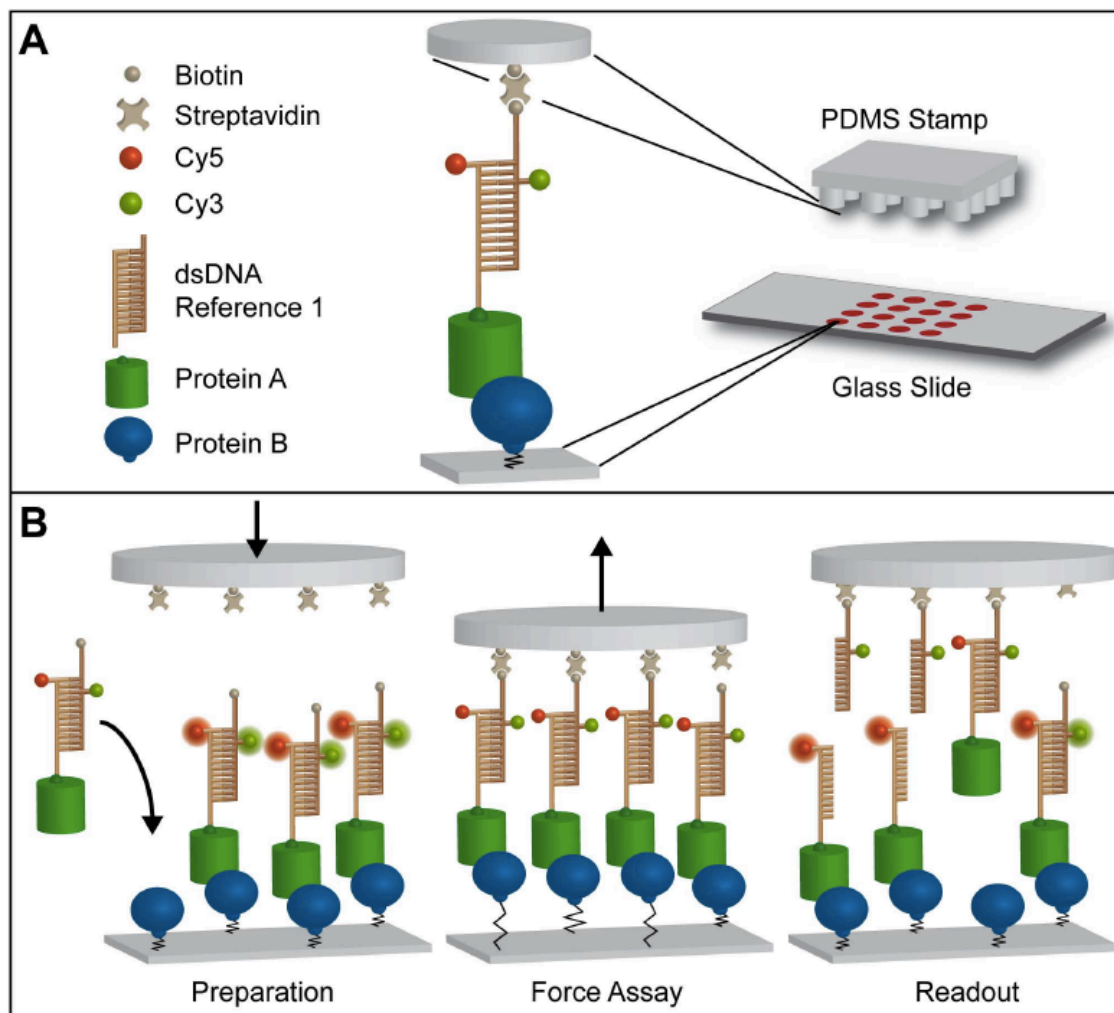


Figure 3.24: Protein-protein Molecular Force Assay. A: schematic representation of a single protein-protein MFB. B: schematic representation of the stamping procedure consisting of MFA. Following molecular complexes assembly on the lower surface, the stamp is lowered allowing biotinylated ends of DNA to bind to SA. During withdrawal of the stamp, force builds up along each MFB until one of the bonds fails. After stamping, the lower surface is scanned in the red and FRET channel to determine the ratio of remaining surface bound molecules. Adapted from [Aschenbrenner et al., 2014].

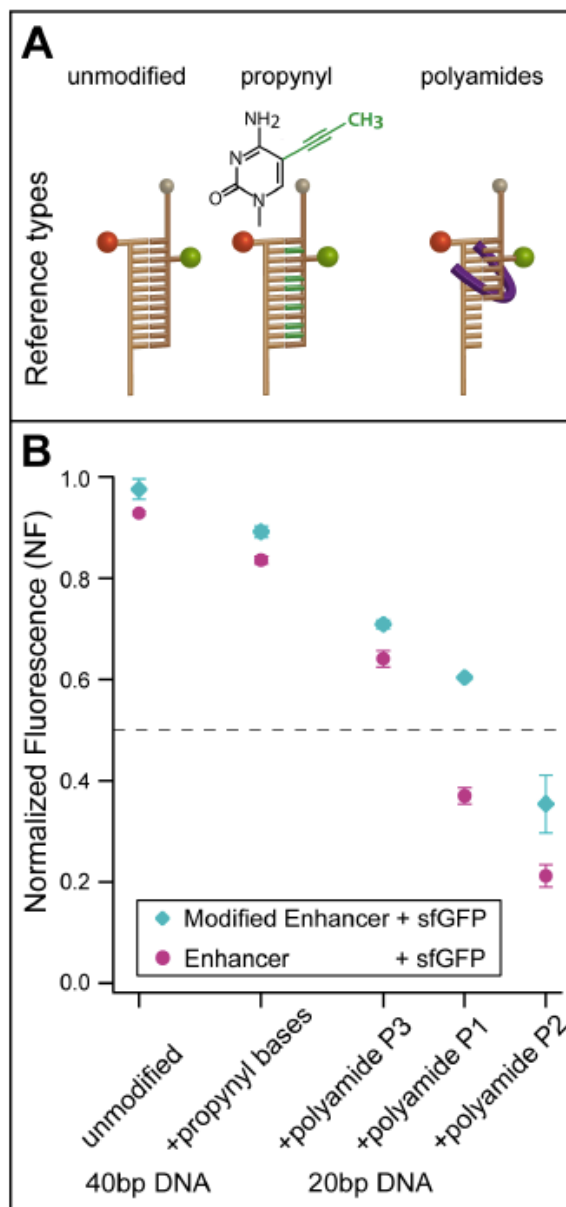


Figure 3.25: Reference DNA modifications for adjustment of MFA sensitivity. A: Reference types - unmodified DNA, intrinsically modified and ligand bound. B: Effect of various reference DNA modifications on the sensitivity of MFA (here measuring sfGFP). Largest spread in NF values was observed for the most balanced bond pair (20 bp DNA + polyamide P1). Adapted from [Aschenbrenner et al., 2014].

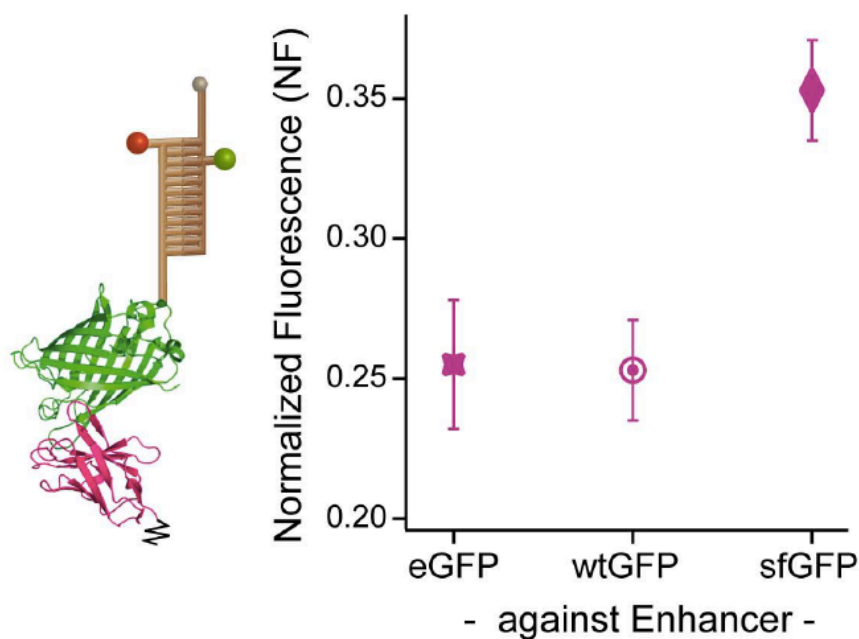


Figure 3.26: Analysis of different GFP variants for Enhancer interaction strength in a Multiplexed Protein-MFA. Left: schematic representation of a single MFB consisting of two bonds in series - the protein complex under study and a DNA duplex as a reference (ribbon model structure of wtGFP (green) and Enhancer (magenta) based on crystal structure from [30], PDB file 3K1K). Right: One example measurement depicts the differences in binding strength of Enhancer tested against wild type, superfolder, and enhanced GFP with the same reference DNA (20bp DNA stabilized with polyamide P1). While eGFP and wtGFP bind to Enhancer with comparable strength, binding of Enhancer to sfGFP is distinctively stronger. All data points are determined in one single stamping process, derived as the mean of several protein spots and displayed with standard deviation error bars. Adapted from [Aschenbrenner et al., 2014].

3.3.4 Energy landscape of Nb-GFP complex

Some of the following experiments were performed together with another PhD student, Philip Severin.

Here, Atomic Force Microscopy (AFM) was exploited to determine rupture forces of the Nanobody and wild-type as well as enhanced GFP. The Nanobody-GFP complex was probed with different pulling velocities ranging from 300 nm/s to 10 $\mu\text{m/s}$. The most probable rupture force (F) was obtained by fitting a Gaussian to the distribution of measured rupture forces and then plotted against the respective loading rate (\dot{F}). The linear two-state Bell-Evans model (see Eq. 1.12) was used to fit the data, with k_{off} - describing the dissociation rate at zero force - fixed at $1.45 \cdot 10^{-4} \text{s}^{-1}$ for wtGFP [Kirchhofer et al., 2010] and $1.24 \cdot 10^{-4} \text{s}^{-1}$ for eGFP [Kubala et al., 2010]. Literature values of off-rates (k_{off}) were used for fitting since the covered range of loading rates was not broad enough to determine the parameter with reasonable accuracy.

We observed separate characteristic force regimes, as shown in Fig. 3.34. The Nanobody bound to eGFP can withstand (within the applied loading rate range) forces from 41- 56 pN, whereas in complex with wtGFP ruptures already at 28 - 45 pN. For increased clarity, the data are presented in this plot without error bars ("width" in the force histograms). One should note that broad distribution of the measured forces is intrinsic to the technique as it stems from thermal fluctuations of the system (more significant at lower force range), and so does not diminish the significance of its results. Linear dependence of force on logarithm of loading rate suggested a single energy barrier along the reaction coordinate imposed by the direction of the acting force. The obtained energy profiles are graphically presented in Fig. 3.35.

Interestingly, we observed a 17 % broader barrier width for single-anchored wtGFP as compared to eGFP, and an even broader one (by 49 %) for double-anchored wtGFP (mean values of $\Delta x = 1.36$ nm for eGFP, $\Delta x = 1.59$ nm for single-anchored wtGFP and $\Delta x = 2.02$ nm for double-anchored wtGFP). Using literature values of K_D : 0.59 nM for eGFP-Nb [Kubala et al., 2010] and 1.4 nM for wtGFP-Nb [Kirchhofer et al., 2010], we obtained binding free energies of $-24.4 k_B T$ for eGFP and $-25.3 k_B T$ for wtGFP. Following Kramers theory [Kramers, 1940; Evans and Williams, 2002], assuming an attempt frequency ν (describing passage of the energy barrier) of the order of 10^7 results in

$$k_{off} = \nu^{\frac{\Delta G^0}{K_B T}} \quad (3.1)$$

$k_{off} \sim 10^4$, that is consistent with the known off rates of this complex.

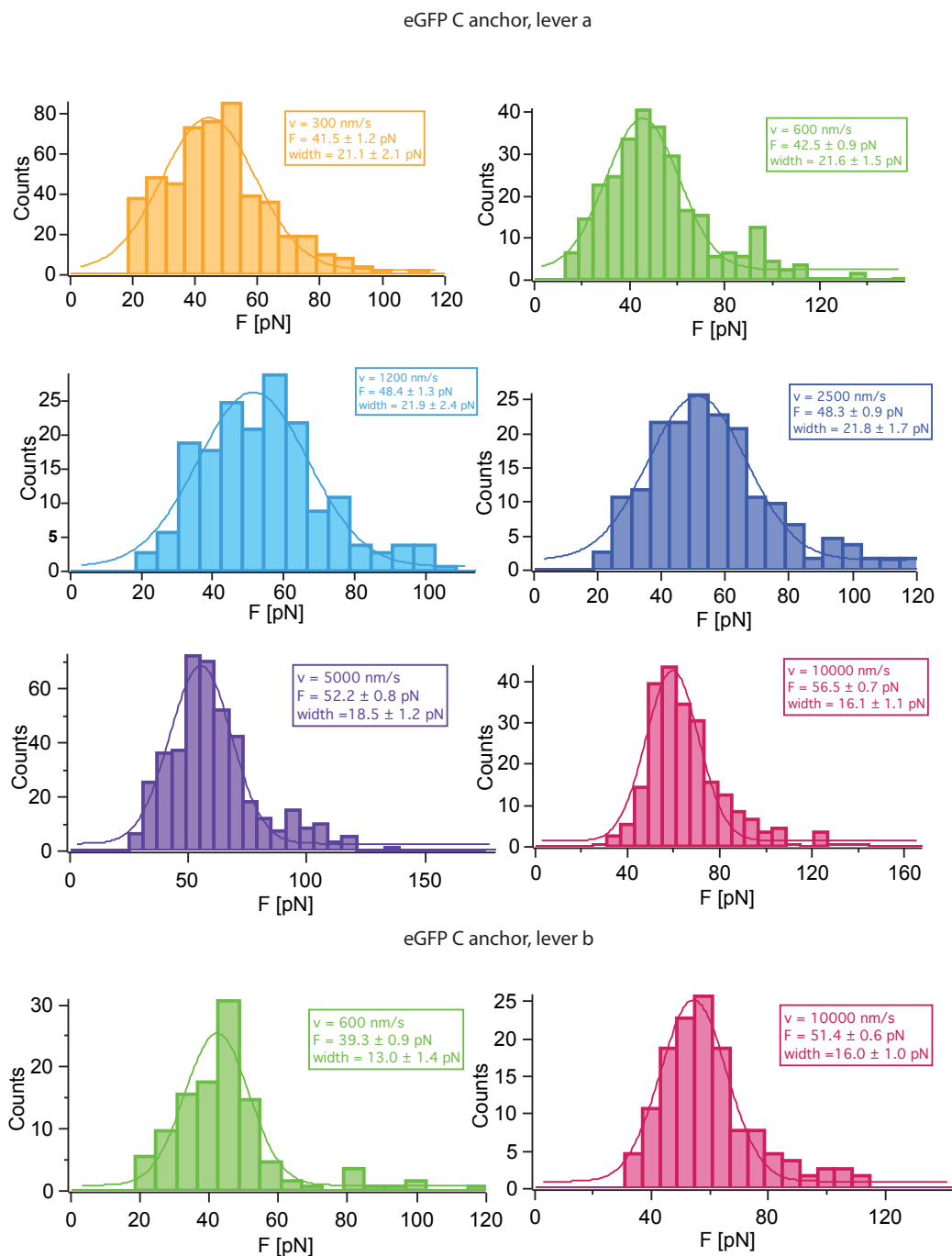


Figure 3.27: Results for a series of rupture force measurements obtained for C-anchored eGFP in complex with the Nb.

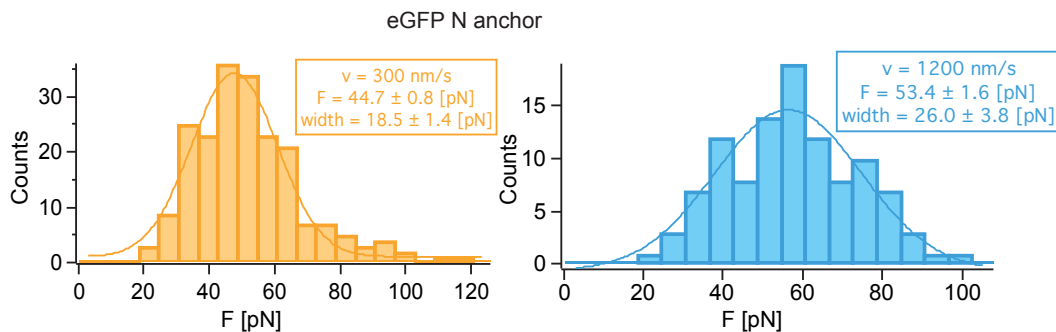


Figure 3.28: Results for a series of rupture force measurements obtained for N-anchored eGFP in complex with the Nb.

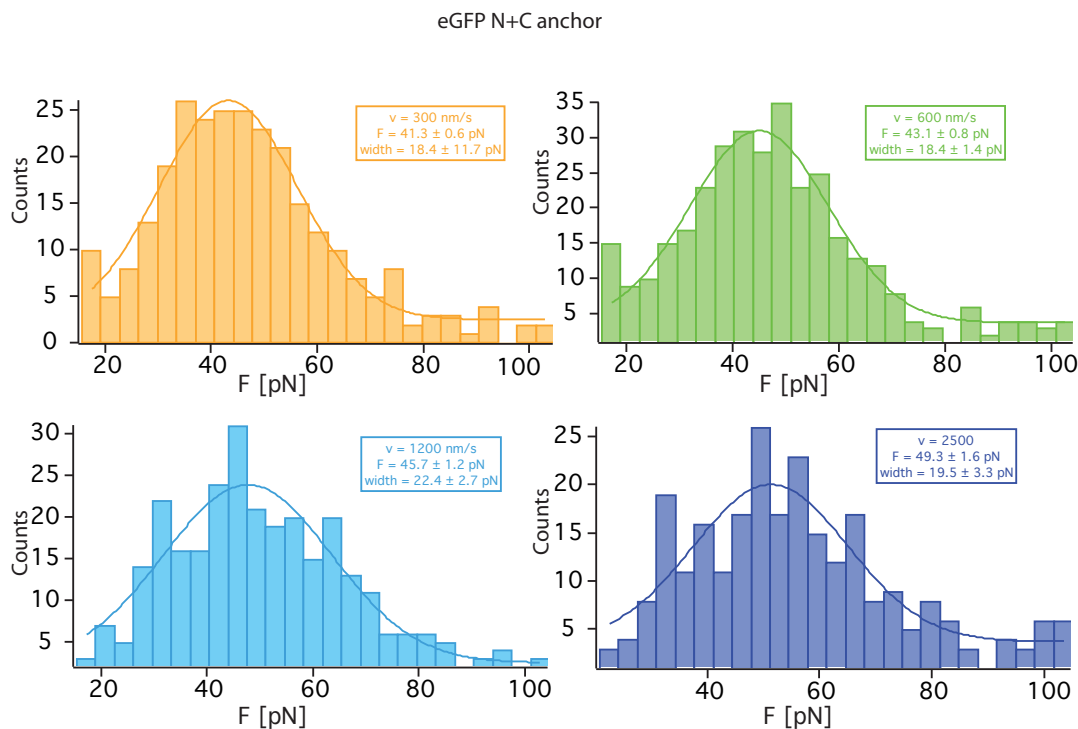


Figure 3.29: Results for a series of rupture force measurements obtained for N+C-anchored eGFP in complex with the Nb.

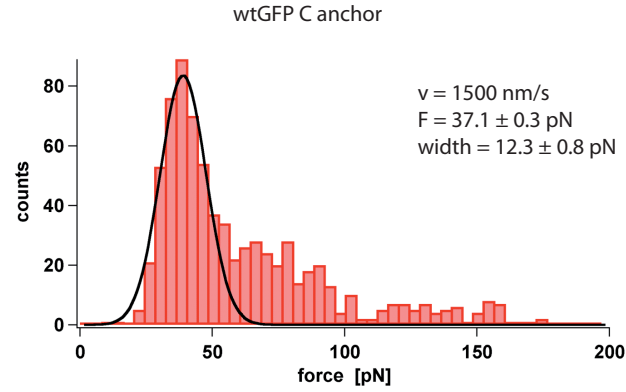


Figure 3.30: Results for a series of rupture force measurements obtained for C-anchored wtGFP in complex with the Nb. (Fig.: P. Severin)

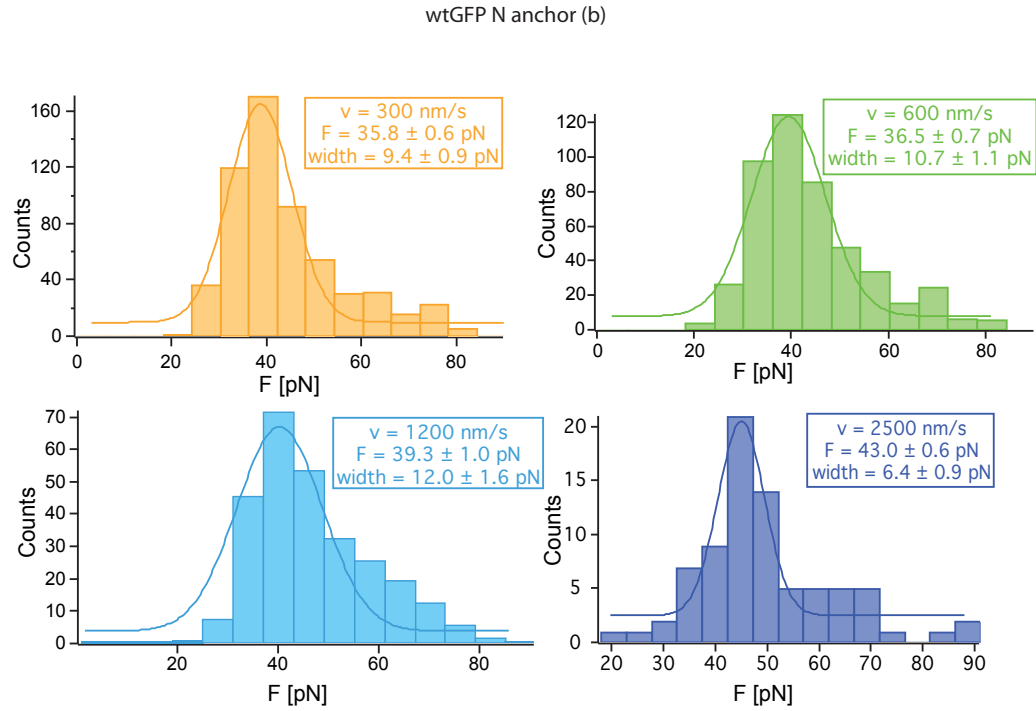


Figure 3.31: Results for a series of rupture force measurements obtained for N-anchored wtGFP (cantilever a) in complex with the Nb.

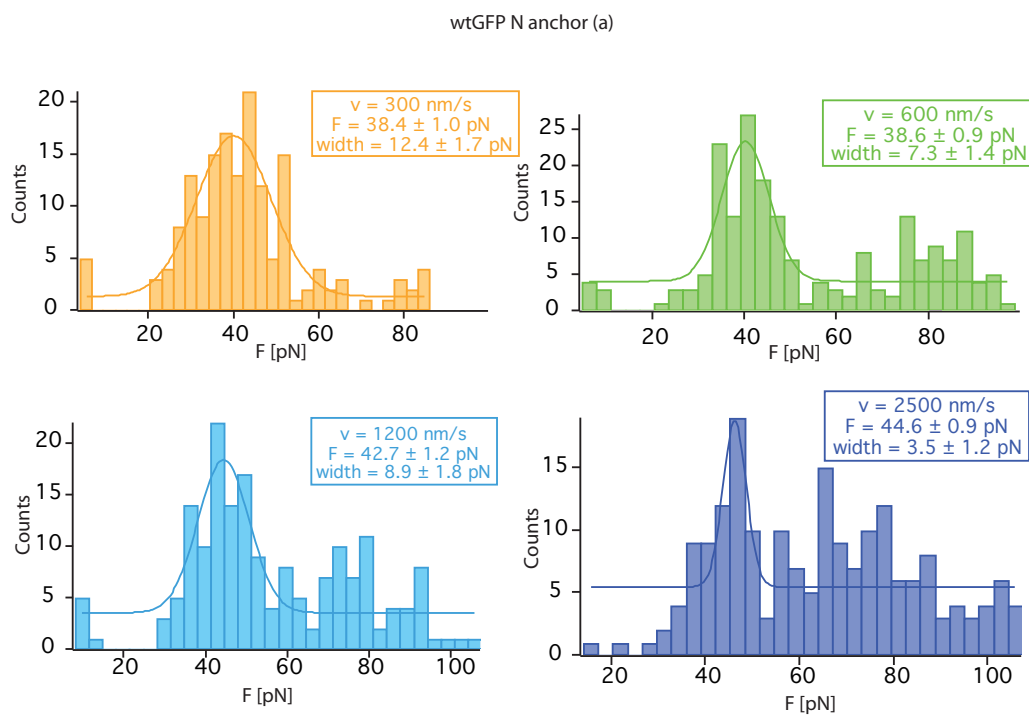


Figure 3.32: Results for a series of rupture force measurements obtained for N-anchored eGFP (cantilever b) in complex with the Nb.

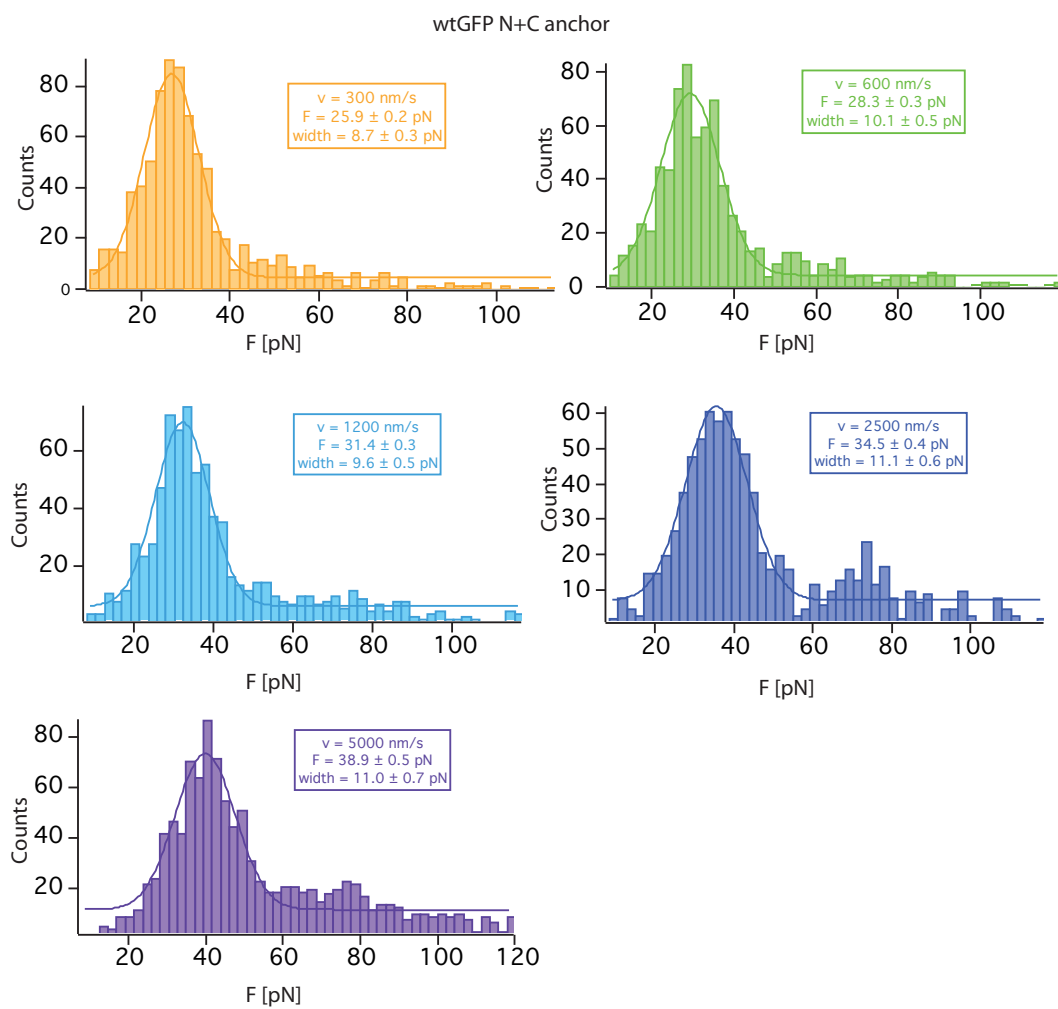


Figure 3.33: Results for a series of rupture force measurements obtained for N+C-anchored eGFP in complex with the Nb.

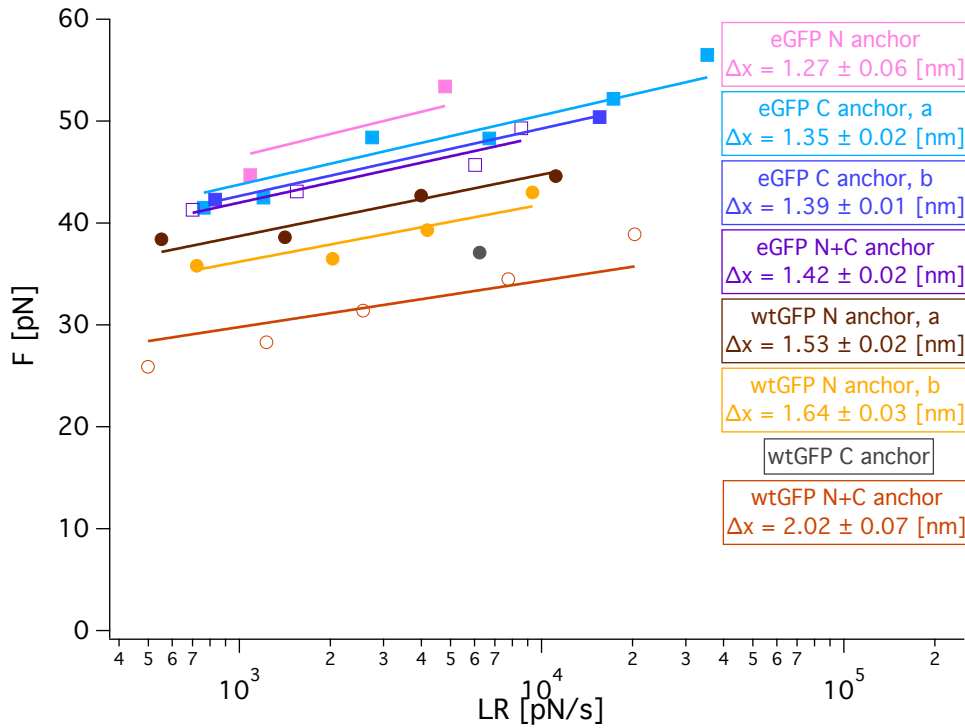


Figure 3.34: Dynamic force spectrum of Nb-GFP complexes obtained based on pulling velocities ranging from 300 nm/s to 10000 nm/s. Data points for eGFP are shown with square markers and wtGFP with circle ones; solid markers denote single-anchored GFP (N- or C-terminally) and open ones double-anchored GFP. Data were fitted to the Bell-Evans model using literature off-rate values for wtGFP ($k_{off} = 1.45 * 10^{-4} s^{-1}$) [Kirchhofer et al., 2010] and eGFP ($k_{off} = 1.24 * 10^{-4} s^{-1}$) [Kubala et al., 2010].

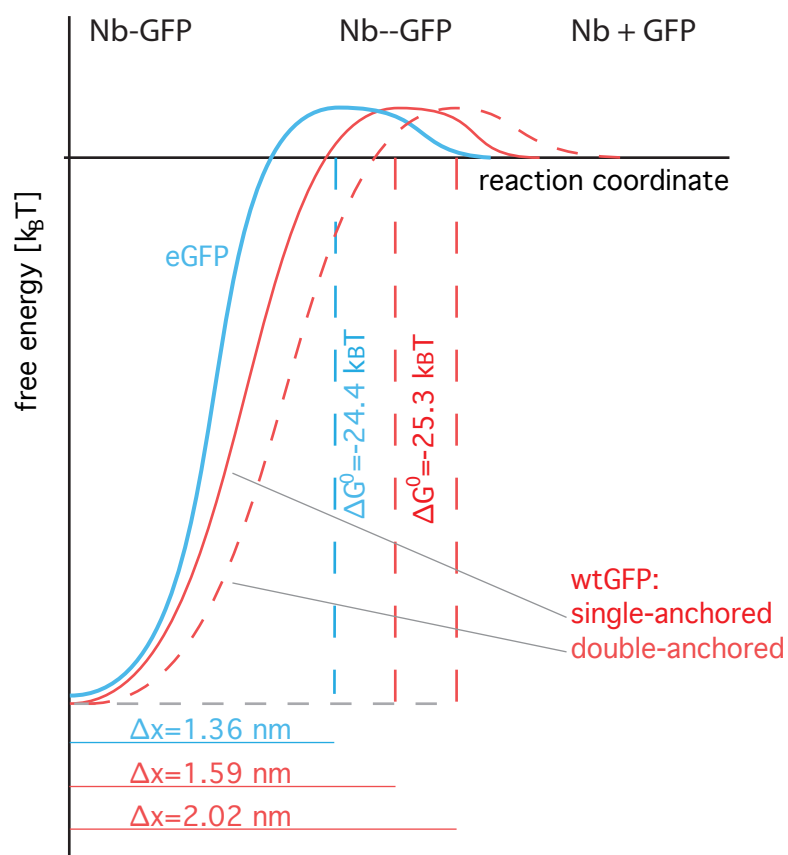


Figure 3.35: Energy profile of the Nb-GFP complex along the direction imposed by the pulling force. The energy barrier appears 17 % shifted: from 1.36 nm (eGFP) to 1.59 nm (single-anchored wtGFP), and even further to 2.02 nm (i.e. by 49 %) for double-anchored wtGFP.

3.3.5 Specificity control in Nb-GFP force spectroscopy

To exclude the possibility of force spectroscopy outcome resulting from nonspecific interactions between the cantilever and the sample surface, we performed measurements on several constellations of cantilever-surface pairs, where one or both of the interacting partners were missing or inactivated. The objective was to compare the picking efficiencies with those of properly prepared samples. The results are presented in Table 3.1.





Schematic representation of the set-up	Set-up and retract speed	curves total	curves selected	peaks	peak ratio
	Experimental set-up 1 m/s	434	226	226	52.1 %
	Nb excess 1 m/s	1024	7	7	0.7 %
	Nb excess 5.88 m/s	1011	36	35	3.5 %
	GFP excess 1 m/s	1001	51	51	5.1 %
	GFP excess 5.88 m/s	1101	59	59	5.4 %
	no Nb 0.798 m/s	1033	35	2	0.3 %
	no Nb 4 m/s	1661	53	7	0.4 %

Table 3.1: Negative control experiments. Comparison of interaction ratios for a typical experimental set-up, one of the interaction partners blocked or missing.

Chapter 4

Discussion

4.1 Streptavidin-biotin bond strength

The well-known and widely used receptor-ligand pair of streptavidin and biotin has already been broadly described by others but available data are not unanimous [Moy et al., 1994; Allen et al., 1996; Wong et al., 1998; Yuan et al., 2000; Lo et al., 2001; Stevens et al., 2002]. Previous AFM approaches (cited above) relied on a statistical interpretation of a series of peaks in the obtained force distribution. The primary peak was attributed to the single-molecule events, and the following ones to multiple ruptures. While such explanation is obviously reasonable, it does not exclude the bias caused by unspecific interactions or values accidentally falling in the range of interest. Here, the rupture force of the complex was characterized by AFM force spectroscopy using the fingerprint provided by the DNA spacer, which ensured that only single-molecule events were analyzed to determine the strength of the interaction. It is of particular importance due to the multivalency of the protein - since a single (tetrameric) SA moiety can accommodate up to four biotins. This allowed to determine the most probable rupture force characterizing the biotin-SA complex as 165.6 ± 3.1 pN. Since values reported in the literature vary greatly and at the same time in most cases the applied loading rates (a parameter significantly affecting the measured force) are not stated, it is not possible to directly compare these results.

Apart from the main peak, the force histogram features also a shoulder towards higher values, which can be explained based on the experiment's geometry. The

tetramers of SA were attached to the cantilever in a random orientation via intrinsic, surface exposed amines. Therefore, of the four biotin-binding pockets of each SA moiety, some were easier accessible (pointing towards the slide surface) than others. However, binding took place with the DNA in a relaxed form and so also the hidden pockets could be approached by the biotinylated end of the DNA. In such case, the DNA stretching and biotin unbinding proceeded along different directions, therefore a higher force was necessary to rupture the biotin-SA complex.

It should be noted here that the measured force value falls into the regime characteristic of force-induced dsDNA melting [Clausen-Schaumann et al., 2000], which may bias the obtained result. Additional measurements involving stabilized DNA duplex (by DNA binders) could help discriminate between strand separation and protein-ligand dissociation. Yet these pilot experiments have proven the feasibility of the assay to access single molecules and further investigate other biomolecular interactions.

4.2 MeCP2-DNA interaction

MeCP2 interaction with methylated DNA has been subjected to extensive studies employing two powerful single-molecule techniques: AFM and MT. We were interested in investigating the phenomenon of DNA loop formation upon MeCP2 binding to methylated CpG sites as suggested in [Ghosh et al., 2010a]. In case of both techniques, MeCP2-stabilized loops should result in the shortening of the contour length of the stretched DNA molecule.

Surface density of DNA depends on a number of factors, including reactivity of the functional groups of the slide and DNA, age of the slides or air exposure prior to use or concentration of the applied DNA. From our experience, even strictly following the preparation procedure does not guarantee reproducible sample quality. Aware of the abovementioned issues, prior to force spectroscopy measurements we performed an EMSA test with a sole purpose of proving MeCP2 ability to bind to the methylated DNA. Band shifts observed in lane 2 and 3 in Fig. 3.3 provide a clear evidence for that, and the shift is more pronounced for higher protein concentration as diluted MeCP2 does not saturate the available binding sites. Since, regarding the AFM samples, it was not possible to determine the exact amount of the DNA bound to the surface, no conclusions regarding stoichiometry would anyway be relevant to the AFM experiment.

The possibility of single-molecule control was central to the experimental design allowing for the detection of MeCP2-induced loop formation. Based on the current state of the research, it is not clear whether the observed looping is stabilized by a single MeCP2 binding to more than one site on the DNA (often referred to as "sandwich" formation) [Georgel et al., 2003; Nikitina et al., 2007] or whether the loops form through dimerization or oligomerization of the protein [Ghosh et al., 2010a]. DNA-bound oligomers have been observed *in vitro* [Georgel et al., 2003] and *in vivo* [Brero et al., 2005], however Klose and Bird [2004] and Adams et al. [2007] challenged their existence before Becker et al. [2013] confirmed the phenomenon and mapped the region of MeCP2 mediating the contact between proteins. Regardless of the actual mode of action, the primary goal of the experiments presented in this thesis was to detect DNA looping by MeCP2 with a single-molecule resolution.

In the first, naïve approach, 1 kb long DNA with 35 methylated CpG sites was used, offering a multitude of loop sizes. The positions and nucleotide context of all the CpG sites are presented in Table 4.1. Upon MeCP2 binding, compaction of the DNA was expected and subsequent stepwise rupture as the ends of the molecule were pulled apart. Indeed, the characteristic B-S fingerprint in the force curves was completely lost upon addition of the protein. The high force peak ("hump") observed in the presence of MeCP2 indicated its interaction with the probed DNA but the ruptures could not be resolved down to single molecule events. Here the issue of surface density came to play; to ensure high picking efficiency, a relatively high density of molecules on the surface was desired, while that translated into shorter molecule-to-molecule distances and increased probability of intermolecular cross-links to occur. Furthermore, multiple intermolecular connections could be attributed to the high density of CpG sites within each DNA molecule. Hence, even probing a single molecule led to pulling a whole net of entangled and interconnected strands.

CpG position	nucleotide context
78	TTATCAAAAG CG GGAAGAATAC
96	ATACATTCAT CG ATAGTAGATG
110	AGTAGATGGAC CG ATATTTCTGT
195	TTATAAAGGCC CG AAGCCCTCTA
215	TATTAAAAAT CG TGGGTAGAAT
252	CCACATAATT CG CGTGTTCCACC
254	ACATAATT CG CGTGTTCCACCTT
409	ATATTTAACAC CG GGTCAGAGCA
443	TTATTAAAAC CG TTAATTACGA
452	CCGTTAATTAC CG ATTTTACCTT
471	CTTCTTTTAC CG TGATAGCAAT
502	TTGCAGACCAC CG AGATACACGC
511	ACGAGATACAC CG CAACAGCTGT
564	CAGATGCTAC CG GGAATGGAAT
603	CTACTGTACT CG GATCGGCTGC
608	GTACTCGGAT CG GCTGCTGGCC
634	AATTGTTGAG CG GGCATCAGCA
710	GACAGAATAC CG AGAAAACCGT
719	CCGAGAAAAC CG TTCAAATCGT
728	CCGTTCAAAT CG TAAATTGCTA
755	AAATCAATAA CG TCAGAAATAT
755	TATTTGCTT CG CATAAGTTGT
774	CCATTAAGT CG CGAGTCATAA
797	ATTAAGT CG CGAGTCATAATA
799	ATAAATTGAC CG GATTTAAGCA
851	TTAATAGTAG CG AAATTTTAA
953	AAGCAATTAA CG ATTAAAATCA
967	TAAAATCAGC CG CAATTGTTTC
979	CAATTGTTT CG CAACAATTTG
1007	AACAATTAGAC CG TTTCATCTGCA
1023	TCTGCATTAC CG CAATAATCAT
1043	ATCTTCAAGG CG TTCCACCACAT
1077	AATTTAGCAC CG GCGTTTAGGG
1080	TTAGCACCGG CG TTTAGGGATT
1106	AGTATGTTTG CG CATTAGTTCA

Table 4.1: Nucleotide context of all 35 CpG sites of 1.1 kb DNA fragment

To gain a better control over the behavior of the pulled strands, we used an *in vitro* methylated DNA construct (otherwise identical with the fully methylated one) with two or three methylated CpG sites, limiting the possible strand shortening distances caused by intramolecular looping. The two methylated sites were separated from each other by 309 bp, that is a distance corresponding to double the persistence length of dsDNA. In the other methylation pattern, the distances between the MeCP2 binding sites were 250 bp or 500 bp. Contrary to the expected data quality improvement - since much less interactions were allowed and the set of predicted shortening lengths was discrete - addition of MeCP2 resulted in a similar high force peak as previously.

However, interesting findings followed one particular AFM experiment, in which - when pulling a fully methylated DNA - the "step" pattern was observed during cantilever retraction. The unusually shaped curves were recorded for hand-controlled cantilever actuation aimed at much more gentle agitation than the automated procedure. The most likely explanation of the observed "steps" assumes two nicks on the opposite strands of one DNA molecule, in a close distance from each other, which upon DNA stretching and shearing would lead to eventual rupture of a double-stranded piece of DNA leaving it attached to the cantilever as schematically presented in Fig. 4.1. Subsequent surface probing resulted in multiple cross-links between the DNA coupled to the cantilever and that on the surface. The overall good quality of the DNA used in the described force spectroscopy experiments explains the rarity of the described observation.

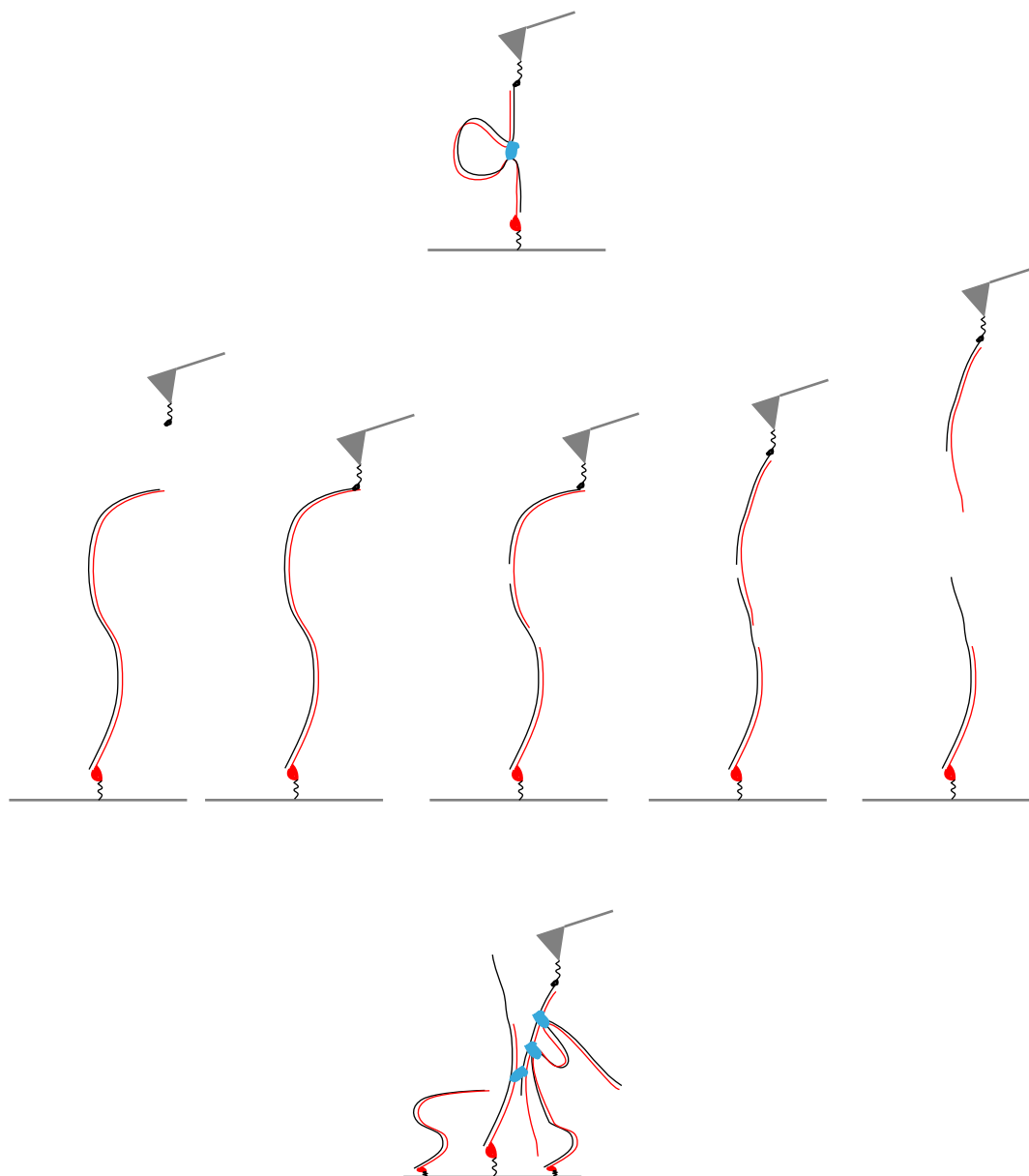


Figure 4.1: Schematic explanation of the observed "step"-pattern in force curves of DNA stretched in presence of MeCP2. The experiment assumes stretching single dsDNA molecules. However, nicks present relatively close to each other on the opposite strands of a DNA molecule result in breaking of the molecule, leaving a dsDNA fragment permanently attached to the cantilever. Subsequently, this fragment probes the surface creating multiple cross-links with DNA on the surface. Each "step" in the force curve represents a single rupture of one such cross-link, leading to a slight increase in the current contour length of the tether. For a short while the system regains flexibility, which is reflected in the increase of force before the next step occurs.

Taking the outcome of the "steps" analysis as a hint, we decided to reach out for another SM technique capable of overcoming the surface density problem encountered with AFM, namely magnetic tweezers (MT). Our first MT experiments were designed so as to reproduce the conditions of the AFM ones and explain the "step" pattern observed there. For this reason, the same 1.1 kb DNA fragment was incorporated into the 5-kb-long MT tether and 1x PBS was used as assay buffer. Since the initial MT trials with 300-bp-loop DNA did not yield any positive results regarding loop detection, we moved on to optimize the assay. First, the loop was extended to 600 bp, then experimental conditions were adjusted to match the optimum for MeCP2. Various reported in literature aspects improving MeCP2 affinity were tested, including high salt conditions [Ghosh et al., 2010a] or stretches of A/T nucleotides adjacent to the binding site [Klose et al., 2005] known to cause DNA bending and widening of the major groove [Ho et al., 2008]. None of these changes brought any improvement to our understanding of the MeCP2-DNA interaction. Both the 600 bp loop DNA and 1.1 kb methylated DNA ruled out the possibility of DNA stiffness being the limiting factor in loop forming. It is important to mention here the statistical background of reasoning in SM techniques. The analysis in both the abovementioned cases (AFM or MT) relies on a very limited (often to single digits) number of molecules picked from a huge batch - be it a few molecules displayed on the cantilever or a few tethers analyzed within an MT experiment. Therefore, proper sample preparation and ensuring its homogeneity as well as high quality is of paramount importance. We controlled the efficiency of enzymatic methylation by subsequent digestion of not fully methylated DNA, so that only properly prepared molecules were applied on the surface.

Strangely, MeCP2 action was clearly apparent in AFM experiments but remained undetectable in all the MT trials. The only significant difference in screening procedure was the waiting time between protein application onto the surface and the measurement itself, which was much longer (about 20 minutes) in case of AFM measurements and just a few minutes in MT. However, since keeping the tethers relaxed at low force for a longer time usually results in an inevitable loss of beads sticking to the flowcell surface, matching this condition was not considered here. This could well be the reason for the lack of loops observed when using the MT technique. A way to test the time requirements characterizing the MeCP2 action on the DNA could be another AFM trial with respectively short equilibration time. On the other hand, the differences in signal detection between these two techniques justify the applied conditions. AFM readout could suffer from too much noise to draw meaningful conclusions.

The satellite peaks recorded for low force traces in Fig. 3.15 a) illustrate the vulnerability of SM measurements to minute contaminants, which - although rare - do occur (e.g. airborne dust). The other two graphs analysing that set of data (Figures 3.14 a) and 3.16 a) with single peaks centered at 0) confirm stability of the tethers' lengths throughout the blank measurement.

Although MeCP2-stabilized loops were imaged in previous works by EM and AFM [Georgel et al., 2003; Nikitina et al., 2007; Ghosh et al., 2010a], recording the process of their formation remains a challenge. A possible explanation for no change in tether behavior upon the addition of the protein could be its unspecific attachment at a second site (by one of its methylation-independent domains as described in 1.5.2, leading to sliding of MeCP2 along the DNA, not detectable with the resolution of the applied techniques. It is common for DNA-binding proteins to bind weakly to an unspecific site and then search for the specific one. This is accomplished by either sliding along the DNA or hopping (referred to as "intersegmental transfer") to more distant places on the same or sometimes also another molecule [Halford and Marko, 2004]. Such mechanism increases the effectiveness of finding the specific binding sites. Indeed, MeCP2 possesses a number of domains capable of unspecific DNA binding: intervening domain (ID), transcription repression domain TRD, C-terminal domain α (CTD- α) [Ghosh et al., 2010b; Kumar et al., 2008]. On the other hand, the overall positive charge of MeCP2, resulting in unspecific binding to the negatively charged DNA backbone [Stuss et al., 2013] could underlie the hump observed in the AFM experiments.

Finally, having tested the MT set-up using EcoRII in the exact same conditions against its capability of loop detection, we showed that it is definitely suited for that purpose, yet the MeCP2-DNA interaction needs to be approached differently - how exactly remains beyond the scope of this work. We decided to leave the preliminary results as a starting point for other studies.

4.3 GFP-Nb

Another biomolecular complex we tried to understand on a single-molecule level was the GFP-Nanobody pair. We chose three different subtypes from the rich repertoire of GFPs: wild-type, enhanced and superfolder GFP (wtGFP, eGFP and sfGFP). The Nb family was represented by one GFP binder (referred to as Enhancer) and its modified form (Modified Enhancer) harboring an additional N-terminal peptide tag. Growing interest in single-molecule manipulation and analysis motivated this study

as detailed understanding of the intermolecular phenomena can not be accomplished based solely on ensemble averaged data from bulk measurements.

4.3.1 Nb-GFP interface

GFP has a structure of a β -barrel with both its N- and C-terminus protruding from the same side of its 3D structure. This enables GFP anchoring to the surface via either one of its termini as well as via both simultaneously, keeping its orientation unchanged. Moreover, upon GFP immobilization, the epitope recognized by the Nanobody is exposed, as it is located on the opposite side of the β -barrel. Similarly, anchoring the Nanobody to the solid support via its C-terminus, should leave its binding site unaffected. Accessibility of the epitope is a prerequisite for efficient single molecule probing of specific interactions, which should not be hindered by unfavorable attachment to the solid support.

Each of the three compatibility-determining regions (CDRs) of the Nanobody contribute to its binding to GFP, accomplished mostly by electrostatic interactions and a single hydrophobic contact. The epitope extends over 672 \AA^2 at the exposed loop region between the strands 6 and 7 of the GFP β -barrel [Kirchhofer et al., 2010].

Site-specific protein attachment provides a controlled and uniform probing geometry, which is crucial for the correct interpretation of the obtained results. In case of protein anchoring utilizing maleimide-thiol chemistry, it is important to ensure that the attachment results solely from the engineered cysteine coupling to surface and that no protein-intrinsic cysteine reacts with maleimide. In its native state, GFP contains two reduced cysteines at positions 48 and 70. Cys70 is buried inside the β -barrel, while Cys48 is partially solvent exposed. However, it is not available for binding to maleimide on the surface, which I tested using unmodified GFP according to a standard surface preparation procedure (data not shown). This proved that coupling of GFP was site-specific as desired.

4.3.2 MFB results

The Molecular Force Balance (MFB) has proven successful in various comparative studies of molecular interactions [Albrecht et al., 2003; Severin et al., 2011; Limmer et al., 2014; Ho et al., 2009]. So far it was, however, limited to DNA samples - much less demanding in terms of experimental conditions and handling. Here, the applicability

of this versatile method was expanded over the vast world of interactions involving proteins. Due to the strict and narrow tolerance characteristic to most proteins, a number of adjustments had to be implemented to ensure integrity and reliability of the assay.

The MFB utilizes the principle of two bonds in series probed simultaneously until, statistically, the weaker one breaks. Therefore, covalently-linked hybrids of protein and DNA were crucial to the functionality of the comparative force assay, thanks to which only the reference or the test bond were in question when under load. The GPF-DNA complexes were formed by reacting the ybbR tag to CoA-derivatized DNA strand as in [Pippig et al., 2014], which turned out to work efficiently.

The GFP-Nb complexes outlived 40 bp DNA in the shear geometry, indicating it can withstand forces of at least 65 pN. No distinction in binding force was observed between eGFP-Nb pair ($NF=0.255 \pm 0.023$) and wtGFP-Nb pair ($NF=0.253 \pm 0.018$), while the NF factor of sfGFP was significantly higher (0.353 ± 0.018). This difference in binding strength can be attributed to the substitutions of five amino acids - two directly contacting the Nanobody and three maintaining hydrophobic interactions. The epitopes of eGFP and wtGFP do not display any differences. Figure 4.2 presents the alignment of all three GFP sequences with highlighted amino acids making up the Nb-binding epitope.

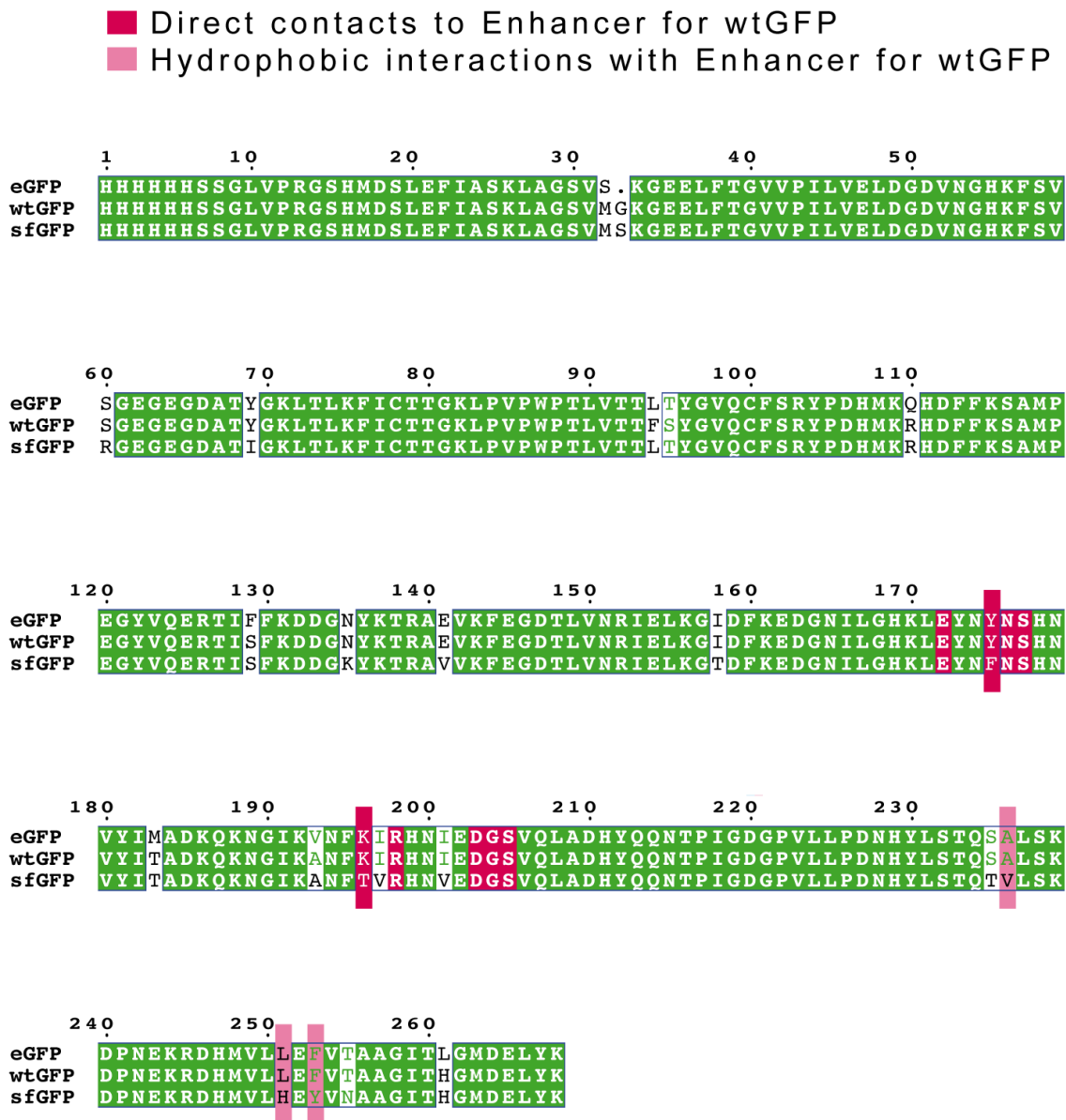


Figure 4.2: Alignment of GFP constructs used in MFB. From: [Aschenbrenner et al., 2014]

Consistently throughout all the MFB measurements, all GFP variants bind stronger to the modified GFP binder than to its "bare" version. This difference can be explained by a difference in isoelectric points of the two Nanobodies, despite their identical epitopes (pI=7.85 in case of the proper GFP binder compared to pI=9.89 for the modified one). Moreover, we were able to demonstrate a lot of flexibility in fine-tuning of the balance by the use of DNA binding ligands. These visibly altered the rupture force characteristic to the DNA oligonucleotides by stabilizing the double-stranded DNA structure. Hence, the sensitivity of the balance could be conveniently set to its maximum - that is around the equilibrium point (where $NF=0.5$). Importantly, modification of the reference (DNA) bond does not influence the Nb-GFP complex, and so for all the different experimental conditions for a given GFP variant, the relation between the binding strengths of the two Nb variants remained unchanged.

The example of DNA modifiers presented here demonstrate the possibility of tuning the sensing capacity of MFB in a broad range. Other ways of DNA stability modulation could also be considered regarding reference bonds, e.g. oligonucleotide-linked polyamide strands [Ryabinin et al., 2004] or tethered major groove amines [Szulik et al., 2013].

4.3.3 AFM results

Intuitively, one could expect a difference in rupture force between single- and double-anchored GFPs. Single attachment point offers much more flexibility for the protein complex to spatially orientate along the acting force, while fixing the GFP at both termini restricts its freedom of movement the more the complex extends. The stiffer two-point attachment should then result in GFP β -barrel held rather vertically upon extension and the Nanobody "peeling off" or sliding from the side of GFP. Indeed, data for wtGFP prove this concept. In single-anchored GFP pulling by Nb, the whole interaction interface of the complex aligned along the pulling direction experiences the rupture at once. Contact between the two protein surfaces is rapidly lost, hence the smaller potential width (Δx). In case of double-anchored GFP, gradual loss of contact between the Nb and its epitope manifests itself with broader potential width and lower force. This distinction however does not apply to the eGFP constructs, which withstand higher forces when pulled on in complex with Nb - high enough to unfold the N-terminal α -helix, which occurs at around 35 pN and contributes additional 2.9 nm to the effective spacer length [Dietz and Rief, 2004]. Hence, the complex - although double-anchored - effectively experiences only a single (shorter)

anchor and behaves accordingly in response to stretching. The alignment of the GFP constructs used in the AFM measurements (based on DNA sequencing results) is presented in Fig. 4.3.

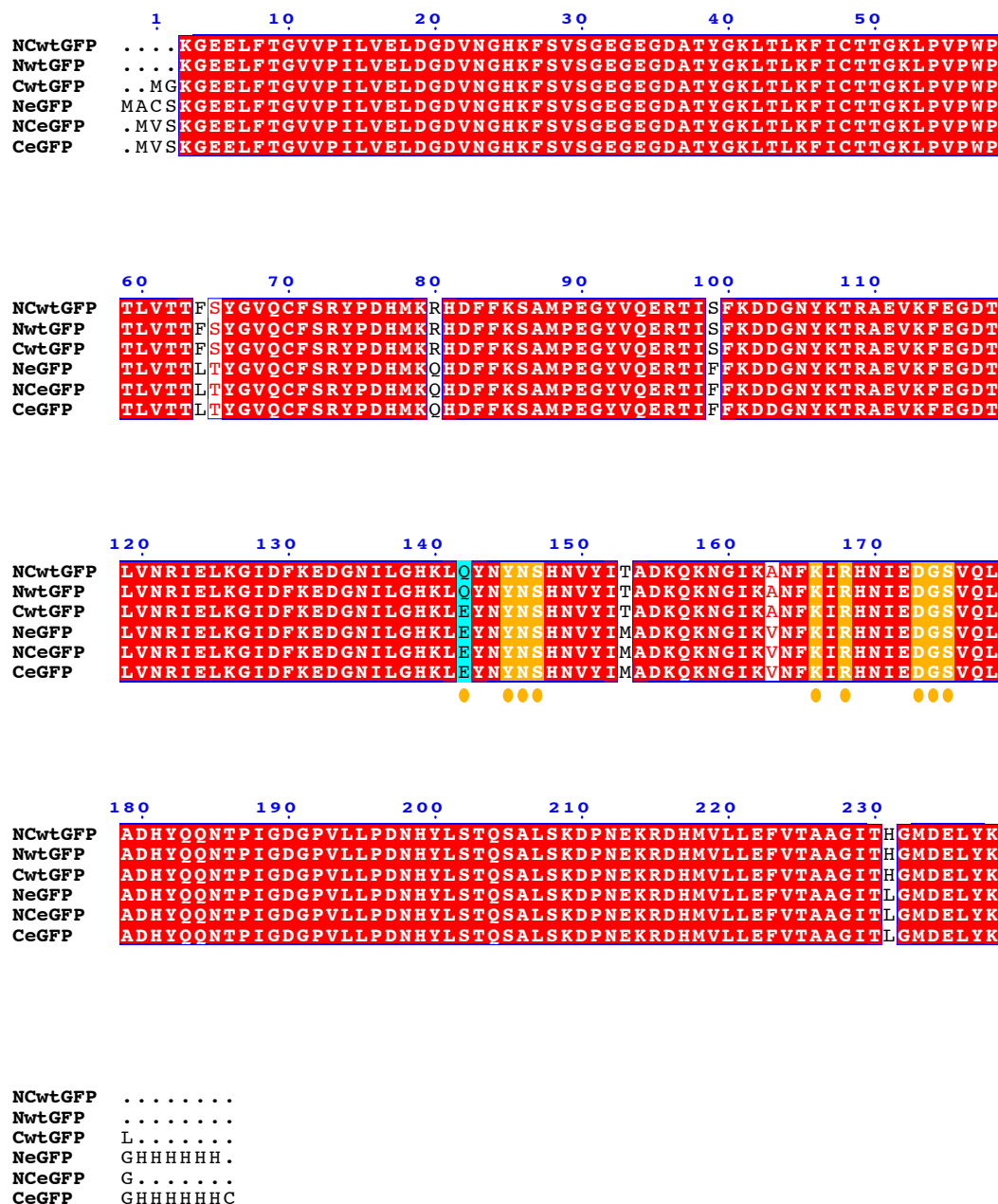


Figure 4.3: Alignment of GFP constructs used in AFM. Orange dots indicate residues in direct contact with the Nanobody; highlighted in orange are the ones conserved in all the measured GFP constructs. Two of the wtGFP constructs display a mutation in one contact site (highlighted in turquoise). Alignment was performed using ClustalW2 (<http://www.ebi.ac.uk/Tools/msa/clustalw2/>).

4.3.4 Specificity of interactions in AFM

In force measurements it is crucial to discriminate specific from unspecific interactions to reduce the impact on the analysis by the latter. In protein unfolding studies this is often accomplished by including an extra domain in the construct, which unfolds at lower force than the protein of interest, yielding a fingerprint in the force-extension curves. The relatively low rupture forces measured for the Nb-GFP complex pose a difficulty in finding a compatible protein signature for this purpose. Therefore we analyzed a number of negative control experiments where binding sites on the Nanobody or GFP were blocked with an excess of the respective binding partner as well as measurements utilizing incompletely functionalized (i.e. lacking the protein) cantilevers or surfaces. In all cases the interaction frequency was drastically reduced as compared to specific Nb-GFP probing.

4.4 Importance of single-molecule studies of protein complexes

In response to the emergence of protein-based single-molecule manipulation techniques, mechanistic analysis of the Nb-GFP interaction bridges the gap between available bulk-derived affinity data and relevant to single molecule force characteristic describing an isolated complex. The fact that the measured forces are in the range of DNA oligonucleotides unbinding [Schumakovitch et al., 2002] makes the Nb-GFP complex a promising candidate as a reference in protein-based comparative force assays. This indicates the applicability of the Nb-GFP complex in determining strength of yet uncharacterized protein pairs. Furthermore, one can imagine the application of Nanobodies as molecular force sensors also *in vivo* - a currently challenging and much desired research direction [Cost et al., 2015].

Single-molecule techniques broaden the horizon of interactions available for identification and detailed investigation, by including the less tight or less stable ones. Weak protein-protein interactions are found particularly among signaling cascades and regulatory pathways [Bhattacharyya et al., 2006; Stein et al., 2009; Bashor et al., 2010]. Characterized by definition by lower stability, they are often missed by classical approaches [Rudolph, 2007; Ohlson, 2008]. Many of them are responsible for the dynamics of intracellular molecular environment and the transient nature reflects their function - after signal propagation the complex dissociates into its stable

constituents. The importance of transient interactions lies in their potential as drug targets, like for instance nutlins used in cancer therapy, stabilizing tumor suppressor p53 [Vassilev et al., 2004] or colchicine stabilizing the dimers of α - and β -tubulin and blocking their polymerization [Ravelli et al., 2004].

4.5 Summary

This work presents examples of the complexity of biomolecular interactions and points out a number of limitations of particular techniques in regard of explaining the mechanisms underlying the subtle differences, which make an approach suitable for one system not necessarily transferrable to another one. Different single-molecule techniques complement each other in their applicability to investigate various biological complexes. Yet very often finding the right approach is not a trivial task.

4.6 Outlook

Given the recent advances in the field of single-molecule manipulation, the Nb-GFP complex offers great opportunities for further expansion, e.g. in the cut-and-paste technology [Kufer et al., 2008]. Direct follow-up experiments at this point could include identifying three different types of Nanobodies suited as handles to immobilize, pick up and deposit elsewhere GFP-tagged proteins. Based on the findings presented in [Kirchhofer et al., 2010], one of the two steps of this GFP takeover could be realized by the pair referred to as Minimizer and Enhancer in the abovementioned publication, since these two binders display such a hierarchical behavior. Thanks to the popularity of the GFP-tag, most proteins have already been fused to the GFP, which makes this strategy straightforward and ready to use once such a GFP-binder based system has been established.

Appendix A

List of abbreviations

- 3D - 3-dimensional
- 5hmC - 5-hydroxymethylcytosine
- Å - Ångstrom
- AFM - Atomic Force Microscope
- bp - basepair
- BG - benzylguanine
- CDR - Complementarity Determining Region
- CE - coupling efficiency
- CoA - Coenzyme A
- Co-IP - Co-Immunoprecipitation
- CpG - C-phosphate-G
- dCTP - deoxycytidine triphosphate
- ddH₂O - double-distilled water
- DMF - dimethylformamide
- DNA - deoxyribonucleic acid
- dsDNA - double-stranded deoxyribonucleic acid
- dNTP - deoxynucleotide
- EDC - 1-Ethyl-3-(3-dimethylaminopropyl)carbodiimide

- dUTP - deoxyuridine triphosphate
- eGFP - enhanced Green Fluorescence Protein
- EMSA - Electrophoretic Mobility Shift Assay
- Fab - Fragment, antigen-binding
- FJC - Freely Jointed Chain
- fN - femtonewton
- FRET - Fluorescence Resonance Energy Transfer
- GA - Gibson Assembly
- GFP - Green Fluorescence Protein
- h - hour
- hAGT - human O6-alkylguanine-DNA alkyl transferase
- HCAb - heavy-chain-only antibody
- HisTag - polyhistidine-tag
- Ig - immunoglobulin
- k_B - Boltzmann constant
- K_d - dissociation constant
- kb - kilobase
- kDa - kilodalton
- LB - lysogeny broth
- MBD - Methyl-DNA Binding Domain
- MeCP2- methyl CpG binding protein 2
- MFA - Molecular Force Assay
- MFB - Molecular Force Balance
- min - minute
- mm - millimeter
- mM - millimolar
- MT - Magnetic Tweezers
- μ l - microliter
- μ M - micromolar

- NA - Neutravidin
- Nb - Nanobody
- NF - normalization factor
- NHS - N-hydroxysuccinimide
- nm - nanometer
- NMR - Nuclear Magnetic Resonance
- PAGE - Polyacrylamide Gel Electrophoresis
- PBS - Phosphate-buffered saline
- PCR - Polymerase Chain Reaction
- PDMS - polydimethylsiloxane
- PEG - Polyethylene Glycol
- PMSF - phenylmethanesulfonyl fluoride
- pN - piconewton
- RNA - Ribonucleic acid
- RTT - Rett Syndrome
- s - second
- SA - streptavidin
- sfGFP - superfolder Green Fluorescence Protein
- SFP - 4'-phosphopantetheinyl transferase
- SM - Single-Molecule
- TCEP - tris(2-carboxyethyl)phosphine
- UHRF1 - Ubiquitin-like containing PHD and RING finger domains 1
- UV - ultraviolet
- v/v - volume/volume
- WDR - WW domain-binding region
- WLC - Wormlike Chain
- wtGFP - wild-type Green Fluorescence Protein
- Y2H - Yeast Two-Hybrid

Appendix B

Declaration

Eidesstattliche Erklärung

Hiermit erkläre ich, dass ich die vorliegende Arbeit eigenständig und ohne fremde Hilfe angefertigt habe. Textpassagen, die wörtlich oder dem Sinn nach auf Publikationen oder Vorträgen anderer Autoren beruhen, sind als solche kenntlich gemacht.

Die Arbeit wurde bisher keiner anderen Prüfungsbehörde vorgelegt und auch noch nicht veröffentlicht.

München, Datum 16.11.2016

Kamila Klamecka

Name (+ Unterschrift)

Bibliography

- Adams, V. H., McBryant, S. J., Wade, P. A., Woodcock, C. L. and Hansen, J. C., 2007. Intrinsic disorder and autonomous domain function in the multifunctional nuclear protein, MeCP2. *Journal of Biological Chemistry* 282(20), pp. 15057–15064.
- Albrecht, C., Blank, K., Lalic-Mülthaler, M., Hirler, S., Mai, T., Gilbert, I., Schiffmann, S., Bayer, T., Clausen-Schaumann, H. and Gaub, H. E., 2003. Dna: A programmable force sensor. *Science* 301(5631), pp. 367–370.
- Allen, S., Davies, J., Dawkes, A. C., Davies, M. C., Edwards, J. C., Parker, M. C., Roberts, C. J., Sefton, J., Tendler, S. J. B. and Williams, P. M., 1996. In situ observation of streptavidin-biotin binding on an immunoassay well surface using an atomic force microscope. *FEBS Letters* 390(2), pp. 161–164.
- Altintas, I., Kok, R. J. and Schiffelers, R. M., 2012. Targeting epidermal growth factor receptor in tumors: from conventional monoclonal antibodies via heavy chain-only antibodies to nanobodies. *Eur J Pharm Sci* 45(4), pp. 399–407.
- Amir, R. E., Van den Veyver, I. B., Wan, M., Tran, C. Q., Francke, U. and Zoghbi, H. Y., 1999. Rett syndrome is caused by mutations in X-linked MECP2, encoding methyl-CpG-binding protein 2. *Nat Genet* 23(2), pp. 185–188.
- Amstutz, P., Koch, H., Binz, H. K., Deuber, S. A. and Plückthun, A., 2006. Rapid selection of specific MAP kinase-binders from designed ankyrin repeat protein libraries. *Protein Engineering Design and Selection* 19(5), pp. 219–229.
- Arbabi Ghahroudi, M., Desmyter, A., Wyns, L., Hamers, R. and Muyldermans, S., 1997. Selection and identification of single domain antibody fragments from camel heavy-chain antibodies. *FEBS Lett* 414(3), pp. 521–6.
- Aschenbrenner, D., Pippig, D. A., Klamecka, K., Limmer, K., Leonhardt, H. and

- Gaub, H. E., 2014. Parallel force assay for protein-protein interactions. *PLoS ONE* 9(12), pp. e115049.
- Baker, S. A., Chen, L., Wilkins, A. D., Yu, P., Lichtarge, O. and Zoghbi, H. Y., 2013. An AT-hook domain in MeCP2 determines the clinical course of Rett syndrome and related disorders. *Cell* 152(5), pp. 984–996.
- Baral, T. N., Magez, S., Stijlemans, B., Conrath, K., Vanhollebeke, B., Pays, E., Muyldermans, S. and De Baetselier, P., 2006. Experimental therapy of African trypanosomiasis with a nanobody-conjugated human trypanolytic factor. *Nat Med* 12(5), pp. 580–4.
- Barchuk, A., Cristino, A., Kucharski, R., Costa, L., Simoes, Z. and Maleszka, R., 2007. Molecular determinants of caste differentiation in the highly eusocial honeybee *Apis mellifera*. *BMC Developmental Biology* 7(1), pp. 70.
- Bashor, C. J., Horwitz, A. A., Peisajovich, S. G. and Lim, W. A., 2010. Rewiring cells: Synthetic biology as a tool to interrogate the organizational principles of living systems. *Annual Review of Biophysics* 39(1), pp. 515–537.
- Becker, A., Allmann, L., Hofstätter, M., Casà, V., Weber, P., Lehmkuhl, A., Herce, H. D. and Cardoso, M. C., 2013. Direct homo- and hetero-interactions of MeCP2 and MBD2. *PLoS ONE* 8(1), pp. e53730.
- Bell, J. T. and Spector, T. D., 2011. A twin approach to unraveling epigenetics. *Trends in Genetics* 27(3), pp. 116 – 125.
- Bhattacharyya, R. P., Reményi, A., Yeh, B. J. and Lim, W. A., 2006. Domains, motifs, and scaffolds: The role of modular interactions in the evolution and wiring of cell signaling circuits. *Annual Review of Biochemistry* 75(1), pp. 655–680.
- Binnig, G., Quate, C. and Gerber, C., 1986. Atomic Force Microscope. *Phys. Rev. Lett.* 56, pp. 930–933.
- Binz, H., Stumpp, M. T., Forrer, P., Amstutz, P. and Pluckthun, A., 2003. Designing repeat proteins: Well-expressed, soluble and stable proteins from combinatorial libraries of consensus ankyrin repeat proteins. *Journal of Molecular Biology* 332(2), pp. 489 – 503.
- Bird, A. P., 1986. CpG-rich islands and the function of DNA methylation. *Nature* 321(6067), pp. 209–213.
- Bogdanović, O. and Veenstra, G., 2009. DNA methylation and methyl-CpG binding

- proteins: developmental requirements and function. *Chromosoma* 118(5), pp. 549–565.
- Brero, A., Easwaran, H. P., Nowak, D., Grunewald, I., Cremer, T., Leonhardt, H. and Cardoso, M. C., 2005. Methyl CpG-binding proteins induce large-scale chromatin reorganization during terminal differentiation. *The Journal of Cell Biology* 169(5), pp. 733–743.
- Broisat, A., Hernot, S., Toczek, J., De Vos, J., Riou, L. M., Martin, S., Ahmadi, M., Thielens, N., Wernery, U., Caveliers, V., Muyldermans, S., Lahoutte, T., Fagret, D., Ghezzi, C. and Devoogdt, N., 2012. Nanobodies targeting mouse/human VCAM1 for the nuclear imaging of atherosclerotic lesions. *Circ Res* 110(7), pp. 927–37.
- Bronner, C., Achour, M., Arima, Y., Chataigneau, T., Saya, H. and Schini-Kerth, V. B., 2007. The {UHRF} family: Oncogenes that are drugable targets for cancer therapy in the near future? *Pharmacology & Therapeutics* 115(3), pp. 419–434.
- Buschdorf, J. P. and Strätling, W. H., 2004. A WW domain binding region in methyl-CpG-binding protein MeCP2: impact on Rett syndrome. *Journal of Molecular Medicine* 82(2), pp. 135–143.
- Butt, H. J. and Jaschke, M., 1995. Calculation of thermal noise in atomic force microscopy. *Nanotechnology* 6(1), pp. 1–7.
- Chaiet, L. and Wolf, F. J., 1964. The properties of streptavidin, a biotin-binding protein produced by *Streptomyces*. *Archives of Biochemistry and Biophysics* 106(0), pp. 1 – 5.
- Chakravarty, R., Goel, S. and Cai, W., 2014. Nanobody: the magic bullet for molecular imaging? *Theranostics* 4(4), pp. 386–98.
- Chalfie, M., 1995. Green Fluorescent Protein. *Photochemistry and Photobiology* 62(4), pp. 651–656.
- Clausen-Schaumann, H., Rief, M., Tolksdorf, C. and Gaub, H. E., 2000. Mechanical stability of single DNA molecules. *Biophysical Journal* 78(4), pp. 1997–2007.
- Colhoun, E. H. and Smith, M. V., 1960. Neurohormonal properties of royal jelly. *Nature* 188(4753), pp. 854–855.
- Cortez-Retamozo, V., Backmann, N., Senter, P. D., Wernery, U., De Baetselier, P., Muyldermans, S. and Revets, H., 2004. Efficient cancer therapy with a nanobody-based conjugate. *Cancer Res* 64(8), pp. 2853–7.

- Cost, A.-L., Ringer, P., Chrostek-Grashoff, A. and Grashoff, C., 2015. How to measure molecular forces in cells: A guide to evaluating genetically-encoded FRET-based tension sensors. *Cellular and Molecular Bioengineering* 8(1), pp. 96–105.
- Crick, F. and Hughes, A., 1950. The physical properties of cytoplasm: A study by means of the magnetic particle method Part I. experimental. *Experimental Cell Research* 1(1), pp. 37–80.
- Daniel, J. M. and Reynolds, A. B., 1999. The catenin p120(ctn) interacts with Kaiso, a novel BTB/POZ domain zinc finger transcription factor. *Molecular and Cellular Biology* 19(5), pp. 3614–3623.
- De Groeve, K., Deschacht, N., De Koninck, C., Caveliers, V., Lahoutte, T., Devoogdt, N., Muyldermans, S., De Baetselier, P. and Raes, G., 2010. Nanobodies as tools for in vivo imaging of specific immune cell types. *J Nucl Med* 51(5), pp. 782–9.
- Dekker, N. H., Abels, J. A., Veenhuizen, P. T. M., Bruinink, M. M. and Dekker, C., 2004. Joining of long double-stranded RNA molecules through controlled overhangs. *Nucleic Acids Research* 32(18), pp. e140–e140.
- D’Huyvetter, M., Aerts, A., Xavier, C., Vaneycken, I., Devoogdt, N., Gijs, M., Impens, N., Baatout, S., Ponsard, B., Muyldermans, S., Caveliers, V. and Lahoutte, T., 2012. Development of ¹⁷⁷Lu-nanobodies for radioimmunotherapy of HER2-positive breast cancer: evaluation of different bifunctional chelators. *Contrast Media Mol Imaging* 7(2), pp. 254–64.
- Dietz, H. and Rief, M., 2004. Exploring the energy landscape of GFP by single-molecule mechanical experiments. *Proceedings of the National Academy of Sciences of the United States of America* 101(46), pp. 16192–16197.
- Els Conrath, K., Lauwereys, M., Wyns, L. and Muyldermans, S., 2001. Camel single-domain antibodies as modular building units in bispecific and bivalent antibody constructs. *Journal of Biological Chemistry* 276(10), pp. 7346–7350.
- Evans, E. and Williams, P., 2002. Dynamic force spectroscopy. In: F. Flyvbjerg, F. JÄijlicher, P. Ormos and F. David (eds), *Physics of bio-molecules and cells. Physique des biomolécules et des cellules*, Les Houches - Ecole d’Ete de Physique Theorique, Vol. 75, Springer Berlin Heidelberg, pp. 145–204.
- Evans, E., Ritchie, K. and Merkel, R., 1995. Sensitive force technique to probe molecular adhesion and structural linkages at biological interfaces. *Biophysical Journal* 68(6), pp. 2580 – 2587.

- Fatemi, M., Hermann, A., Gowher, H. and Jeltsch, A., 2002. Dnmt3a and Dnmt1 functionally cooperate during de novo methylation of DNA. *European Journal of Biochemistry* 269(20), pp. 4981–4984.
- Filion, G. J. P., Zhenilo, S., Salozhin, S., Yamada, D., Prokhortchouk, E. and Defossez, P.-A., 2006. A family of human zinc finger proteins that bind methylated DNA and repress transcription. *Molecular and Cellular Biology* 26(1), pp. 169–181.
- Flower, D. R., 1996. The lipocalin protein family: structure and function. *Biochemical Journal* 318(Pt 1), pp. 1–14.
- Fraga, M. F., Ballestar, E., Paz, M. F., Ropero, S., Setien, F., Ballestar, M. L., Heine-Suner, D., Cigudosa, J. C., Urioste, M., Benitez, J., Boix-Chornet, M., Sanchez-Aguilera, A., Ling, C., Carlsson, E., Poulsen, P., Vaag, A., Stephan, Z., Spector, T. D., Wu, Y.-Z., Plass, C. and Esteller, M., 2005. Epigenetic differences arise during the lifetime of monozygotic twins. *Proceedings of the National Academy of Sciences of the United States of America* 102(30), pp. 10604–10609.
- Freitag, S., Le Trong, I., Klumb, L., Stayton, P. S. and Stenkamp, R. E., 1997. Structural studies of the streptavidin binding loop. *Protein Science : A Publication of the Protein Society* 6(6), pp. 1157–1166.
- Gainkam, L. O., Huang, L., Caveliers, V., Keyaerts, M., Hernot, S., Vaneycken, I., Vanhove, C., Revets, H., De Baetselier, P. and Lahoutte, T., 2008. Comparison of the biodistribution and tumor targeting of two 99mTc-labeled anti-EGFR nanobodies in mice, using pinhole SPECT/micro-CT. *J Nucl Med* 49(5), pp. 788–95.
- Georgel, P. T., Horowitz-Scherer, R. A., Adkins, N., Woodcock, C. L., Wade, P. A. and Hansen, J. C., 2003. Chromatin compaction by human MeCP2: Assembly of novel secondary chromatin structures in the absence of DNA methylation. *Journal of Biological Chemistry* 278(34), pp. 32181–32188.
- Ghosh, R. P., Horowitz-Scherer, R. A., Nikitina, T., Gierasch, L. M. and Woodcock, C. L., 2008. Rett syndrome-causing mutations in human MeCP2 result in diverse structural changes that impact folding and DNA interactions. *Journal of Biological Chemistry* 283(29), pp. 20523–20534.
- Ghosh, R. P., Horowitz-Scherer, R. A., Nikitina, T., Shlyakhtenko, L. S. and Woodcock, C. L., 2010a. MeCP2 binds cooperatively to its substrate and competes with histone H1 for chromatin binding sites. *Molecular and Cellular Biology* 30(19), pp. 4656–4670.

- Ghosh, R. P., Nikitina, T., Horowitz-Scherer, R. A., Gierasch, L. M., Uversky, V. N., Hite, K., Hansen, J. C. and Woodcock, C. L., 2010b. Unique physical properties and interactions of the domains of methylated DNA binding protein 2. *Biochemistry* 49(20), pp. 4395–4410.
- Goethals, L. R., Bos, T. J., Baeyens, L., De Geeter, F., Devoogdt, N. and Lahoutte, T., 2014. Camelid reporter gene imaging: a generic method for in vivo cell tracking. *EJNMMI Res* 4, pp. 32.
- Gosse, C. and Croquette, V., 2002. Magnetic Tweezers: Micromanipulation and force measurement at the molecular level. *Biophysical Journal* 82(6), pp. 3314 – 3329.
- Green, N. M., 1975. Avidin. *Advances in Protein Chemistry*, Vol. 29, Academic Press, pp. 85 – 133.
- Halford, S. E. and Marko, J. F., 2004. How do site-specific DNA-binding proteins find their targets? *Nucleic Acids Research* 32(10), pp. 3040–3052.
- Hamers-Casterman, C., Atarhouch, T., Muyldermans, S., Robinson, G., Hammers, C., Songa, E. B., Bendahman, N. and Hammers, R., 1993. Naturally occurring antibodies devoid of light chains. *Nature* 363, pp. 446–448.
- Hendrich, B. and Bird, A., 1998. Identification and characterization of a family of mammalian methyl-CpG binding proteins. *Molecular and Cellular Biology* 18(11), pp. 6538–6547.
- Herce, H. D., Deng, W., Helma, J., Leonhardt, H. and Cardoso, M. C., 2013. Visualization and targeted disruption of protein interactions in living cells. *Nat Commun* 4, pp. 2660.
- Hmila, I., Saerens, D., Ben Abderrazek, R., Vincke, C., Abidi, N., Benlasfar, Z., Govaert, J., El Ayeb, M., Bouhaouala-Zahar, B. and Muyldermans, S., 2010. A bispecific nanobody to provide full protection against lethal scorpion envenoming. *FASEB J* 24(9), pp. 3479–89.
- Ho, D., Dose, C., Albrecht, C. H., Severin, P., Falter, K., Dervan, P. B. and Gaub, H. E., 2009. Quantitative detection of small molecule/DNA complexes employing a force-based and label-free dna-microarray. *Biophysical Journal* 96(11), pp. 4661 – 4671.
- Ho, K. L., McNae, I. W., Schmiedeberg, L., Klose, R. J., Bird, A. P. and Walkinshaw, M. D., 2008. MeCP2 binding to {DNA} depends upon hydration at methyl-CpG. *Molecular Cell* 29(4), pp. 525 – 531.

- Holliday, R., 2006. Epigenetics: A historical overview. *Epigenetics* 1(2), pp. 76–80.
- Hopfner, R., Mousli, M., Jeltsch, J.-M., Voulgaris, A., Lutz, Y., Marin, C., Bellocq, J.-P., Oudet, P. and Bronner, C., 2000. ICBP90, a novel human CCAAT binding protein, involved in the regulation of topoisomerase IIalpha expression. *Cancer Research* 60(1), pp. 121–128.
- Howarth, M., Chinnapen, D. J.-F., Gerrow, K., Dorrestein, P. C., Grandy, M. R., Kelleher, N. L., El-Husseini, A. and Ting, A. Y., 2006. A monovalent streptavidin with a single femtomolar biotin binding site. *Nat Meth* 3(4), pp. 267–273.
- Jeltsch, A., 2006. On the enzymatic properties of Dnmt1: Specificity, processivity, mechanism of linear diffusion and allosteric regulation of the enzyme. *Epigenetics* 1(2), pp. 63–66.
- Jørgensen, H. F., Ben-Porath, I. and Bird, A. P., 2004. Mbd1 is recruited to both methylated and nonmethylated CpGs via distinct DNA binding domains. *Molecular and Cellular Biology* 24(8), pp. 3387–3395.
- Kirchhofer, A., Helma, J., Schmidthals, K., Frauer, C., Cui, S., Karcher, A., Pellis, M., Muyldermans, S., Casas-Delucchi, C. S., Cardoso, M. C., Leonhardt, H., Hopfner, K. P. and Rothbauer, U., 2010. Modulation of protein properties in living cells using nanobodies. *Nat Struct Mol Biol* 17(1), pp. 133–8.
- Klose, R. J. and Bird, A. P., 2004. MeCP2 behaves as an elongated monomer that does not stably associate with the Sin3a chromatin remodeling complex. *Journal of Biological Chemistry* 279(45), pp. 46490–46496.
- Klose, R. J., Sarraf, S. A., Schmiedeberg, L., McDermott, S. M., Stancheva, I. and Bird, A. P., 2005. DNA binding selectivity of MeCP2 due to a requirement for A/T sequences adjacent to methyl-CpG. *Molecular Cell* 19(5), pp. 667–678.
- Kohler, G. and Milstein, C., 1975. Continuous cultures of fused cells secreting antibody of predefined specificity. *Nature* 256(5517), pp. 495–497.
- Koide, A., Bailey, C. W., Huang, X. and Koide, S., 1998. The fibronectin type III domain as a scaffold for novel binding proteins. *Journal of Molecular Biology* 284(4), pp. 1141 – 1151.
- Kramers, H., 1940. Brownian motion in a field of force and the diffusion model of chemical reactions. *Physica* 7(4), pp. 284 – 304.
- Kubala, M. H., Kovtun, O., Alexandrov, K. and Collins, B. M., 2010. Structural and

- thermodynamic analysis of the GFP:GFP-nanobody complex. *Protein Sci* 19(12), pp. 2389–401.
- Kufer, S. K., Puchner, E. M., Gump, H., Liedl, T. and Gaub, H. E., 2008. Single-Molecule Cut-and-Paste surface assembly. *Science* 319(5863), pp. 594–596.
- Kumar, A., Kamboj, S., Malone, B. M., Kudo, S., Twiss, J. L., Czymmek, K. J., LaSalle, J. M. and Schanen, N. C., 2008. Analysis of protein domains and Rett syndrome mutations indicate that multiple regions influence chromatin-binding dynamics of the chromatin-associated protein MECP2 in vivo. *Journal of cell science* 121(Pt 7), pp. 1128–1137.
- Kurzban, G., Gitlin, G., Bayer, E., Wilchek, M. and Horowitz, P., 1990. Biotin binding changes the conformation and decreases tryptophan accessibility of streptavidin. *Journal of Protein Chemistry* 9(6), pp. 673–682.
- Lansdorp, B. M. and Saleh, O. A., 2012. Power spectrum and Allan variance methods for calibrating single-molecule video-tracking instruments. *The Review of Scientific Instruments* 83(2), pp. 025115.
- Lewis, J. D., Meehan, R. R., Henzel, W. J., Maurer-Fogy, I., Jeppesen, P., Klein, F. and Bird, A., 1992. Purification, sequence, and cellular localization of a novel chromosomal protein that binds to methylated DNA. *Cell* 69(6), pp. 905–914.
- Limmer, K., Pippig, D. A., Aschenbrenner, D. and Gaub, H. E., 2014. A force-based, parallel assay for the quantification of protein-DNA interactions. *PLoS One*.
- Lo, Y.-S., Zhu, Y.-J., and Thomas P. Beebe, J., 2001. Loading-rate dependence of individual ligand receptor bond-rupture forces studied by atomic force microscopy. *Langmuir* 17(12), pp. 3741–3748.
- Marko, J. F. and Siggia, E. D., 1995. Statistical mechanics of supercoiled DNA. *Phys. Rev. E* 52, pp. 2912–2938.
- Marttila, A. T., Laitinen, O. H., Airenne, K. J., Kulik, T., Bayer, E. A., Wilchek, M. and Kulomaa, M. S., 2000. Recombinant NeutraLite avidin: a non-glycosylated, acidic mutant of chicken avidin that exhibits high affinity for biotin and low non-specific binding properties. *{FEBS} Letters* 467(1), pp. 31 – 36.
- Mohr, F., Döhner, K., Buske, C. and Rawat, V. P. S., 2010. Tet genes: new players in DNA demethylation and important determinants for stemness. *Experimental Hematology* 39(3), pp. 272–281.

- Morfill, J., Kühner, F., Blank, K., Lugmaier, R. A., Sedlmair, J. and Gaub, H. E., 2007. B-S transition in short oligonucleotides. *Biophysical Journal* 93(7), pp. 2400–2409.
- Morin, J. G. and Hastings, J. W., 1971. Energy transfer in a bioluminescent system. *Journal of Cellular Physiology* 77(3), pp. 313–318.
- Moy, V., Florin, E. and Gaub, H., 1994. Intermolecular forces and energies between ligands and receptors. *Science* 266(5183), pp. 257–259.
- Muyldermans, S., Atarhouch, T., Saldanha, J., Barbosa, J. and Hamers, R., 1994. Sequence and structure of VH domain from naturally occurring camel heavy chain immunoglobulins lacking light chains. *Protein Engineering* 7(9), pp. 1129–1135.
- Nan, X., Meehan, R. R. and Bird, A., 1993. Dissection of the methyl-CpG binding domain from the chromosomal protein MeCP2. *Nucleic Acids Research* 21(21), pp. 4886–4892.
- Nikitina, T., Shi, X., Ghosh, R. P., Horowitz-Scherer, R. A., Hansen, J. C. and Woodcock, C. L., 2007. Multiple modes of interaction between the methylated DNA binding protein MeCP2 and chromatin. *Molecular and Cellular Biology* 27(3), pp. 864–877.
- Nord, K., Gunneriusson, E., Ringdahl, J., Stahl, S., Uhlen, M. and Nygren, P.-A., 1996. Binding proteins selected from combinatorial libraries of an alpha-helical bacterial receptor domain. *Nat Biotech* 15(8), pp. 772–777.
- Oberhauser, A. F., Hansma, P. K., Carrion-Vazquez, M. and Fernandez, J. M., 2001. Stepwise unfolding of titin under force-clamp atomic force microscopy. *Proceedings of the National Academy of Sciences* 98(2), pp. 468–472.
- Ohlson, S., 2008. Designing transient binding drugs: A new concept for drug discovery. *Drug Discovery Today* 13(9
), pp. 433 – 439.
- Overbeke, W. V., Verhelle, A., Everaert, I., Zwaenepoel, O., Vandekerckhove, J., Cuvelier, C., Derave, W. and Gettemans, J., 2014. Chaperone nanobodies protect gelsolin against MT1-MMP degradation and alleviate amyloid burden in the gelsolin amyloidosis mouse model. *Mol Ther* pp. 1768–1778.
- Parry, L. and Clarke, A. R., 2011. The roles of the methyl-CpG binding proteins in cancer. *Genes & Cancer* 2(6), pp. 618–630.
- Paul, W. E., 2003. *Fundamental immunology*. 5th edn, Lippincott, Philadelphia.

- Pédélecq, J.-D., Cabantous, S., Tran, T., Terwilliger, T. C. and Waldo, G. S., 2006. Engineering and characterization of a superfolder green fluorescent protein. *Nat Biotech* 24(1), pp. 79–88.
- Petronis, A., 2006. Epigenetics and twins: three variations on the theme. *Trends in Genetics* 22(7), pp. 347 – 350.
- Pippig, D. A., Baumann, F., Strackharn, M., Aschenbrenner, D. and Gaub, H. E., 2014. Protein-DNA chimeras for nano assembly. *ACS Nano* 8(7), pp. 6551–6555.
- Pradhan, S., Bacolla, A., Wells, R. D. and Roberts, R. J., 1999. Recombinant human DNA (cytosine-5) methyltransferase: I. expression, purification, and comparison of de novo and maintenance methylation. *Journal of Biological Chemistry* 274(46), pp. 33002–33010.
- Prasher, D. C., Eckenrode, V. K., Ward, W. W., Prendergast, F. G. and Cormier, M. J., 1992. Primary structure of the *aequorea victoria* green-fluorescent protein. *Gene* 111(2), pp. 229 – 233.
- Ravelli, R. B. G., Gigant, B., Curmi, P. A., Jourdain, I., Lachkar, S., Sobel, A. and Knossow, M., 2004. Insight into tubulin regulation from a complex with colchicine and a stathmin-like domain. *Nature* 428(6979), pp. 198–202.
- Rothbauer, U., Zolghadr, K., Tillib, S., Nowak, D., Schermelleh, L., Gahl, A., Backmann, N., Conrath, K., Muyldermans, S., Cardoso, M. C. and Leonhardt, H., 2006. Targeting and tracing antigens in live cells with fluorescent nanobodies. *Nat Methods* 3(11), pp. 887–9.
- Rudolph, J., 2007. Inhibiting transient protein-protein interactions: lessons from the Cdc25 protein tyrosine phosphatases. *Nat Rev Cancer* 7(3), pp. 202–211.
- Ryabinin, V. A., Boutorine, A. S., Hélène, C., Pyshnyi, D. V. and Sinyakov, A. N., 2004. Oligonucleotide–minor groove binder conjugates and their complexes with complementary DNA: Effect of conjugate structural factors on the thermal stability of duplexes. *Nucleosides, Nucleotides and Nucleic Acids* 23(5), pp. 789–803.
- Schumakovitch, I., Grange, W., Strunz, T., Bertoncini, P., Güntherodt, H.-J. and Hegner, M., 2002. Temperature dependence of unbinding forces between complementary DNA strands. *Biophysical Journal* 82(1 Pt 1), pp. 517–521.
- Severin, P. M. D. and Gaub, H. E., 2012. DNA-protein binding force chip. *Small* 8(21), pp. 3269–3273.

- Severin, P. M. D., Ho, D. and Gaub, H. E., 2011. A high throughput molecular force assay for protein-DNA interactions. *Lab Chip* 11, pp. 856–862.
- Shimomura, O., Johnson, F. H. and Saiga, Y., 1962. Extraction, purification and properties of aequorin, a bioluminescent protein from the luminous hydromedusan, *Aequorea*. *Journal of Cellular and Comparative Physiology* 59(3), pp. 223–239.
- Singh, S., Murphy, B. and O'Reilly, R., 2002. Epigenetic contributors to the discordance of monozygotic twins. *Clinical Genetics* 62(2), pp. 97–103.
- Stein, A., Pache, R. A., Bernadó, P., Pons, M. and Aloy, P., 2009. Dynamic interactions of proteins in complex networks: a more structured view. *FEBS Journal* 276(19), pp. 5390–5405.
- Stevens, M. M., Allen, S., Davies, M. C., Roberts, C. J., Schacht, E., Tendler, S. J. B., VanSteenkiste, S., and Williams, P. M., 2002. The development, characterization, and demonstration of a versatile immobilization strategy for biomolecular force measurements. *Langmuir* 18(17), pp. 6659–6665.
- Stijlemans, B., Caljon, G., Natesan, S. K., Saerens, D., Conrath, K., Perez-Morga, D., Skepper, J. N., Nikolaou, A., Brys, L., Pays, E., Magez, S., Field, M. C., De Baetselier, P. and Muyldermans, S., 2011. High affinity nanobodies against the Trypanosome brucei VSG are potent trypanolytic agents that block endocytosis. *PLoS Pathog* 7(6), pp. e1002072.
- Stumpp, M. T., Binz, H. K. and Amstutz, P., 2008. DARPins: A new generation of protein therapeutics. *Drug Discovery Today* 13(15–16), pp. 695 – 701.
- Stuss, D. P., Cheema, M., Ng, M. K., Martinez de Paz, A., Williamson, B., Missiaen, K., Cosman, J. D., McPhee, D., Esteller, M., Hendzel, M., Delaney, K. and Ausió, J., 2013. Impaired in vivo binding of MeCP2 to chromatin in the absence of its DNA methyl-binding domain. *Nucleic Acids Research* 41(9), pp. 4888–4900.
- Szulik, M. W., Voehler, M. W., Ganguly, M., Gold, B. and Stone, M. P., 2013. Site-specific stabilization of DNA by a tethered major groove amine, 7-aminomethyl-7-deaza-2'-deoxyguanosine. *Biochemistry* 52(43), pp. 7659–7668.
- Vandenbroucke, K., de Haard, H., Beirnaert, E., Dreier, T., Lauwereys, M., Huyck, L., Van Huysse, J., Demetter, P., Steidler, L., Remaut, E., Cuvelier, C. and Rot-tiers, P., 2009. Orally administered *L. lactis* secreting an anti-TNF Nanobody demonstrate efficacy in chronic colitis. *Mucosal Immunol* 3(1), pp. 49–56.
- Vaneycken, I., D'Huyvetter, M., Hernot, S., De Vos, J., Xavier, C., Devoogdt, N.,

- Caveliers, V. and Lahoutte, T., 2011. Immuno-imaging using nanobodies. *Curr Opin Biotechnol* 22(6), pp. 877–81.
- Vaneycken, I., Govaert, J., Vincke, C., Caveliers, V., Lahoutte, T., De Baetselier, P., Raes, G., Bossuyt, A., Muyldermans, S. and Devoogdt, N., 2010. In vitro analysis and in vivo tumor targeting of a humanized, grafted nanobody in mice using pinhole SPECT/micro-CT. *J Nucl Med* 51(7), pp. 1099–106.
- Vassilev, L. T., Vu, B. T., Graves, B., Carvajal, D., Podlaski, F., Filipovic, Z., Kong, N., Kammlott, U., Lukacs, C., Klein, C. et al., 2004. In vivo activation of the p53 pathway by small-molecule antagonists of MDM2. *Science* 303(5659), pp. 844–848.
- Vilfan, I., Lipfert, J., Koster, D., Lemay, S. and Dekker, N., 2009. Magnetic tweezers for single-molecule experiments. In: P. Hinterdorfer and A. Oijen (eds), *Handbook of Single-Molecule Biophysics*, Springer US, pp. 371–395.
- Vincke, C., Loris, R., Saerens, D., Martinez-Rodriguez, S., Muyldermans, S. and Conrath, K., 2009. General strategy to humanize a camelid single-domain antibody and identification of a universal humanized nanobody scaffold. *J Biol Chem* 284(5), pp. 3273–84.
- Vogel, M., Keller-Gautschi, E., Baumann, M. J., Amstutz, P., Ruf, C., Kricek, F. and Stadler, B. M., 2007. Designed ankyrin repeat proteins as anti-idiotypic-binding molecules. *Annals of the New York Academy of Sciences* 1109(1), pp. 9–18.
- Wade, P. A., Geggion, A., Jones, P. L., Ballestar, E., Aubry, F. and Wolffe, A. P., 1999. Mi-2 complex couples DNA methylation to chromatin remodelling and histone deacetylation. *Nat Genet* 23(1), pp. 62–66.
- Ward, W. W., Cody, C. W., Hart, R. C. and Cormier, M. J., 1980. Spectrophotometric identity of the energy transfer chromophores in Renilla and Aequorea green-fluorescent proteins. *Photochemistry and Photobiology* 31(6), pp. 611–615.
- Watson, J. D. and Crick, F. H. C., 1953. Molecular structure of nucleic acids: A structure for deoxyribose nucleic acid. *Nature* 171(4356), pp. 737–738.
- Weber, P. C., Ohlendorf, D. H., Wendoloski and Salemme, F. R., 1989. Structural Origins of High-Affinity Biotin Binding to Streptavidin. *Science* 243, pp. 85–88.
- Wong, S. S., Joselevich, E., Woolley, A. T., Cheung, C. L. and Lieber, C. M., 1998. Covalently functionalized nanotubes as nanometre- sized probes in chemistry and biology. *Nature* 394(6688), pp. 52–55.

- Yasui, D. H., Peddada, S., Bieda, M. C., Vallero, R. O., Hogart, A., Nagarajan, R. P., Thatcher, K. N., Farnham, P. J. and LaSalle, J. M., 2007. Integrated epigenomic analyses of neuronal MeCP2 reveal a role for long-range interaction with active genes. *Proceedings of the National Academy of Sciences* 104(49), pp. 19416–19421.
- Yin, J., Lin, A. J., Golan, D. E. and Walsh, C. T., 2006. Site-specific protein labeling by sfp phosphopantetheinyl transferase. *Nat. Protocols* 1(1), pp. 280–285.
- Yuan, C., Chen, A., Kolb, P., and Moy*, V. T., 2000. Energy landscape of streptavidin–biotin complexes measured by atomic force microscopy. *Biochemistry* 39(33), pp. 10219–10223.
- Zhang, G., Gurtu, V. and Kain, S. R., 1996. An enhanced green fluorescent protein allows sensitive detection of gene transfer in mammalian cells. *Biochemical and biophysical research communications* 227(3), pp. 707–711.
- Zheng, F., Put, S., Bouwens, L., Lahoutte, T., Matthys, P., Muyldermans, S., De Baetselier, P., Devoogdt, N., Raes, G. and Schoonooghe, S., 2014. Molecular imaging with macrophage CR1g-targeting nanobodies for early and preclinical diagnosis in a mouse model of rheumatoid arthritis. *J Nucl Med* 55(5), pp. 824–9.

Acknowledgements

I wish to thank Professor Heinrich Leonhardt and Professor Hermann Gaub for raising the idea of a joint project, thanks to which I had a chance to work in two amazing labs. I am grateful for the superb work environment you provided, inspiring projects, motivating discussions and your supportive attitude. It is Professor Leonhardt who directed my attention to the nano-aspects of biology and Professor Gaub who introduced me to manipulation at the nanoscale level, as well as gave me a beginner's crash course in alpine skiing.

I am grateful to Professor Dimitris Vlassopoulos and Professor Kostas Tokatlidis for the training I received in their labs at FORTH, Greece, which paved the way to starting my PhD.

I would like to express my gratitude to all those who contributed to this thesis.

In particular I thank:

Philip Severin, Daniela Aschenbrenner and Lukas Milles for their enthusiasm and active involvement in the projects we were part of.

Diana Pippig for solving the unsolvable. Thank you for sharing your intuitive approach and always looking for non-hackneyed solutions.

Philipp Meyer and Philipp Walker for their help and constructive exchange of ideas.

Jonas Helma, Carina Frauer and Garwin Pichler for sharing their expertise.

Stefan Stahl and Mathias Strackharn for helping me maneuver in the single-molecule world.

Manuela Milden of Cardoso lab and Carina Frauer for providing MeCP2.

Angelika Kardinal and Thomas Nicolaus for excellent technical support.

Przemo Polewski for his inexhaustible IT support.

Diana, Przemo, Carina, Udo and Marek for critically reading the drafts of my thesis.

Marilena Pinto, Dr Marie-Christine Blüm and Dr Susanne Hennig from the CeNS-IDK office for taking care of the rich content of the IDK program. I also appreciate the generous financial support by CeNS and NIM.

Kasia Krzemień for being of immense help in the IDK activities and for all the time and fun we shared, not only the science-related bits.

A huge thank you goes to all members of LS Leonhardt and LS Gaub ‘Gambicrew’ for the amazing team spirit in both scientific and non-scientific activities.

Last but not least I thank my husband Marek for being there for me, for your patience and understanding. I thank our sons Eryk and Emil, who have been my constant inspiration, as well as our families for all the support. Dziękuję za Wasze wsparcie!

Curriculum Vitae

Personal

Name: Kamila Klamecka

Education

MSc in Materials Engineering (Nanotechnology), Adam Mickiewicz University of Poznań, Poland (2009)

MSc in Biotechnology, Poznań University of Life Sciences, Poland (2008)

Academic training

PhD candidate at the Faculty of Biology, Ludwig Maximilians University of München, groups of Prof. Dr Heinrich Leonhardt and Prof. Dr Hermann Gaub (11/2009 - present)

research assistant, group of Prof. Dr Kostas Tokatlidis, FORTH-IMBB, Heraklion, Greece (2 months, 2009)

research assistant, group of Prof. Dr Dimitris Vlassopoulos, FORTH-IESL, Heraklion, Greece (4 months, 2008 - 2009)

research assistant, group of Dr Andreas Dahl, MPI for Molecular Genetics, Berlin, Germany (5 months, 2007 - 2008)

Scholarships

2011-2015 member of Nanosystems Initiative Munich-Graduate Program

2009-2013 International Doctorate Program IDK-NanoBioTechnology scholarship by Elite Network of Bavaria

2006/2007 European Mobility Scheme for Physics Students scholarship by European Physical Society for six months' studies at the University of Copenhagen, Denmark

2005-2007 Scholarship by Ministry of National Education of Poland (twice)

Publications

Klamecka K, Severin PM, Milles LF, Gaub HE, Leonhardt H. *Energy profile of nanobody-GFP complex under force*. Phys Biol. 2015 Sep 10;12(5)

Aschenbrenner D, Pippig DA, Klamecka K, Limmer K, Leonhardt H, Gaub HE *Parallel force assay for protein-protein interactions*. PLoS One. 2014 Dec 29;9(12)

Banachowicz E, Patkowski A, Meier G, Klamecka K, Gapiński J *Successful FCS experiment in nonstandard conditions*. Langmuir. 2014 Jul 29;30(29):8945-55.